K-K and π-K Scattering Lengths at Maximal Isospin from Lattice QCD

Dissertation
zur
Erlangung des Doktorgrades (Dr. rer. nat.)
der
Mathematisch-Naturwissenschaftlichen Fakultät
der
Rheinischen Friedrich-Wilhelms-Universität Bonn

von
Christopher Helmes
aus
Gelsenkirchen

Bonn, 26.11.2018

Dieser Forschungsbericht wurde als Dissertation von der
Mathematisch-Naturwissenschaftlichen Fakultät der Universität Bonn angenommen und ist
auf dem Hochschulschriftenserver der ULB Bonn
`http://hss.ulb.uni-bonn.de/diss_online` elektronisch publiziert.

1. Gutachter:	Prof. Dr. Carsten Urbach
2. Gutachter:	Prof. Dr. Bastian Kubis
Tag der Promotion:	15.03.2019
Erscheinungsjahr:	2019

ABSTRACT

The current work presents calculations of the elastic scattering length a_0 for systems of two Kaons and one pion and one Kaon, respectively. The values for a_0 have been obtained from lattice QCD simulations with $N_f = 2 + 1 + 1$ dynamical flavors in the sea. The gauge configurations used in this work have been generated by the European twisted mass collaboration (ETMC) and comprise pion masses in the range 230 to 450 MeV at 3 distinct lattice spacings. The gauge configurations are realized in a maximally twisted mass setup. For the valence sector we adopt a mixed action approach with one doublet of mass degenerate light quarks and one Osterwalder-Seiler valence strange quark at different values of the strange quark mass. Within the framework of stochastic Laplacian-Heaviside (sLapH) quark field smearing we calculate the two point correlation functions of the K^+ and π^+, respectively and the four point correlation function of the π^+-K^+ and the K^+-K^+ system. Thermal pollution is handled via a ratio of shifted correlation functions (K^+-K^+) and two variants of weighting-and-shifting the correlation functions. The energies extracted from the four and two point functions are used to calculate the scattering length a_0 for each system via Lüscher's method. Because of the unphysical quark masses, necessary for stable simulations, chiral inter- and extrapolations of the data are in order. We employ two procedures to fix the strange quark mass to its physical value, the Kaon mass at leading order chiral perturbation theory and its next to leading order form. For K^+-K^+ we resort to a combined chiral and continuum extrapolation, linear in the light quark mass, to arrive at the physical light quark mass. Thus we find

$$M_K a_0 = -0.385(16)_{\text{stat}}(^{+0}_{-12})_{m_s}(^{+0}_{-5})_{Z_P}(4)_{r_f}\,, \tag{1}$$

with systematic uncertainties stemming from the quark mass fixing (m_s), the renormalization procedure (Z_P) and the neglect of higher order terms in the expansion of the energy shift in terms of the a_0 and the inverse lattice volume. In the extrapolation the lattice artifact is found to be negligible. In the case of π^+-K^+ we extrapolate to the physical pion mass following the next to leading order for the scattering length in SU(3) ChPT. Here we find at the physical point

$$\mu_{\pi K}\, a_0^{3/2} = -0.0463(17)\,. \tag{2}$$

In this analysis we are not able to resolve possible lattice artifacts.

A further result of this study is that Chiral perturbation theory works well for the systems under considerations. For maximal isospin scattering lengths higher order terms of ChPT contribute only mildly to the leading order behavior.

The chapters Chapters 5 and 6 of this cumulative thesis have been published in [1, 2], please cf. next page.

List of Publications

[1] C. Helmes et al.,
Hadron-Hadron Interactions from $N_f = 2 + 1 + 1$ lattice QCD: Isospin-1 KK scattering length,
Phys. Rev. **D96** (2017) 034510, arXiv: 1703.04737 [hep-lat] (cit. on pp. iii, 49).

[2] C. Helmes et al.,
Hadron-Hadron interactions from $N_f = 2 + 1 + 1$ lattice QCD: $I = 3/2$ πK scattering length,
Phys. Rev. **D** ((in press)), arXiv: 1809.08886 [hep-lat] (cit. on pp. iii, 67).

DANKSAGUNG

Im folgenden möchte ich mich bei all den Menschen bedanken, ohne die diese Arbeit nicht zustande gekommen wäre.

Zuerst gilt mein Dank Prof. Dr. Carsten Urbach, der mir ermöglichte, mich in den vergangenen 4 Jahren mit diesen herausfordernden Problemen zu beschäftigen und immer ein offenes Ohr und hilfreiche Ratschläge hatte, wenn ich nicht weiter kam.

Außerdem möchte ich mich herzlich bei den Mitgliedern unserer Arbeitsgruppe für viele anregende Diskussionen und eine allzeit freundliche Arbeitsatmosphäre bedanken. Hervorheben möchte ich dabei Dr. Bartosz Kostrzewa für seine verständlichen Erklärungen komplexer Zusammenhänge und Hinweise auf mögliche Komplikationen bei der Durchführung der Analyse. Martin Ueding bin ich für zahlreiche Ratschläge und Antworten zu Softwarefrage jdeder Natur zu Dank verpflichtet. Markus Werner danke ich für viele Eingriffe in den Kontraktionscode, die diese Analyse möglich gemacht haben, sowie hilfreiche Diskussionen zu sehr vielfältigen physikalischen Themen. Dr. Marcus Petschlies danke ich für das Korrekturlesen der gesamten Dissertation sowie Hinweisen zu deren Verbesserung. Diese Forschungsarbeit wurde aus Mitteln des chinesisch-deutschen Sonderforschungsbereichs CRC110: “Symmetries and the Emergence of Structure” finanziert. Hierfür möchte ich mich bei Prof. Dr. Dr. h.c. Ulf-G. Meißner bedanken.

Darüber hinaus gibt es in meinem privaten Umfeld, Menschen, die mit ihrer moralischen Unterstützung maßgeblich dazu beigetragen haben, dass ich nicht vorzeitig das Handtuch warf. Sehr wichtig waren dabei meine Eltern, Kerstin Helmes und Hans-Joachim Helmes, sowie meine Schwester Ricarda Helmes. Meiner Freundin Vera Jaritz gilt mein besonderer Dank für ihre lange Geduld und viele Vorschläge zu einer pragmatischen Herangehensweise an diverse Probleme.

Diese Arbeit wäre außerdem nicht ohne die Mitglieder der Theorieabteilung des HISKP zustande gekommen: Vielen Dank an dieser Stelle.

CONTENTS

CHAPTER 1

INTRODUCTION

The Standard Model of particle physics has been successful in describing how matter is built from quarks and leptons. The nonet of pseudoscalar mesons as depicted in Figure 1.1, can be described via group theory regarding the 3 lightest quark flavors up (u), down (d) and strange (s). As will be detailed later the 3 lightest flavors of quarks and antiquarks can be ordered into

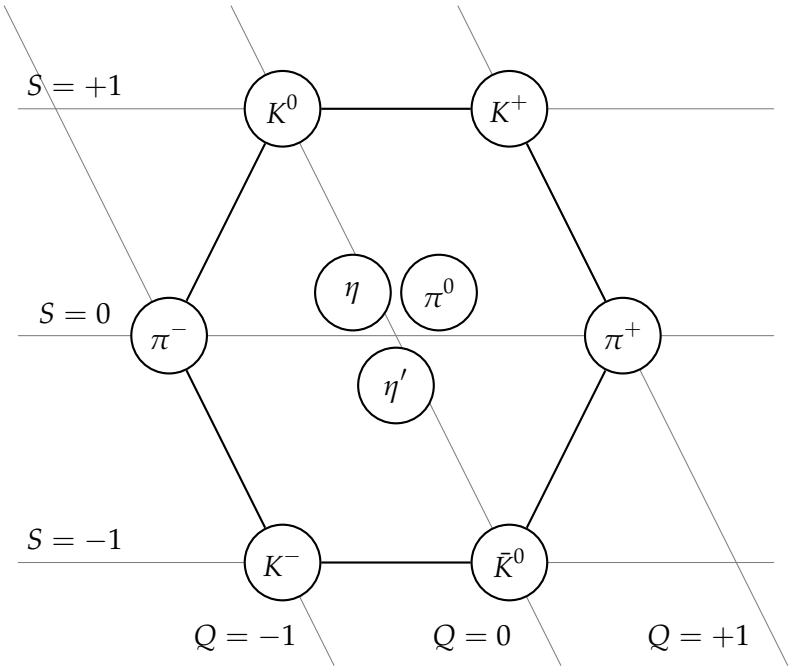

Figure 1.1: The pseudoscalar meson nonet with lines of constant electrical charge Q and constant strangeness S.

a triplet (**3**) of SU(3) and its complex conjugate representation ($\bar{\mathbf{3}}$). The tensor product of the two representations can be decomposed into the direct sum of one octet **8** and one singlet **1**

$$\mathbf{3} \otimes \bar{\mathbf{3}} = \mathbf{8} \oplus \mathbf{1}\,. \tag{1.1}$$

The members of this nonet are called mesons and are composed of one quark and one antiquark. As will be detailed in Section 2.1 the octet states are of particular interest because they are assumed to play the role of the Goldstone bosons of the spontaneously broken chiral symmetry. This is supported by the mass gap between the pseudoscalar and vector octet states. Due to this circumstance it is mandatory to understand the dynamical behavior of the members of the pseudoscalar octet. The main goal of this thesis is to shed some light on the elastic interaction of π- and K-mesons. Because these interactions happen at low energies lattice QCD is a formidable tool to tackle this matter. It is an ab-initio approach which does not need further assumptions on the interactions than a formulation of the strong interaction, quantum chromodynamics (QCD). This is accomplished by simulating QCD on a hybercubic space-time via Monte Carlo methods on high performance computers. Despite the nice feature of only a few assumptions current simulations are just beginning to reach the realm of physical quark masses. Thus one needs an extrapolation procedure to arrive at physical conditions. In order to do so we will employ Chiral Perturbation Theory (ChPT). It is an effective theory relying on the expansion around light meson masses and momenta. During the expansion process unknown unphysical constants appear which need to be fixed via further input data. In this framework quark mass dependent formulae are derived allowing for an extrapolation in the quark masses. The unknown constants alluded to above can then be fixed via fits to simulated lattice data. Because of the discretization procedure needed for the simulation process also continuum limits need to be taken in the end.

Experimentally π-K-interactions are not easily accessible because pions and kaons only form as intermediate states in high energy collisions. Owing to this it is difficult to determine scattering parameters like the scattering length or the effective range, experimentally. At the same time such low energy interactions could play an important role inside neutron stars where low energy mesons can be generated easily. Currently the DIRAC collaboration is measuring the lifetime of the bound π-K system. Its lifetime depends, among others, on a precise knowledge of the π-K scattering length, a_0. Besides lattice QCD determinations only purely theoretical estimates using Roy-Steiner equations or Chiral Perturbation Theory for a_0 are available. The present work adds to this circumstance by providing the first continuum extrapolated value of the scattering length. As we will see we improve significantly on the statistical uncertainty of a_0. This is possible by employing a novel quark field smearing scheme introduced in Ref. [3] combined with the $N_f = 2 + 1 + 1$ gauge field configurations of the European Twisted Mass Collaboration (ETMC) at three distinct values of the lattice spacing.

This thesis is organized as follows. Chapter 2 shortly recaptures the theoretical fundamentals of QCD, Chiral Perturbation Theory and the discretization of the strong interaction via lattice QCD in the twisted mass formalism. We then proceed to introduce the correlation functions for the processes under investigation and necessary spectroscopy in Chapter 3. In Chapter 4 we shortly present the Hybrid Monte Carlo algorithm and improvement methods for gauge configurations and correlation functions. Chapters 5 and 6 comprise the main results of this thesis, namely an investigation of the kaon-kaon and the pion-kaon scattering length at maximal isospin, respectively. The thesis is concluded by Chapter 7 where a final discussion and outlook to possible future applications is given.

CHAPTER 2

THEORETICAL BACKGROUND

Similar to the electric charge in Quantum Electrodynamics the so called color charge is used to describe strong interactions in the formalism of Quantum Chromodynamics (QCD). We introduce the Lagrangian density and discuss its respective symmetries in Section 2.1. In addition we give an overview on the quantization of QCD in the path integral formalism and parametrize scattering processes. Furthermore we give an effective perturbative description of low energy phenomena in form of Chiral Perturbation Theory (ChPT), cf. Section 2.2. As a non-perturbative approach to QCD we translate the continuum formulations of Section 2.1 to euclidean space-time in Section 2.3 and discretize space-time in Section 2.4. This leads us to the formulation of lattice QCD (lQCD) which enables the numerical simulations of the strong interaction.

2.1 FUNDAMENTALS OF CONTINUUM QCD

2.1.1 THE LAGRANGIAN DENSITY OF QCD

QCD is a quantized field theory with infinite degrees of freedom. It is best described within the Lagrange formalism where a Lagrangian density $\mathcal{L}$ can be formulated. Since a full treatment of $\mathcal{L}$ is out of the scope of this work we will only state its mathematical form and shortly explain its features. A more thorough introduction can be found e.g. in Refs. [4, 5]. The fundamental building blocks of strongly interacting matter are quarks and gluons. Quarks have a rest mass and are believed to be fundamental fermions like electrons whereas gluons are massless vector bosons which play the role of exchange particles of the strong interaction. Quarks differ from electrons in their mass and electric charge, which comes in multiplicities of 1/3. They exist in six flavors (up, down, strange, charm, bottom, top) ordered into three doublets

$$\begin{pmatrix} u \\ d \end{pmatrix}, \quad \begin{pmatrix} c \\ s \end{pmatrix}, \quad \begin{pmatrix} t \\ b \end{pmatrix}. \tag{2.1}$$

In addition to the mediation of the strong interaction each gluon carries one color charge and one anti-color charge. From a field-theoretical point of view this behavior is described by QCD being a non-abelian local gauge theory, described by $\mathrm{SU}(3)_C$, where C stands for color. During

strong interactions color charges are exchanged between the participating particles. One of the most striking features of strongly interacting particles is the display of confinement, i.e. any observable object needs to be color neutral. Expressed differently, single quarks cannot be observed directly.

The Lagrangian density of QCD, $\mathcal{L}_{\mathrm{QCD}}$, reads

$$\mathcal{L}_{\mathrm{QCD}}(\bar{\psi}, \psi, A) = -\frac{1}{4} F^{a,\mu\nu}(x) F^{a}_{\mu\nu}(x) + \sum_{f} \bar{\psi}_f(x) \left(i\not{D} - M_{ff} \right) \psi(x)_f \,, \tag{2.2}$$

where ψ_f denotes a vector made out of three Dirac spinors $\psi_f = (\psi_{a,f}, \psi_{b,f}, \psi_{c,f})^T$ of a single quark flavor f, with color degrees of freedom, labeled a,b and c, $\bar{\psi}_f$ its adjoint representation and M_{ff} the corresponding entry of the mass matrix. The three components of ψ_f denote three color degrees of freedom. The covariant derivative $\not{D}$ reads

$$\not{D}_\mu = \gamma^\mu (\partial_\mu + i g A^a_\mu \frac{\lambda^c_a}{2}) \,, \tag{2.3}$$

with the Dirac matrices γ^μ given in appendix A.1 and the gluon fields $A^a_\mu(x)$. It is a modification of the free Lagrangian density implementing local gauge invariance with respect to non-abelian local SU(3) transformations. The representation of these transformations $U(g(x))$ read

$$U(g(x)) = \exp\left(-i \sum_{a=1}^{8} \frac{\lambda^a}{2} \theta^a(x) \right) \,, \tag{2.4}$$

with the eight real valued functions $\theta^a(x)$, $a = 1, \ldots, 8$ and λ^a denoting the Gell-Mann matrices acting in color space. Based on local invariance the fields A^a_μ have to transform under $U(g(x))$ like

$$A_\mu = \sum_{a=1}^{8} \frac{\lambda^a}{2} A^a_\mu \to U(g(x)) A_\mu U^\dagger(g(x)) + \frac{i}{g} \partial_\mu U(g(x))^\dagger U(g(x)) \,. \tag{2.5}$$

The transformations act on ψ_f via $\psi_f(x) \to U(g(x))\psi_f(x)$. As a last ingredient the term

$$\mathcal{L}_{\mathrm{kin}} = -\frac{1}{4} F^{a,\mu\nu}(x) F^{a}_{\mu\nu}(x) \,, \tag{2.6}$$

encodes the dynamical behavior of the gluons. The important difference is that the gluons themselves carry charge and thus have self-interactions. Owing to that the eight field strength tensors $F^a_{\mu\nu}$ read

$$F^a_{\mu\nu}(x) = \partial_\mu A^a_\nu(x) - \partial_\nu A^a_\mu(x) - g f_{abc} A^b_\mu(x) A^c_\nu(x) \,, \tag{2.7}$$

with f_{abc} denoting the structure constants of the Lie-algebra underlying SU(3). The field

strength tensors transform like

$$F_{\mu\nu} = \sum_{a=1}^{8} \frac{\lambda^a}{2} F^a_{\mu\nu} \to U(g(x)) F_{\mu\nu} U^\dagger(g(x)) \,. \tag{2.8}$$

With the gauge covariant derivative given by Equation (2.3) the Lagrangian density of Equation (2.2) is symmetric under $\mathrm{SU}(3)_C$. Color charge is confined inside hadrons, such that no free color charged particles can be observed. Further exact symmetries are spatial reflections, time reversal and parity. As a consequence Equation (2.2) is also invariant under their combined action. Furthermore Equation (2.2) is Lorentz invariant. In addition to these exact symmetries Equation (2.2) exhibits a few approximate symmetries. In comparison to the heavy quarks (c, t, b), the masses of the three lighter quarks (u, d, s) can be neglected. Further going to the chiral limit $m_u = m_d = m_s = 0$ the Lagrangian density would be invariant under global $\mathrm{SU}(3)_V$ vector transformations of the form

$$\psi = \begin{pmatrix} u \\ d \\ s \end{pmatrix} \to \exp(-i\theta\lambda)\psi \,, \tag{2.9}$$

where the Gell-Mann matrices λ now act in flavor space and θ is an arbitrary eight-vector. Since the strange quark is much heavier than the u and d quark, a better choice is the isospin symmetry $\mathrm{SU}(2)$ of the doublet $(u, d)^T$

$$\psi = \begin{pmatrix} u \\ d \end{pmatrix} \to \exp(-i\theta\tau)\psi \,, \tag{2.10}$$

where the generators τ are now given by the Pauli matrices acting in flavor space and θ is an arbitrary three vector parametrizing the rotation. The symmetry under the transformation Equation (2.10) is broken by the quark mass difference of the u and d quark mass

$$\Delta m = m_u - m_d \,. \tag{2.11}$$

Returning to the chiral limit of 3 vanishing light quark masses the Lagrangian density of QCD also exhibits a hidden symmetry which is sponataneously broken. In the case of three flavors (u, d, s) and vanishing quark masses ($m_u = m_d = m_s = 0$) Equation (2.2) exhibits an exact $\mathrm{U}(3) \times \mathrm{U}(3) = \mathrm{SU}(3)_L \times \mathrm{SU}(3)_R \times \mathrm{U}(1)_V \times \mathrm{U}(1)_A$ symmetry, where the indices L and R denote left and right handed quarks, respectively and V and A vector and axial, respectively. The axial symmetry is anomalously broken by quantum effects during the quantization of the theory, see Refs. [6, 7], whereas the vector symmetry remains exact. The Noether currents of the left and right handed symmetries $SU(3)_L \times SU(3)_R$ can be linearly combined into eight Vector and eight Axial currents, denoted by V_a and A_a, respectively. Because the vacuum is not invariant under the Noether charge Q_{Aa} belonging to A_a, there have to exist 8 massless Goldstone bosons, which is the dimension of the left and right handed groups. The vector and axial currents, as well as the non singlet scalar density and pseudoscalar density can be

expressed (for $\mathrm{SU}(3)_V$) as

$$V_a^\mu = \bar{\psi}\gamma^\mu\lambda_a\psi \qquad A_a^\mu = \bar{\psi}\gamma^\mu\gamma^5\lambda_a\psi \tag{2.12}$$

$$S = \bar{\psi}\psi \qquad P_a = i\bar{\psi}\gamma_5\lambda_a\psi\,, \tag{2.13}$$

2.1.2 QCD IN THE PATH INTEGRAL FORMALISM

The action S which is the integral of the Lagrangian density over the four dimensional space-time,

$$S = \int \mathrm{d}^4x\,\mathcal{L} = S_F + S_G\,, \tag{2.14}$$

can be used to quantize QCD in the path integral formalism. Splitting the action into a fermionic (S_F) and a gauge (S_G) contribution will prove useful when discretizing the action. Matrix elements are given by the path integral

$$\langle\Omega|\mathcal{T}(\psi_1,\ldots,\psi_n)|\Omega\rangle = \frac{1}{Z}\int \mathrm{D}\psi\;\mathrm{D}\bar{\psi}\;\mathrm{D}A\;\psi_1(x)\ldots\psi_n(x)\exp\left(iS[\bar{\psi},\psi,A]\right)\,, \tag{2.15}$$

where Ω is the vacuum state of the theory, $\mathcal{T}$ denotes time ordering and the $\psi_i(x)$ are quantum fields. Because spinor fields obey anti-commutation relations, as opposed to commutation relations for classical fields, the fields $\psi(x)$ are anti-commuting Grassmann fields. Their algebraic properties and their differentiation and integration rules can be found in Ref. [8]. The integration measure used in Equation (2.15) is a product of integration measures over all possible paths

$$\int \mathrm{D}\psi\; = \prod_{i=1}^{\infty}\int \mathrm{d}\psi(x_i)\;. \tag{2.16}$$

The product in Equation (2.16) means a product over all possible paths. For a numerical treatment the product needs to be finite and thus discrete. In addition we have introduced the partition function Z in Equation (2.15). For QCD it reads

$$Z = \int \mathrm{D}\psi\;\mathrm{D}\bar{\psi}\;\mathrm{D}A\;\exp\left(iS[\bar{\psi},\psi,A]\right)\,. \tag{2.17}$$

In Equation (2.14) we have split up the action in contributions stemming from the fermionic (S_F) and the gluonic (S_G) part of Equation (2.2). Instead of evaluating the path integral of the n-point function Equation (2.15) the generating functional can be used to calculate n-point functions as detailed, for example, in Ref. [9]. Introducing an external spinor valued field $J(x)$ the generating functional is defined as

$$\mathcal{Z}[J] = \int \mathrm{D}\psi\;\mathrm{D}\bar{\psi}\;\mathrm{D}A\;\exp\left(i\int \mathrm{d}^4x\left(\mathcal{L}(\bar{\psi},\psi,A) + \bar{J}(x)\psi(x) + \bar{\psi}(x)J(x)\right)\right)\,, \tag{2.18}$$

where we have suppressed the color and Dirac indices for legibility. A given n-point function Equation (2.15) can then be calculated using the functional derivative with respect to each

coordinate

$$\langle\Omega|\mathcal{T}(\psi_1(x),\ldots,\psi_n(x))|\Omega\rangle = \frac{1}{\mathcal{Z}[0]}\left(-i\frac{\delta}{\delta J(x_1)}\right)\ldots\left(-i\frac{\delta}{\delta J(x_n)}\right)\mathcal{Z}[J]|_{J=0}\,. \tag{2.19}$$

2.1.3 PARAMETRIZATION OF SCATTERING PROCESSES

The processes under investigation in this thesis take place at low interaction energies. Therefore a non-relativistic description is sufficient. In addition the interactions are elastic and happen below their respective 4-particle energy threshold. The scattering particles furthermore are spinless, such that the wave functions of these bosonic systems need to be symmetric. For two particles with masses (momenta) m_1 ($\vec{p}$) and m_2 ($\vec{q}$), respectively, their total non-interacting energy E_0 is given via the superposition principle

$$E_0 = E_1(\vec{p}) + E_2(\vec{q}) \tag{2.20}$$

$$E_i(k) = \frac{\vec{k}^2}{2m_i} \tag{2.21}$$

Hadronic scattering processes at low interaction energies are conveniently described by the S-matrix in a non-relativistic manner. Since the form of the interaction often is not known exactly, in the S-matrix approach we examine asymptotic states of particles at $t = \pm\infty$ where the interaction takes place at $t = 0$. Let $\psi = |\vec{p}_i, \vec{q}_i\rangle$ denote the incoming wave function at $t = -\infty$ and $\varphi = \langle\vec{p}_f, \vec{q}_f|$ be the outgoing wave function at $t = +\infty$. The elements of the S-matrix are then defined via,

$$S_{fi} = \langle\vec{p}_f, \vec{q}_f|S|\vec{p}_i, \vec{q}_i\rangle\ . \tag{2.22}$$

The S-matrix is unitary, $S^\dagger S = \mathbb{1}$. Because the product $S^\dagger S$ amounts to a sum of probabilities over all possible transitions they have to add up to $\mathbb{1}$. Furthermore it is Lorentz invariant. Owing to the probability property of matrix elements there is always the possibility that ψ goes to φ without interaction. Therefore separating the non-interacting part of the S-matrix from its interacting part we rewrite

$$S = 1 + iT\,, \tag{2.23}$$

defining the T-matrix. It is related to the QCD scattering amplitude $\mathcal{T}(\vec{p}_f, \vec{q}_f|\vec{p}_i, \vec{q}_i)$ by

$$\langle\vec{p}_f, \vec{q}_f|iT|\vec{p}_i, \vec{q}_i\rangle = (2\pi)^4\delta(E_i - E_f)\delta^3(\vec{P}_i - \vec{P}_f)\mathcal{T}(\vec{p}_f, \vec{q}_f|\vec{p}_i, \vec{q}_i)\,. \tag{2.24}$$

Here the δ-distributions define total energy and momentum conservation.

The scattering amplitude $\mathcal{T}(\vec{p}_f, \vec{q}_f|\vec{p}_i, \vec{q}_i)$ in turn can also be obtained using the The Lehmann-Symanzik-Zimmermann (LSZ) reduction formula, see e.g. Ref. [9]. It relates S-matrix elements

to n-point functions. In the case of bosons as interacting particles it reads

$$\begin{aligned} S_{fi} &= \text{disconnected parts} \\ &+ (iN^{1/2})^{n+l} \int \mathrm{d}^4y_1 \ldots \mathrm{d}^4x_l \, \exp\left(i \sum_{k=1}^{n} p_k y_k - \sum_{r=1}^{l} q_r x_r \right) \\ &\times (\Box_{y_1} + m^2) \ldots (\Box_{x_l} + m^2) \, \langle \Omega | \mathcal{T}[\phi(y_1) \ldots \phi(x_l)] | \Omega \rangle \, , \end{aligned} \tag{2.25}$$

where the inverse Klein-Gordon propagators ensure that the particles are all on-shell, N is the normalization of each state and we evaluate everything in momentum space. A more thorough treatment of this reduction technique can be found in Ref. [9] The T-matrix element $\langle \varphi_f | iT | \psi_i \rangle$ is given by the second summand in Equation (2.25) which features the full time ordered n-point function. The n-point function can be calculated using functional derivatives of the generating functional as in eq. (2.19). The T-matrix, and hence the scattering amplitude can be expressed via a Born series

$$\begin{aligned} \mathcal{T}(\vec{p}\,', \vec{p}) &= \hat{V}(\vec{p}\,', \vec{p}) \\ &+ \sum_{n=0}^{\infty} \frac{(-1)^n}{2^n} \int \frac{\mathrm{d}^3k_1}{(2\pi)^3} \ldots \int \frac{\mathrm{d}^3k_n}{(2\pi)^3} \hat{V}(\vec{p}\,', \vec{k}_1) G_E(\vec{k}_1) \hat{V}(\vec{k}_1, \vec{k}_2) G_E(\vec{k}_2) \ldots \hat{V}(\vec{k}_n, \vec{p}) \, . \end{aligned} \tag{2.26}$$

Here G_E denotes the retarded Green's function

$$G_E(\vec{k}) = (\epsilon(\vec{k}) - E + i\epsilon)^{-1} \, , \tag{2.27}$$

and $\hat{V}(\vec{k})$ the Fourier transformed spherical potential of the interaction.

$$\hat{V}(\vec{k}', \vec{k}) = \int \mathrm{d}^3z \, \Big(\exp(-i(\vec{k}' - \vec{k})z) + \exp(-i(\vec{k} - \vec{k}')z) \Big) \, V(z) \, . \tag{2.28}$$

The scattering amplitude depends on the relative momenta of the two particles only. Hence the arguments $\vec{p}\,'$ and $\vec{p}$ of Equation (2.26) are $\vec{p}\,' = \vec{p}_f - \vec{q}_f$ and $\vec{p} = \vec{p}_i - \vec{q}_i$. In the center of mass frame, defined by $\vec{P}_i = \vec{p}_i + \vec{q}_i = 0$, the non-relativistic scattering amplitude of Equation (2.24) can be expanded into partial waves

$$\mathcal{T} = -\frac{4\pi}{\mu_{12}} \sum_{\ell=0}^{\infty} (2\ell + 1) P_\ell(\cos\vartheta) t_\ell \, , \tag{2.29}$$

with the reduced mass

$$\mu_{12} = \frac{m_1 m_2}{m_1 + m_2} \, . \tag{2.30}$$

Now $t_\ell(k)$ are the partial wave amplitudes, $P_\ell(\cos\vartheta)$ the Legendre polynomials of first kind and the factor $(2\ell + 1)$ accounts for the degeneracy of each partial wave. Allowing for inelasticity of the interaction and invoking the optical theorem leads to the general form of the

partial wave amplitudes,

$$t_\ell(k) = \frac{1}{2ik}\left[\eta_\ell(k)\exp(2i\delta_\ell(k)) - 1\right] , \tag{2.31}$$

where we have introduced the momentum dependent scattering phase shift $\delta_\ell(k)$, and a parameter for the inelasticity of the scattering

$$\eta_\ell(k) \leqslant 1 , \tag{2.32}$$

which for our case of elastic scattering is $\eta_\ell(k) = 1$. Since we are dealing with short ranged potentials, matching the wave function inside and outside the potential leads to the effective range approximation for s-wave scattering ($\ell = 0$),

$$k\cot\delta_0(k) = -\frac{1}{a_0} + \frac{1}{2}r_0k^2 . \tag{2.33}$$

This defines the scattering length a_0 and the effective range r_0 which are completely sufficient to describe elastic scattering processes because terms of order $\mathcal{O}\left(k^4\right)$ and higher can be ignored. The sign of the scattering length changes depending on the behavior of the scattering

$$\mathrm{sgn}(a_0) = \begin{cases} +1 , & \text{repulsive} \\ -1 , & \text{attractive} \end{cases} . \tag{2.34}$$

2.2 FUNDAMENTALS OF CHIRAL PERTURBATION THEORY

The scattering processes under investigation in this thesis occur at low energies compared to the QCD scale $\Lambda_{\mathrm{QCD}} \approx 1\,\mathrm{GeV}$. The large value of the strong coupling constant, α_s, at low energies prevents the application of ordinary Perturbation Theory to these processes. One way to proceed is the application of Chiral Perturbation Theory (ChPT) to make statements about low energy phenomena. A more detailed introduction can be found in Ref. [10]. After transforming the Lagrangian density into an effective form and inspecting its Noether currents we end up with a description of the interaction processes at hand in terms of the light degrees of freedom. The effective Lagrangian density $\mathcal{L}_{\mathrm{eff}}$ is only known up to low energy constants (LECs), as explained below. As mentioned in Chapter 1 lattice QCD simulations are run at non-physical values of quark masses. In the end we will combine the data obtained from lQCD calculations and the description of the data's chiral behavior in terms of ChPT to extrapolate our findings to physical values of the input parameters (physical meson masses and decay constants).

This section shortly defines what constitutes an effective field theory. After that we state the effective Lagrangian density to obtain predictions from and conclude with the expressions for the scattering lengths in the maximum isospin channels of K-K and π-K interactions.

2.2.1 EFFECTIVE FIELD THEORIES

ChPT is based on the assumption that for certain processes only low energy degrees of freedom are relevant whereas high energy degrees of freedom do not play a role in the interactions at hand such that they can be integrated out [10]. Effective field theories rely on the fact that scales, like for instance hadron masses, are intrinsically separated. In fact the pseudoscalar masses of the pions, the kaons and the η-meson are well separated from heavier hadron masses like for instance baryons. This separation can be expressed via

$$M_\ell \ll \Lambda \approx M_h\,, \tag{2.35}$$

where ℓ and h stand for light and heavy, respectively. It follows that the hadrons with masses around Λ do not take part at low energy processes and therefore are not important for the dynamics of these processes. An effective theory aims at replacing the underlying Lagrangian density by an effective form with different degrees of freedom. Neglecting the heavy degrees of freedom results in an unrenormalized theory with unknown coupling constants. These low energy constants (LEC) are unknown a priori and have to be determined either by calculation, by input from experiments or by fits to simulated data. The effective Lagrangian density needs to respect the same symmetries as the underlying theory because its interaction terms are also determined from the symmetries of the underlying theory. In total a successful construction of an effective Lagrangian is based on a low energy expansion from terms invariant under the symmetries of the underlying theory.

2.2.2 EFFECTIVE LAGRANGIAN DENSITY

Chiral Perturbation Theory is based on a conjecture made by Weinberg in Ref. [11]. This conjecture relates the S-matrix of a quantum field theory with a perturbative expansion of the most general effective Lagrangian density describing that quantum field theory. For this to work the expansion of $\mathcal{L}_{\text{eff}}$ has to be compatible with the underlying symmetries of the quantum field theory under inspection to all orders. Therefore one is left with two tasks:

1. Organization of the effective Lagrangian

2. Assessment of the importance of diagrams stemming from interaction terms

Item 1 can be taken care of by using Weinberg's power counting scheme. This scheme is based on an expansion of the effective Lagrangian in terms of momenta. Four derivatives (∂_μ) generate four momenta (p_μ), whereas squared meson masses are associated with squares of four momenta, when on-shell. In this sense the effective Lagrangian density, $\mathcal{L}_{\text{eff}}$, can be expanded in powers of momenta and masses

$$\mathcal{L}_{\text{eff}} = \mathcal{L}^{(2)} + \mathcal{L}^{(4)} + \mathcal{L}^{(6)} + \dots , \tag{2.36}$$

denoted by the superscripts in Equation (2.36). The occurrence of only even terms is explained by Lorentz invariance of the QCD Lagrangian density and the absence of $\mathcal{L}^{(0)}$ by the fact that it just adds an irrelevant constant. To construct an effective Lagrangian density one first decides up to which order the expansion of Equation (2.36) should be carried out. Then one collects for each power all possible terms obeying the symmetries of the theory one is interested in. For QCD we want $\mathcal{L}_{\text{eff}}$ to be invariant under $\mathrm{SU}(3)_L \times \mathrm{SU}(3)_R \times \mathrm{U}(1)_V$ in the chiral limit. Switching on quark masses should induce chiral symmetry breaking as described in Section 2.1. As an example we outline the expansion at leading order, first in the chiral limit and then incorporating quark masses. The low energy regime of QCD is dominated by the Goldstone bosons. In the chiral limit the quark masses vanish, $M = \mathrm{diag}(m_u, m_d, m_s) = 0$, and $\mathcal{L}_{\text{eff}}$ should be invariant under the isospin $\mathrm{SU}(3)$ group such that the eight Goldstone bosons $\Phi_a(x)$ associated with the eight generators λ_a of fields are the degrees of freedom. Following Ref. [10] the dynamical variables thus are given by $U(x) \in \mathrm{SU}(3)$,

$$\begin{aligned} U(x) &= \exp\left(i\frac{\Phi(x)}{F_0}\right), \\ \Phi(x) &= \sum_{a=1}^{8} \lambda_a \Phi_a(x) = \begin{pmatrix} \pi^0 + \eta/\sqrt{3} & \sqrt{2}\pi^+ & \sqrt{2}K^+ \\ \sqrt{2}\pi^- & -\pi^0 + \eta/\sqrt{3} & \sqrt{2}K^0 \\ \sqrt{2}K^- & \sqrt{2}\,\overline{K}^0 & 2\eta/\sqrt{3} \end{pmatrix}. \end{aligned} \tag{2.37}$$

The constant F_0 is associated with the weak pion decay $\pi^+ \longrightarrow \ell\nu_\ell$ in the chiral limit. It determines the coupling strength of a Goldstone boson to the axial vector current, cf. [10]

$$\left\langle \Omega \,\middle|\, J_L^{\mu,a}(0) \,\middle|\, \phi^b(p) \right\rangle = -ip_\mu \frac{F_0}{2}\delta_{ab}, \tag{2.38}$$

where we have made use of the expansion of the left handed axial current $J_L^{\mu,a}(x)$ up to order $\mathcal{O}\left(\phi^2\right)$ as shown in Ref. [10]

$$J_L^{\mu,a}(0) = i\frac{F_0^2}{4}\mathrm{tr}\left(\lambda_a \partial^\mu U^\dagger U\right) . \tag{2.39}$$

Its numerical value has to be determined via phenomenological input. It is given by $F_0 \approx 93\,\mathrm{MeV}$. Depending on the normalization of the Φ-field, the experimental value of the charged pion decay constant f_π differs by a factor of $\sqrt{2}$. In what follows we will work with $f_\pi = \sqrt{2}F_0 = 131.52\,\mathrm{MeV}$. The matrix $U(x)$ transforms under $R \in \mathrm{SU}(3)_R$ and $L \in \mathrm{SU}(3)_L$ like

$$U(x) \to U(x)' = RU(x)L^\dagger \tag{2.40}$$

The most general $\mathcal{L}_{\mathrm{eff}}$ at leading order with the minimal number of derivatives and a global $\mathrm{SU}(3)_L \times \mathrm{SU}(3)_R$ invariance is then given by

$$\mathcal{L}^{(2)} = \frac{F_0}{2}\mathrm{tr}(\partial_\mu U \partial^\mu U^\dagger) \tag{2.41}$$

In the physical Lagrangian density the quark masses explicitly break the global $\mathrm{SU}(3)_L \times \mathrm{SU}(3)_R$ symmetry, leading to massive Goldstone bosons. The quark mass matrix M is inserted into $\mathcal{L}_{\mathrm{eff}}$ via the assumption that it transforms like

$$M \to M' = RML^\dagger , \tag{2.42}$$

and expands the Lagrange density $\mathcal{L}(U, M)$. At leading order this results in

$$\mathcal{L}^{(2)} = \frac{F_0}{2}\mathrm{tr}(\partial_\mu U \partial^\mu U^\dagger) + \frac{F_0^2 B_0}{2}\mathrm{tr}(MU^\dagger + UM^\dagger) , \tag{2.43}$$

where the second term is invariant under Equation (2.42) and Equation (2.40). An important result of ChPT at leading order are the Gell-Mann-Oakes-Renner (GMOR) relations, as obtained from developing the second term in Equation (2.43) to second order in the momentum p and taking the isospin symmetric limit $m_u = m_d = m_\ell$, as done in Ref. [10]. Thus the masses of the Goldstone bosons π, K and η are obtained as

$$\begin{aligned} M_\pi^2 &= 2B_0 m_\ell \\ M_K^2 &= B_0(m_\ell + m_s) \\ M_\eta^2 &= \frac{2}{3}B_0(m_\ell + 2m_s) . \end{aligned} \tag{2.44}$$

The GMOR relations imply the Gell-Mann-Okubo formula

$$M_\eta^2 = \frac{1}{3}(4M_K^2 - M_\pi^2) \tag{2.45}$$

2.2.3 SCATTERING LENGTHS AT NEXT TO LEADING ORDER

The up and down quark form an isospin doublet $I = (1/2, -1/2)^T$, reflecting SU(2) flavor symmetry. This leads to the decomposition

$$\mathbf{2} \otimes \mathbf{2} = \mathbf{3} \oplus \mathbf{1}\,, \tag{2.46}$$

with total isospin $I = 1$ for the triplet and $I = 0$ for the singlet. The triplet states $\langle I, I_3 \rangle$ are the pions

$$\begin{pmatrix} \pi^+ \\ \pi^0 \\ \pi^- \end{pmatrix} = \begin{pmatrix} |1,+1\rangle \\ |1,0\rangle \\ |1,-1\rangle \end{pmatrix} \tag{2.47}$$

The strange quark has isospin $I = 0$ such that the Kaon's isospin configuration is completly determined by the light quark:

$$K^+ = \left|\frac{1}{2}, \frac{1}{2}\right\rangle\,, \quad K^- = \left|\frac{1}{2}, -\frac{1}{2}\right\rangle \tag{2.48}$$

$$K^0 = \left|\frac{1}{2}, -\frac{1}{2}\right\rangle\,, \quad \bar{K}^0 = \left|\frac{1}{2}, \frac{1}{2}\right\rangle\,. \tag{2.49}$$

The kinematics of interactions of 2 hadrons are described by the Mandelstam variables for four momenta p_i, $i = 1, \ldots, 4$

$$s = (p_1 + p_2)^2 = (p_3 + p_4)^2\,, \tag{2.50}$$

$$t = (p_2 - p_4)^2 = (p_1 - p_3)^2\,, \tag{2.51}$$

$$u = (p_2 - p_3)^2 = (p_1 - p_4)^2\,, \tag{2.52}$$

$$s + t + u = \sum_i p_i^2\,, \quad p_i^2 = m_i^2\,. \tag{2.53}$$

The elastic process $\pi^+ K^+ \to \pi^+ K^+$ has isospin $I_3 = 3/2$, wehreas, for instance, the isospin of π^- and K^+ can couple to $|I, I_3\rangle = |3/2, -1/2\rangle$ and $|I, I_3\rangle = |1/2, -1/2\rangle$, respectively. With the amplitudes of isospin $I_3 = 1$ and $I_3 = 0$ it is possible to construct amplitudes whose diagrams are even/odd under exchange of the Mandelstam variables s and u. In Ref. [12] these amplitudes have been defined as

$$\mathcal{T}^+ = \frac{1}{\sqrt{6}}\mathcal{T}^0(\pi\pi \to K\bar{K}) = \frac{1}{3}(\mathcal{T}^{1/2} + 2\mathcal{T}^{3/2})\,, \tag{2.54}$$

$$\mathcal{T}^- = \frac{1}{2}\mathcal{T}^1(\pi\pi \to K\bar{K}) = \frac{1}{3}(\mathcal{T}^{1/2} - \mathcal{T}^{3/2})\,. \tag{2.55}$$

With a Lagrangian density at given order it is possible to calculate T-matrix elements and scattering amplitudes $\mathcal{T}$ for specific scattering processes using the formulae in Section 2.1.3. The general procedure which also allows to calculate off-shell matrix elements has been developed in Ref. [13]. The starting point is the S-matrix element of the interaction depicted in Figure 2.1.

In our case it is given by

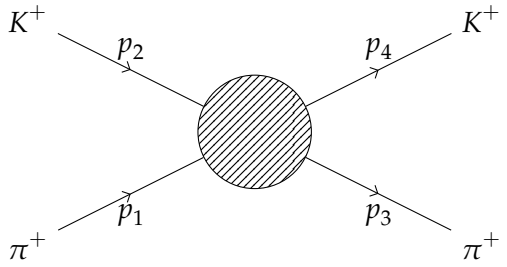

Figure 2.1: Diagram for elastig π-K scattering the arrows denote propagators with their respective 4 momenta p_i. The dashed shaded area depicts the elastic interaction of the two particles.

$$S_{fi} = \langle \pi^+(p_3)K^+(p_4), \text{out} \,|\, S \,|\, \pi^+(p_1)K^+(p_2), \text{in} \rangle \ . \tag{2.56}$$

Employing the LSZ reduction formula Equation (2.25) and the generating functional Equation (2.19) the scattering amplitude $\mathcal{T}^{3/2}$ for the process $\pi^+K^+ \to \pi^+K^+$ has been calculated in Ref. [14]. From the amplitude $\mathcal{T}^{3/2}$ the scattering length can be calculated using the effective range expansion as explained in section 2.1.3. In the basis of the even/odd amplitudes the scattering lengths are given at next-to-leading order in SU(3) ChPT in Equations (12) and (13) in Ref. [15]. For convenience they are listed in the appendix of Chapter 6. From these the isospin $1/2$ and isospin $3/2$ scattering lengths can be constructed equivalent to the combinations of the amplitudes, cf. Ref. [15]

$$a_0^{3/2} = a_0^+ - a_0^- \tag{2.57}$$

$$a_0^{1/2} = a_0^+ + 2a_0^- \tag{2.58}$$

Furthermore multiplying Equation (2.57) by the reduced mass of the π-K system following Equation (2.30) and plugging in the expressions for $a^\pm$ one arrives at

$$\begin{aligned} \mu_{\pi K}\, a_0^{3/2} = -0.0463(17) = \frac{\mu_{\pi K}^2}{4\pi f_\pi^2} \Bigg[& \frac{32 M_\pi M_K}{f_\pi^2} L_{\pi K}(\Lambda_\chi) - 1 - \frac{16 M_\pi^2}{f_\pi^2} L_5(\Lambda_\chi) \\ & + \frac{1}{16\pi^2 f_\pi^2} \chi_{\text{NLO}}^{3/2}(\Lambda_\chi, M_\pi, M_K, M_\eta) \Bigg] \ . \end{aligned} \tag{2.59}$$

In Equation (2.59) the LECs L_5 and $L_{\pi K}$ occur, with $L_{\pi K}$ being a combination of several other LECs:

$$L_{\pi K} = 2L_1 + 2L_2 + L_3 - 2L_4 - \frac{L_5}{2} + 2L_6 + L_8 \, . \tag{2.60}$$

The functions $\chi_{\text{NLO}^{3/2}}$ and $\chi_{\text{NLO}^{1/2}}$ summarize next to leading order corrections to the scattering length. They can be constructed from the corrections $\chi_{\text{NLO}}^{\pm}$ given in the appendix of the publication in Chapter 6. The LECs appearing in Equation (2.59) stem from the NLO form of the chiral Lagrangian density, stated in Ref. [14].

2.3 QCD AND SCATTERING IN HYPERCUBIC SPACE-TIME

In this section we reformulate the methods of Chapter 2 in a way such that numerical calculations become feasible. This non perturbative ab-initio approach to QCD is called lattice QCD (lQCD). The reformulation involves rotating the time dimension of Minkowski space to the imaginary axis. The Euclidean space time obtained by this rotation is then discretized into a four dimensional hypercube. We discuss the discretization With Lüscher's method, introduced in Section 2.3.2, we describe a way to access scattering observables in our lattice formulation. of the QCD gauge field first in Section 2.3.1. The discretization of fermions is presented in greater detail in Section 2.4.

2.3.1 THE LATTICE AS A REGULATOR

The oscillatory behavior of the weight function $\exp iS$ in the n-point function Equation (2.15), known as sign problem prevents a numerical evaluation. Another problem are ultraviolet divergences when trying to calculate the path integral. To address the oscillations we now change from Minkowski to Euclidean space-time by a Wick rotation of the time axis $t \to -i\tau$, τ is called Euclidean time. This change of variables transforms the metric of space-time from the Minkowski formulation ($g_{\mu\nu}$) to the Euclidean one ($\delta_{\mu\nu}$):

$$g_{\mu\nu} = \mathrm{diag}(1,-1,-1,-1) \overset{t\to -i\tau}{\longrightarrow} \delta_{\mu\nu} = \mathrm{diag}(-1,-1,-1,-1)\,. \tag{2.61}$$

The rotation transforms the oscillatory exponential in Equation (2.15) like

$$\exp\left(i\int \mathrm{d}t\mathcal{L}_M\right) \to \exp\left(-\int \mathrm{d}t\mathcal{L}_E\right)\,, \tag{2.62}$$

provided the Dirac matrices, cf. Appendix A.1, the integration measure and the spinor valued fields are adjusted accordingly. Thus the n-point function of Equation (2.15) is changed to

$$\langle\Omega|\mathcal{T}(\psi_1,\ldots,\psi_n)|\Omega\rangle = \frac{1}{Z}\int \mathrm{D}\psi\ \mathrm{D}\bar{\psi}\ \mathrm{D}A\ \psi_1\cdots\psi_n \exp(-S_E[\bar{\psi},\psi,A])\,, \tag{2.63}$$

with according changes in Z as well. The Euclidean action S_E now reads

$$S_E = S_F + S_G = \int\left(\mathrm{d}^4x \sum_f \bar{\psi}_f(x)(\gamma_\mu D^\mu + m_f)\psi_f(x) - \frac{1}{4}F^{a,\mu\nu}(x)F^a_{\mu\nu}(x)\right)\,. \tag{2.64}$$

Splitting up the action into a fermionic (S_F) and a gluonic (S_G) part carries over from Minkowski space to the Euclidean space. Since we inserted fermions as Grassmann numbers their calculus would complicate a numerical sampling of the path integral. A way forward is to perform the integrals over the Grassmann-valued fields $\bar{\psi}$ and ψ analytically. The Gaussian integral over Grassmann variables,

$$\int \mathrm{D}\bar{\psi}\ \mathrm{D}\psi\ \exp\left(-\int \mathrm{d}^4x\,\bar{\psi}D\psi\right) = \det D\,, \tag{2.65}$$

for an operator D, yields for the expectation value

$$\langle \mathcal{O} \rangle = \frac{1}{Z} \int \mathrm{D}A \, \det(D) \mathcal{O}(A, D^{-1}(A)) \exp(-S_G[A]) \,, \tag{2.66}$$

where D is the Dirac operator of the action S_E and D^{-1} denotes fermionic propagators. With $\mathcal{O}(A, D^{-1})$ we denote the time ordered product of fermionic fields $\psi(x)$ which depends on the fermionic propagator and the gauge field. The determinant can be incorporated into Equation (2.66), again, this time as an integral over complex numbers $\phi^\dagger$ and ϕ which obey bosonic statistics

$$\langle \mathcal{O} \rangle = \frac{1}{Z} \int \mathrm{D}\phi^\dagger \, \mathrm{D}\phi \, \mathrm{D}A \, \mathcal{O}(A, D^{-1}(A)) \exp(-S_G[A] - \phi^\dagger D^{-1} \phi) \,. \tag{2.67}$$

In this way we avoid the combinatorics stemming from the Grassmann integrals and still determine the fermionic determinant. What is left to do is to invert the Dirac Matrix D which still is demanding numerically but no principal problem. Thus we can now treat the exponential factor in Equation (2.63) as a probability distribution.

When evaluating the estimator Equation (2.67) we will encounter ultraviolet divergences in the integration over the different degrees of freedom (ψ) for high momenta. To cure this we introduce a sharp high momentum cutoff by discretizing Euclidean space-time on a 4 dimensional hypercubic lattice

$$\Lambda = \left\{ n = \nu a \;\middle|\; \nu \in \mathrm{Z}^4 \right\} . \tag{2.68}$$

In this discretization prescription a is the lattice spacing. We here assume equal spacing for the temporal and all spatial directions. For completness we denote the basis of Z^4 by

$$B = \{ \, \mu \mid \mu = 1, \ldots, 4 \, \} \, . \tag{2.69}$$

The discretization necessitates a reformulation of the Euclidean action S_E. For the time being we note that in principle any discretization of S_E is allowed as long as the continuum action is recovered when sending $a \to 0$.

The discretization of space-time given in Equation (2.68) entails a redefinition of the gauge field A_μ introduced in section 2.1. On the lattice the gauge field is represented by gauge link matrices $U_\mu(n)$ via

$$U_\mu(n) = \exp(iaA_\mu(n)) \,, \tag{2.70}$$

These SU(3) matrices are the elementary gauge transporters [8] on the lattice. A set of gauge link matrices

$$\mathrm{Y} = \left\{ U_\mu(n) \;\middle|\; n \in \Lambda \right\} \tag{2.71}$$

is called a gauge field configuration. The gauge links transport color charge along a given direction μ as depicted in fig. 2.2. At the lattice boundaries we adopt periodic boundary

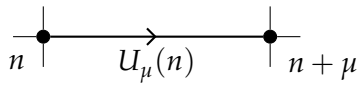

(a) Forward gauge transporter

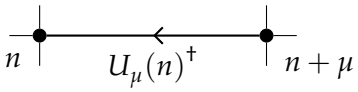

(b) Backward gauge transporter

Figure 2.2: Gauge links transporting color charge in the forward and backward direction, labeled $U_\mu(n)$ and $U_\mu^\dagger(n)$, respectively.

conditions for the gauge fields such that

$$U_\mu(n + L\mu_i) = U_\mu(n)\,. \tag{2.72}$$

In the context of the four-dimensional Euclidean lattice defined in Equation (2.68) the definition of the spinor quark fields change as well. Instead of being continuous spinors the quark fields are now defined on the lattice sites only. Furthermore each quark field carries indices for color charge, Dirac component and flavor. For legibility reasons we will suppress these indices in the following, assuming that they become clear from the context.

2.3.2 SCATTERING IN A FINITE BOX

When evaluated inside a box of finite volume L^3 the energy spectrum of hadrons becomes discrete. This is in contrast to the infinite volume case where the energy spectrum is continuous. In addition, if the box is small enough, it will squeeze the cloud of particles around the hadron stemming from its polarization of the vacuum. This squeezing causes a shift in the measured energies of the hadronic system. In the following we will concentrate on systems of two interacting mesons at rest inside such a finite box and impose periodic spatial boundary conditions, such that wave functions of particles read

$$\psi(x^0, \vec{x}) = \psi(x^0, \vec{x} + \vec{n}L)\,, \qquad \vec{n} \in \mathbb{Z}^3\,. \tag{2.73}$$

In Refs. [16, 17] M. Lüscher derived the volume dependence of these energy shifts and connected them to infinite volume scattering parameters, like the scattering length and the scattering phase shift. The total energy E of two interacting particles inside the box is given by their energies and a shift δE:

$$E = \sqrt{m_i^2 + \vec{p}_i^{\,2}} + \sqrt{m_j^2 + \vec{p}_j^{\,2}} + \delta E\,, \tag{2.74}$$

where the subscripts i and j denote different particles with masses m_i and m_j, respectively, $\vec{p}_{i,j}$ are the discrete three momenta of the particles

$$\vec{p}_i = \frac{2\pi}{L}\vec{n}_i\,, \vec{n}_i \in \mathbb{Z}^3 \tag{2.75}$$

and δE denotes the energy shift due to interactions of the particles involved. For completeness we note that here the center of mass of the system is at rest which implies $\vec{p}_i = -\vec{p}_j$ such that

the total energy is given by

$$E = m_1 + m_2 + \delta E \,. \tag{2.76}$$

Extensions to this formalism in direction to moving particles with different momenta have been developed in Ref. [18]. The energy shift happens for two reasons as detailed in Ref. [17]. On the one hand periodicity of the volume induces particle propagation around the lattice, an effect which decays exponentially with L [16]. On the other hand the direct interaction of the mesons at hand entails corrections to the free energy in powers of $1/L$.

To see this we sketch Lüscher's line of argument in the non-relativistic case and its generalization to the relativistic case of quantum field theory as was done in Ref. [17]. The argument is based on the Born series approximation [19] of the non-relativistic scattering amplitude of two particles with masses m_i and m_j and the expansion of the Eigenvalue of the full Hamiltonian of the system.

To this end let $H = H_0 + V$ denote the full Hamilton operator of the interacting meson system in a finite volume L^3. H_0 is the free Hamilton operator acting on the bosonic wave function $\psi(x, y)$ of the two particle system

$$H_0 = -\frac{\widetilde{\Delta}_x + \widetilde{\Delta}_y}{2m} \,. \tag{2.77}$$

The interaction potential V acts on $\psi(x, y)$ via

$$V\psi(x, y) = V(x - y)\psi(x, y) \,. \tag{2.78}$$

The eigenfunctions ψ_0 to H_0 can be labeled by the meson momenta $\vec{p}$ and $\vec{q}$

$$H_0 \left|\vec{p}, \vec{q}\right\rangle = E_0 \left|\vec{p}, \vec{q}\right\rangle \,. \tag{2.79}$$

The total energy E of the interacting system can be expanded in an infinite power series with parameters ϵ taken to $\epsilon = 1$ afterwards

$$E = E_0 + \epsilon r(E) \,, \tag{2.80}$$

$$E = \sum_{\nu=0}^{\infty} \epsilon^\nu E_\nu \,. \tag{2.81}$$

The function $r(z)$ is the non-degenerate perturbative expansion of the full Hamiltonian H in terms of the free two particle wave function and the poles at $z = E_0$ removed by

$$Q_0 = 1 - \left|\psi_0\right\rangle \left\langle\psi_0\right| \,. \tag{2.82}$$

It is then defined via

$$r(z) = \left\langle \psi_0 \middle| V \sum_{n=0}^{\infty} \left(\frac{Q_0}{z - H_0} V \right)^n \middle| \psi_0 \right\rangle \,. \tag{2.83}$$

Equation (2.81) leads to a recursion relation for E in ν. Setting $\epsilon = 1$ the recursion relation becomes

$$\begin{aligned} E &= E_0 + \sum_{\nu=1}^{\infty} E_\nu \\ E_\nu &= \sum_{j_1}^{\nu} \dots \sum_{j_\nu}^{\nu} C(j_1, \dots, j_\nu) r_{j_1} r_{j_2} \dots r_{j_\nu} , \end{aligned} \tag{2.84}$$

where the r_j are the summands of the Taylor series of $r(E_0)$

$$r_j = \frac{1}{j!} \frac{\partial^j}{\partial z^j} r(z)|_{z=E_0} \tag{2.85}$$

The first energy correction is given by $E_1 = r_0$ and is just $r(z)$ evaluated at $z = E_0$. Evaluation of the series in finite volume yields

$$\begin{aligned} r_0 = \frac{1}{2L^3} \Bigg(\hat{V}(0,0) + \sum_{n=1}^{\infty} \left(\frac{-1}{2L^3} \right)^n \sum_{k_1 \neq 0} \dots \sum_{k_n \neq 0} \\ \hat{V}(0,\vec{k_1}) \frac{m}{k_1^2} \hat{V}(k_1,k_2) \frac{m}{k_2^2} \dots \hat{V}(k_n,0) \Bigg) , \end{aligned} \tag{2.86}$$

where the sums do not include the poles of the intermediate propagators. The operator valued potential $\hat{V}$ is the Fourier transform of the spatial potential

$$\hat{V}(k_1,k_2) = \int \mathrm{d}^3 z \, \{ \exp[-i(k_1-k_2)z] + \exp[-i(k_2-k_1)z] \} \, V(z) . \tag{2.87}$$

This series resembles the Born series of the scattering amplitude Equation (2.26) with the difference of integrals being replaced by sums. In Ref. [17] a generalized momentum sum, accounting for the mismatch between the infinite volume integral and the 3-dimensional finite volume sum was derived. Sums of the type occuring in Equation (2.86) can be evaluated with the help of the generalized momentum sum [17] which yields an expansion of the energy corrections E_ν in powers of the potential V and inverse box size L^{-1}. So far the matching has been established for the quantum mechanical Born series only and a generalization to Quantum field theories is still to be made. M. Lüscher establishes this generalization in Ref. [17]. The main point here is the replacement of the Born series by a geometric series of the four point function using the Bethe-Salpeter kernel. Further differences are alleviated as well, cf. Ref [17].

Using the connection whose derivation was sketched above yields the relation between the energy shift, the elastic s-wave scattering length a_0 and the effective range r_f

$$\delta E_{12} = -\frac{2\pi a_0}{\mu_{12} L^3} \left(1 + c_1 \frac{a_0}{L} + c_2 \frac{a_0^2}{L^2} + c_3 \frac{a_0^3}{L^3} \right) - \frac{4\pi^2 a_0^3}{\mu_{12} L^6} r_f + \mathcal{O}(L^{-7}) . \tag{2.88}$$

The coefficients $c_1, \dots, c_3$ stem from the numerical evaluation of Lüscher's Zeta function, given

in Ref. [17] as

$$c_1 = -2.837297\,, \quad c_2 = 6.375183\,, \quad c_3 = -8.311951\,. \tag{2.89}$$

2.4 DISCRETIZATION SCHEMES OF QCD

We still need to specify a discretization scheme for the fermionic and gluonic actions S_F and S_G, respectively. To this end we here discuss different discretizations of the fermionic part of Equation (2.64), namely Wilson fermions, Wilson twisted mass fermions and Osterwalder-Seiler fermions. For the gauge part of Equation (2.64) we will focus on the Iwasaki gauge action as introduced in Ref. [20].

2.4.1 WILSON QUARKS

One of many discretization schemes is to discretize fermions like Wilson proposed in Ref. []. The Wilson Dirac operator reads

$$D_W = \sum_{\mu=0}^{3} \frac{1}{2} \left(\gamma_\mu (\nabla_\mu + \nabla_\mu^*) - ar \nabla_\mu \nabla_\mu^* \right) , \tag{2.90}$$

with the gauge covariant lattice derivative for one flavor f

$$\nabla_\mu \psi_f(x) = \frac{1}{a} \left(U_\mu(x) \psi_f(x + a\hat{\mu}) - \psi_f(x) \right) \tag{2.91}$$

$$\nabla_\mu^* \psi_f(x) = \frac{1}{a} \left(\psi_f(x) - U_\mu(x - a\hat{\mu}) \psi_f(x - a\hat{\mu}) \right) . \tag{2.92}$$

The matrices $U_\mu(x)$ are the link variables introduced in Section 2.3.1. In Equation (2.90) the term proportional to a is called Wilson term. In the current work the Wilson parameter r is set to $r = 1$. The Wilson term decouples excess fermions, stemming from the discretization procedure of the naive Dirac propagator in momentum space, by assigning them a heavier effective mass, as shown in detail in Ref. [8]. The corresponding action now reads

$$S_F^W = \sum_{x \in \Lambda} \bar{\psi}(x) (D_W + m_0) \psi(x) . \tag{2.93}$$

Apart from removing doublers from the eigenvalue spectrum of the Dirac propagator this action respects parity, charge conjugation unitarity and has an exact $U(N_f)$ symmetry, with N_f being the number of quark flavors under consideration. In addition it displays γ_5-hermiticity:

$$\gamma_5 D_W^\dagger \gamma_5 = D_W . \tag{2.94}$$

Nevertheless there are also a few drawbacks. At finite lattice spacing the presence of the Wilson term breaks all axial symmetries, for example chiral symmetry. Furthermore the bare mass m_0 receives a linearly divergent contribution via $m_{\text{crit}} \propto 1/a$. Thus the renormalized quark mass m_R is given by

$$m_R = Z_m (m_0 - m_{\text{crit}}) , \tag{2.95}$$

with Z_m being a multiplicative renormalization constant. As a last disadvantage we mention that discretization effects with the Wilson Fermion action are of order $\mathcal{O}(a)$.

The additive renormalization of the quark mass can pose a problem in numerical simulations because typically a physical quark mass corresponds to a negative bare quark mass m_0. A missing lower bound on the eigenvalue spectrum of the bare quark mass can complicate things further, as shown in Refs. [21, 22]. To see this we define the hermitian operator

$$Q = \gamma_5(D_W + m_0)\,,\; Q = Q^\dagger \tag{2.96}$$

and its eigenfunctions and eigenvalues via

$$Q\phi_i(x) = \lambda_i\phi_i(x)\,. \tag{2.97}$$

Now we evaluate a pseudoscalar correlation function [21, 22] with the help of Equation (2.66):

$$\begin{aligned} C_{\mathrm{PS}}(x-y) &= \left\langle \bar{\psi}(x)\gamma_5\frac{\tau_1}{2}\psi(x)\bar{\psi}(y)\gamma_5\frac{\tau_1}{2}\psi(y)\right\rangle \\ &= \frac{1}{2Z}\int \mathrm{D}U\ \det(Q^2)\mathrm{tr}(Q^{-1}(y,x)Q^{-1}(x,y))\exp(-S_G[U]) \\ &= \frac{1}{2Z}\int \mathrm{D}U\ \prod_i \lambda_i^2 \sum_{k,\ell}\frac{1}{\lambda_k\lambda_\ell}\phi_k(x)\phi_k^*(x)\phi_\ell(y)\phi_\ell^*(y)\,. \end{aligned} \tag{2.98}$$

Gauge configurations with small eigenvalues λ_i are called "exceptional configurations". In nowadays numerical simulations the determinant in Equation (2.98) cancels potentially small eigenvalues stemming from the trace over the quark propagators and thus avoids the problem of exceptional configurations. Nevertheless in earlier days it was common to simulate in the quenched approximation, i.e. $\det(Q^2) = 1$, in order to save computing time. There exceptional configurations posed a severe problem in the evaluation of correlation functions.

2.4.2 TWISTED MASS FORMALISM

A cure to exceptional configurations came in form of the twisted mass (tm) formulation of lQCD, as we will describe in the following. Nowadays twisted mass fermions mainly are used because they automatically improve a class of quantities up to order $\mathcal{O}(a)$ in lattice artifacts such that the remaining lattice artifacts of these operators are of order $\mathcal{O}\left(a^2\right)$ or higher.

LIGHT SECTOR

In the continuum the twisted mass action $S_{F,\mathrm{tm}}$ for a mass degenerate doublet of quarks $\chi_\ell = (\chi_u, \chi_d)^T$ is given by

$$S_{F,\mathrm{tm}}^{\mathrm{cont}} = \int \mathrm{d}^4x\,\bar{\chi}_\ell(x)(\not{D} + m_q + i\mu_q\gamma_5\tau_3)\chi_\ell(x)\,, \tag{2.99}$$

where μ_q is the bare twisted mass and τ_3 the third Pauli matrix acting in flavor space. The standard and twisted mass continuum action can be related via a chiral transformation of the

quark fields

$$\bar{\psi}(x) = \bar{\chi}(x)R(\omega)\,, \quad \psi(x) = R(\omega)\chi(x)\,, \quad R(\omega) = \exp\left(i\omega\gamma_5\frac{\tau_3}{2}\right)\,, \tag{2.100}$$

the fermionic continuum action Equation (2.14) is recovered, provided

$$\tan\omega = \frac{\mu_q}{m_q}\,, \tag{2.101}$$

holds. The mass then is given by

$$M = \sqrt{m_q^2 + \mu_q^2}\,. \tag{2.102}$$

In the continuum case twisted QCD and standard QCD are exactly related by the chiral transformation Equation (2.100) and all symmetries of QCD carry over. This relation can be seen by replacing the mass terms of Equation (2.99) as

$$m_q + i\mu_q\gamma_5\tau_3 = M\left(\cos(\omega) + i\sin(\omega)\gamma_5\tau_3\right) = M\exp(i\gamma_5\omega\tau_3)\,, \tag{2.103}$$

and using the chiral rotations of Equation (2.100) to obtain the continuum action of QCD. As a consequence of this exact relation also correlation functions of standard QCD and twisted mass QCD are related via the same transformation. The currents in the twisted basis are obtained by transforming the multiplets in Equation (2.13) to the twisted basis using Equation (2.100). Following Ref. [21], these relations read

$$\begin{aligned}
A_1'^{\mu} &= \cos(\alpha)A_1^{\mu} + \sin(\alpha)V_2^{\mu}\,, & V_1'^{\mu} &= \cos(\alpha)V_1^{\mu} + \sin(\alpha)A_2^{\mu}\,,\\
A_2'^{\mu} &= \cos(\alpha)A_2^{\mu} - \sin(\alpha)V_1^{\mu}\,, & V_2'^{\mu} &= \cos(\alpha)V_2^{\mu} - \sin(\alpha)A_1^{\mu}\,,\\
A_3'^{\mu} &= A_3^{\mu}\,, & V_3'^{\mu} &= V_3^{\mu}\,,\\
P_a' &= P_a\,, (a = 1,2)\,, & S_0' &= \cos(\alpha)S_0 + 2iP_3\,,\\
P_3' &= \cos(\alpha)P_3 + is\frac{1}{2}S_0\,.
\end{aligned} \tag{2.104, 2.105}$$

When regularizing twisted mass QCD with Wilson quarks the action reads

$$S_{F,\mathrm{tm}} = \sum_x \bar{\chi}(x)(D_W + m_0 + i\mu_q\gamma_5\tau_3)\chi(x)\,, \tag{2.106}$$

and the axial symmetry of Equation (2.99) is broken by the Wilson term. The pure Wilson action and the twisted mass Wilson action only coincide again in the continuum limit.

Owing to the flavor structure of the twisted mass term the Dirac operator changes flavor on application of γ_5 from left and right:

$$\begin{aligned}
D_d &= \gamma_5 D_u^{\dagger}\gamma_5\\
D_u &= \gamma_5 D_d^{\dagger}\gamma_5\,.
\end{aligned} \tag{2.107}$$

Here the subscripts u and d denote the upper and lower part of the twisted mass Dirac operator, respectively.

With the twisted mass Dirac operator

$$Q + i\mu_q \gamma_5 \tau_3 \,, \tag{2.108}$$

the 2 flavor determinant now reads

$$\det(Q + i\mu_q \gamma_5 \tau_3) = \det \begin{pmatrix} Q + i\mu_q & 0 \\ 0 & Q - i\mu_q \end{pmatrix} = \det(Q^2 + \mu_q^2) > 0 \,. \tag{2.109}$$

Thus the twisted mass term ensures a positive real determinant, necessary for calculating quark propagators, provided $\mu_q \neq 0$.

AUTOMATIC ORDER $\mathcal{O}(a)$ IMPROVEMENT

Observables evaluated with standard Wilson fermions have contributions which are linear in the lattice spacing. These contributions are called order $\mathcal{O}(a)$ lattice artifacts and necessitate a continuum extrapolation of these observables. Using Symanzik improvement, as described in Ref. [21] and references therein, the Sheikoleslami-Wohlert counterterm added to the Wilson action cancels order $\mathcal{O}(a)$ artifacts of the spectrum of particle energies. This is in contrast to the case when matrix elements are the observables of interest. Then for each operator entering the observable one needs to separately tune one set of counterterms for each observable.

In the case of twisted mass fermions at "full" or "maximal" twist it can be shown that all parity even operators possess lattice artifacts which are at least of order $\mathcal{O}(a^2)$.

Tuning the action to maximal twist amounts to setting the twist angle to $\omega = \pi/2$, as described in detail in Ref. [22]. This can be achieved by setting the renormalized quark mass m_R to zero as can be seen from

$$\tan\omega = \frac{\mu_R}{m_R} \,. \tag{2.110}$$

Following the argumentation in Ref. [22], since m_R is given by Equation (2.95) it is enough to set the untwisted mass m_0 to its critical value $m_0 = m_{\text{crit}}$. One possible way to achieve this is to tune the untwisted mass to the value where the PCAC mass m_{PCAC} vanishes

$$m_{\text{PCAC}} = \frac{\langle \partial_0 A_0^a(x) P^a(0) \rangle}{2 \langle P^a(x) P^a(0) \rangle} = \frac{Z_P}{Z_A} m_R \,, \quad a = 1,2 \,. \tag{2.111}$$

Here P^a and A_0^a refer to the multiplet currents of Equation (2.105) and Z_P and Z_A are the pseudoscalar and axial vector renormalization constants. Note that no renormalization constants need to be determined when tuning to m_{crit}.

HEAVY SECTOR

So far we only considered one doublet of mass degenerate light quarks. Compared to the second generation of quarks (s, c), treating the first generation as mass degenerate is a valid approximation because the masses of the u and d quark are much smaller compared to the masses of s and c quark. Too maintain the structure of the fermionic determinant additional flavors can only be inserted in doublets. Mass non degenerate quarks, like the charm and strange quarks can be introduced in a twisted mass way by using the action

$$S_h = \sum_x \bar{\chi}_h(x)(D_W + m_q + i\mu_\sigma\gamma_5\tau_1 + \mu_\delta\tau_3)\chi_h(x)\,, \tag{2.112}$$

where $\chi_h(x)$ now describes a mass non-degenerate doublet of quarks $\chi_h = (\chi_c, \chi_s)^T$. The choice of Pauli matrices in Equation (2.112) is such that the desirable properties already discussed in the light case carry over completely at maximal twist. Calculating the fermionic determinant analogous to the case of the light sector yields

$$\det(Q + i\mu_\sigma\gamma_5\tau_1 + \mu_\delta\tau_3) = \det\begin{pmatrix} Q+\mu_\sigma & i\mu_\sigma\gamma_5 \\ i\mu_\sigma\gamma_5 & Q-\mu_\sigma \end{pmatrix} = \det(Q^2 - \mu_\delta^2 + \mu_\sigma^2)\,. \tag{2.113}$$

Thus the fermionic determinant of the non-degenerate doublet stays positive provided

$$\sqrt{m_q^2 + \mu_\sigma^2} \;>\; \mu_\delta$$

holds. The connection between the chiral and the physical basis for the heavy quark doublet reads

$$\bar{\psi}_h(x) = \bar{\chi}_h(x)R_h(\omega_h)\,, \quad \psi_h(x) = R_h(\omega_h)\chi_h(x)\,, \quad R_h(\omega_h) = \exp\left(i\omega_h\gamma_5\frac{\tau_1}{2}\right)\,, \tag{2.114}$$

where the doublets $\bar{\chi}_h$ and χ_h are in the twisted basis and $\bar{\psi}_h$ and ψ_h are the corresponding doublets in the physical basis. The difference to Equation (2.100) lies in the choice of τ_1, as opposed to τ_3, and a different twist angle ω_h, instead of ω. Analogously to the light sector the bare quark masses of the strange quark and the charm quark, m_s and m_c, respectively, are now given by

$$m_{c/s} = M \pm \mu_\delta\,, \tag{2.115}$$

with M being the polar mass

$$M = \sqrt{m_q^2 + \mu_\sigma^2}\,. \tag{2.116}$$

Again in the case of full twist the bare quark masses are completely determined by the parameters μ_σ and μ_δ, provided m_{crit} is tuned to cancel m_q. As has been worked out in Ref. [23], the heavy quark masses are then renormalized with the Pseudoscalar and Scalar renormalization

constants, Z_P and Z_S, respectively,

$$m^R_{c/s} = \frac{1}{Z_P}\left(\mu_\sigma \pm \frac{Z_P}{Z_S}\mu_\delta\right) . \tag{2.117}$$

When a non-degenerate doublet is introduced into the action operators with strange and charm quarks receive flavor mixing contributions. This happens because at finite lattice spacing with Wilson twisted mass (Wtm) non-degenerate quarks K and D meson states do exist in a mixed flavor-parity sector ($s/c,-/+$) as opposed to the continuum case. As a consequence K and D meson states mix during the calculation of correlation functions. A more detailed discussion of this issue and possible solutions can be found in Ref. [24].

2.4.3 OSTERWALDER-SEILER QUARKS

The problem of flavor and parity mixing can be solved by regularizing the non-degenerate valence sector in a different way than the sea sector. Such a mixed action setup can be realized with so called Osterwalder-Seiler quarks. Thus we are able to implement valence strange quarks by using a different Dirac operator of the form

$$D_s = D_\mathrm{W} + m_0 + i\mu_s\gamma_5\tau_3 , \tag{2.118}$$

with an additional degenerate doublet of quarks $q_s = (q_s^+, q_s^-)^T$. Automatic order $\mathcal{O}(a)$ improvement only stays valid at maximal twist. Therefore the additional flavor is inserted as a degenerate doublet. Thus at maximal twist the upper and lower quark mass are of the same modulus, $|\mu_s|$, but possess opposite signs. As a consequence lattice quantities using different components of the doublet q_s will differ by lattice artifacts of order $\mathcal{O}(a^2)$ and only coincide in the continuum. This approach avoids complications stemming from the mass splitting term in Equation (2.112). In addition it renders the valence strange quark mass tunable by allowing for different bare quark parameters μ_s. Furthermore, as was shown in Ref. [23] automatic order $\mathcal{O}(a)$ improvement stays valid when taking m_0 to be the same m_crit as for the light sector. Nevertheless all these nice features come at a price: The usage of OS-valence quarks explicitly breaks unitarity between the sea and the valence quarks such that one would have to take into account the mismatching between valence and sea strange quark mass when interpolating in μ_s.

Realizing the heavy sector via OS-quarks would introduce the unphysical doublet members already at the level of the gauge configuration. As a consequence the resulting fermion determinant would need to be treated in order to cancel the unwanted contributions.

2.4.4 GAUGE ACTION

The gauge action S_G used in the simulations for this work is the Iwasaki gauge action, introduced in [20]. Because the generation of gauge configurations is not in the focus of this thesis we will only briefly state the mathematical form of the gauge action and discuss the choice of

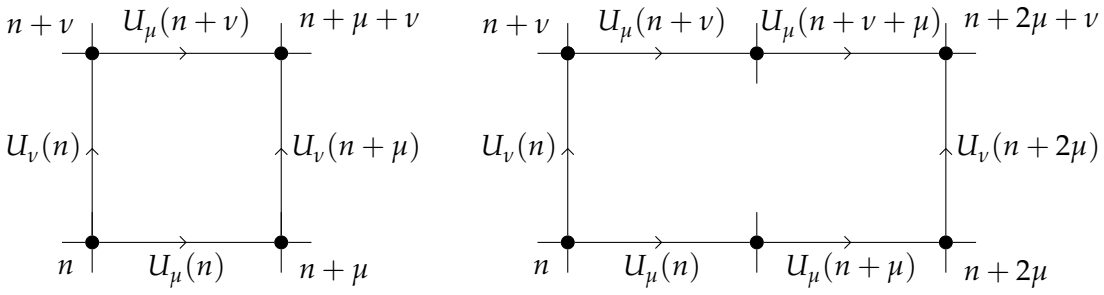

(a) Gauge link plaquette $U_{\mu\nu}^{1\times1}$ (b) Wilson loop $U_{\mu\nu}^{1\times2}$

Figure 2.3: The closed path objects $U_{\mu\nu}^{m\times n}$ entering the Iwasaki gauge action.

parameters. The Iwasaki gauge action reads

$$S_G(U) = \frac{\beta}{6}\sum_n\sum_{\mu\neq\nu}\left\{b_0\left[\mathbb{1}-\mathrm{Re\,tr}\left(U_{\mu\nu}^{1\times1}(n)\right)\right]+2b_1\left[\mathbb{1}-\mathrm{Re\,tr}\left(U_{\mu\nu}^{1\times2}(n)\right)\right]\right\}, \tag{2.119}$$
$$\beta = \frac{6}{g^2},$$

where β is the inverse bare coupling constant of the theory. The quantities inside the traces are the gauge invariant plaquette and the 1×2 Wilson loop depicted in Figure 2.3

Those quantities are 2 dimensional gauge invariant products of link variables along closed paths $\mathscr{L}(m,n)$ with $m\,,n\in\mathbb{Z}$ labeling the extension to two dimensions.

$$U_{\mu\nu}^{m\times n}(n) = \prod_{(x,\eta)\in\mathscr{L}(m,n)} U_\eta(x)\,. \tag{2.120}$$

With the choices $b_1 = 0\,, b_0 = 2$ Wilson's gauge action, cf. Ref. [25], is recovered. In the continuum limit $a\to0$ both formulations of the gauge action transform into the continuum gauge action. In Ref. [26] it has been shown that simulations employing Wilson's gauge action exhibit a first order phase transition for certain values of the gauge coupling parameter β and the critical mass m_{crit}. To ameliorate this behavior the parameters values

$$b_0 = 1-8b_1, \quad b_1 = -0.331\,, \tag{2.121}$$

smooth the behavior of the phase transition, as was shown in Ref. [27]

CHAPTER 3

CORRELATION FUNCTIONS AND HADRON SPECTROSCOPY

The overall goal of any lattice simulation is the numerical evaluation of matrix elements or n-point functions as introduced in Section 2.1.2. Ultimately, we are interested in the scattering length a_0 and the effective range r_f of the K^+-K^+ and the π^+-K^+ system. As shown in Section 2.3.2, these two physical quantities are connected to the finite volume energy of the system. In the following we present the formalism how to obtain these energy values from simulated lattice data.

3.1 CALCULATING CORRELATION FUNCTIONS

Quantum field theoretical correlation functions are composed of creation and annihilation operators. The correlation we are interested in is the excitation of a two meson system from the vacuum at time t and its annihilation at some time t'. For mesons, made out of one quark and one antiquark, the creation/annihilation operators are quark bilinears. In the context of lattice QCD they are also referred to as interpolating fields. The creation operators of the pion ($\mathcal{O}^\dagger_\pi$) and the kaon ($\mathcal{O}^\dagger_K$), for instance, read

$$\mathcal{O}^\dagger_{p,\pi}(t) = \sum_x e^{ipx} \bar{d}(x,t) i\gamma_5 u(x,t)\,, \tag{3.1}$$

$$\mathcal{O}^\dagger_{p,K}(t) = \sum_x e^{ipx} \bar{s}^+(x,t) i\gamma_5 u(x,t)\,, \tag{3.2}$$

where we have made the assumption of choosing the OS strange quark with positive sign in its mass value and introduced the projection to a possible momentum p via the discretized Fourier transform. The corresponding annihilation operators are obtained by adjoining the creation operators. In the remainder we restrict ourselves to the case of vanishing momentum $p = 0$. A

correlation function creating a pion at euclidean time t' and annihilating it at t can be written as

$$\begin{aligned} C_\pi(t-t') &= \left\langle \mathcal{O}_\pi(t)\mathcal{O}_\pi^\dagger(t') \right\rangle \\ &= \left\langle \bar{u}(x,t)i\gamma_5 d(x,t)\bar{d}(x',t')i\gamma_5 u(x',t') \right\rangle \\ &= -\mathrm{tr}\left(i\gamma_5 D_u^{-1}(x|x')i\gamma_5 D_d^{-1}(x'|x) \right) . \end{aligned} \tag{3.3}$$

Here we have Wick-contracted the correlation function to arrive at a trace involving color and 3-dimensional space. The objects $D_f^{-1}(x|x')$ are the Dirac propagators for quark flavor f, encoding the propagation of a quark of flavor f from x' to x.

3.1.1 CORRELATOR DIAGRAMS

Wick contractions like Equation (3.3) can also be represented diagrammatically. The last line in Equation (3.3) features one Dirac propagator for each of the quark flavors. A graphical representation of $C_\pi(t-t')$ is given in Figure 3.1. The quarks propagate from the π^+ vertices (white circle) at x' to x. Using Equation (2.107) the d quark propagator is calculated from the u quark propagator. When regarding two meson systems the decomposition into diagrams gets

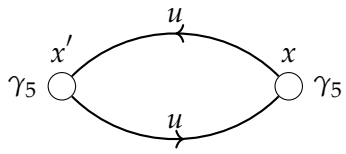

Figure 3.1: Connected diagram of $C_\pi(t-t')$. White circles denote the pion at initial (left) and final time (right). In addition the vertex factor from the meson interpolator is given. Quark propagation occurs along the lines.

more involved. For the case of maximal isospin scattering the Correlation function decomposes into a direct part and a cross correlated part, as depicted in Figure 3.2, for the case of π^+-K^+-scattering. Time runs from left to right for each diagram. The gray circles denote a K^+ whereas the white circles depict the π^+ with the according vertex factors stemming from the interpolators. The propagators resulting from the Wick contraction are shown as labeled arrows. The Correlation function of a single Kaon is constructed in full analogy to the single pion case. To calculate the full correlation functions each diagram first gets calculated individually. This process is called contraction. After the contractions have been done the full diagram is calculated according to the decomposition just discussed.

In the case of K^+-K^+-scattering the same types of diagrams come into play. The only differences are the flavor structure at the vertices and the fact that two strange quark propagators are needed compared to only one in the case of π^+-K^+.

As a remark we note that sometimes traces over a single quark flavor can occur, as for instance when doing Wick contractions of the π^0. Because of a worse signal-to-noise ratio compared to fully connected contributions, their analysis is more involved. These disconnected contributions do not occur for the interpolators used in this work.

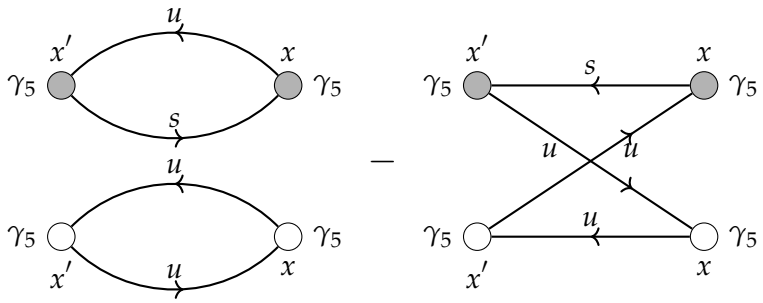

Figure 3.2: Diagram decomposition of $C_{\pi K}(t - t')$ into a direct and a cross correlated part. Kaons are denoted as gray circles, pions as white circles. In addition the arrows depict the quark propagation for each diagram.

3.2 TRANSFER MATRIX FORMALISM

In Section 2.1.2 we have seen that correlation functions can be expressed in the path integral formalism. Another possibility is the formulation in terms of the spectral decomposition. In the Heisenberg picture the euclidean correlation function for two interpolating operators $\mathcal{O}$ is given by

$$\left\langle \mathcal{O}(t_f, x_f)\mathcal{O}^\dagger(t_i, x_i)\right\rangle_T = \lim_{T\to\infty}\frac{1}{Z}\mathrm{tr}\left(e^{-\left(T-\left(t_f-t_i\right)\right)\widehat{H}}\mathcal{O}^\dagger(x_f)e^{-\left(t_f-t_i\right)\widehat{H}}\mathcal{O}(x_i)\right), \tag{3.4}$$

with normalization

$$Z = \mathrm{tr}\left(e^{-T\widehat{H}}\right). \tag{3.5}$$

In this notation the trace is the trace of a statistical density operator and is meant as a sum over all possible eigenstates of $\widehat{H}$. The operator $\widehat{H}$ is the Hamilton operator of the interaction in the Heisenberg picture, the subscripts i and f denote initial and final state, respectively and T is the total time extent of the lattice. Using completeness and restricting oneself to finite times T one obtains

$$\langle \mathcal{O}\left(t_f, x_f\right)\mathcal{O}^\dagger(t_i, x_i)\rangle_T = \frac{1}{Z}\sum_{m,n} e^{-\left(T-\left(t_f-t_i\right)\right)E_m}\langle m|\mathcal{O}(x_f)|n\rangle\, e^{-\left(t_f-t_i\right)E_n}\langle n|\mathcal{O}(x_i)|m\rangle, \tag{3.6}$$

where $E_{m,n}$ are eigenstate energies of $\hat{H}$. When taking the limit $T \to \infty$ only terms with $E_m = 0$ survive and one arrives at

$$\left\langle \mathcal{O}(t_f, x_f)\mathcal{O}^\dagger(t_i, x_i)\right\rangle = \frac{1}{Z}\sum_n \langle\Omega|\mathcal{O}(x_f)|n\rangle\langle n|\mathcal{O}(x_i)|\Omega\rangle\, e^{-tE_n}. \tag{3.7}$$

For finite times T higher energy states contribute to the spectral decomposition Equation (3.6). These contributions are larger at early times t and wash out towards later times. This happens because the interpolators $\mathcal{O}$ do not couple only to their continuum counterparts but also to all lattice interpolators with the same quantum numbers. To extract the ground state energy

nevertheless, one usually inspects the data for $C(t)$ at late enough times. In the course of this inspection it is useful to define the effective mass $m_{\text{eff}}(t)$ as

$$m_{\text{eff}}(t+0.5) = \ln \frac{C(t)}{C(t+1)} \,. \tag{3.8}$$

The region where excited states have decayed away sufficiently can then be identified as a plateau in a plot of m_{eff} vs. t' and the ground state energy of the correlation function can then be extracted via a fit of the form

$$C(t) \propto A_0^2 \left(e^{-tE_0} \pm e^{-(T-t)E_0} \right) \tag{3.9}$$

to the data. The ground state of a two point correlation function then shows a cosh-like $(+)$ or sinh-like $(-)$ behavior.

3.3 THERMAL POLLUTION OF CORRELATION FUNCTIONS

As mentioned in Section 3.2 the interpolators $\mathcal{O}$ overlap with all states $\langle n|$ having the same quantum numbers as the state one is interested in. In the case of more than two mesons appearing in the correlation function states with the same quantum numbers as the ground state affect the late time behavior of correlation functions. In effective mass plots states like this usually show up as downward bends towards late times. These states can be constant in time or time dependent. Both kind of states are discussed for the case of two pions at isospin $I_3 = 2$ and nonzero momentum in Ref. [28]. In the following we will present examples for both kinds of pollution and possible means to overcome these obstacles.

3.3.1 TIME INDEPENDENT POLLUTION

An example of a thermal state shows up when inspecting the 4-point correlation function of two kaons with $t' = 0$

$$\begin{aligned} C_{KK}(t) &= \left\langle O_{KK}(t) O_{KK}^{\dagger}(0) \right\rangle \,, \\ \mathcal{O}_{KK}(t) &= \sum_{x,x'} \bar{s}^{+}(x,t)\, i\gamma_5\, d(x,t)\; \bar{s}^{+}(x',t)\, i\gamma_5\, d(x',t) \,. \end{aligned} \tag{3.10}$$

The spectral decomposition at finite T of this correlation function reads (cf. Equation (3.6))

$$C_{KK}(t) = \frac{1}{Z} \sum_{n,m} e^{-TE_m} e^{-t(E_n - E_m)} \, \langle m|\mathcal{O}_{KK}|n\rangle \, \langle n|\mathcal{O}_{KK}^{\dagger}|m\rangle \,. \tag{3.11}$$

The ground state we are interested in shows up when $E_n = E_{KK}$ and $E_m = 0$, which contributes

$$C_{KK}^{0}(t) \propto e^{-t(E_{KK})} \, \langle \Omega|\mathcal{O}_{KK}|KK\rangle \, \langle KK|\mathcal{O}_{KK}^{\dagger}|\Omega\rangle \tag{3.12}$$

to Equation (3.11). Another contribution that is also possible is

$$C^1_{KK}(t) \propto e^{-TE_K} \langle \bar{K}|\mathcal{O}_{KK}|K\rangle \langle \bar{K}|\mathcal{O}^\dagger_{KK}|K\rangle \,, \tag{3.13}$$

where the time dependent exponential cancels due to the energy difference $\Delta E = E_m - E_n$, when taking $m = n = K$. One way to remove such states is to shift the correlation function by a certain amount of time slices. Redefining $\tilde{t} = t - t'$ and defining $\delta t > 0$ a new correlation function $C'_{KK}(t)$ is obtained by calculating

$$C'_{KK}(\tilde{t}) = C_{KK}(t) - C_{KK}(t + \delta t)\,, \tag{3.14}$$

which cancels the thermal contribution Equation (3.13) exactly and modifies the amplitudes of Equation (3.12) by a constant factor.

For the present work we take a different approach, first presented in Ref. [29] and also used in Ref. [30]. Instead of calculating the total energy E_{KK} from Equation (3.14) it is possible to obtain the energy shift δE directly from the ratio of shifted correlation functions

$$R(t + a/2) = \frac{C_{KK}(t) - C_{KK}(t+1)}{C^2_K(t) - C^2_K(t+1)}\,, \tag{3.15}$$

which behaves like

$$\begin{aligned} R(t + a/2) &= A\left(\cosh\left(\delta E_{KK} t'\right) + \sinh\left(\delta E_{KK} t'\right) \coth\left(2E_K t'\right)\right)\,, \\ t' &= t + a/2 - T/2\,. \end{aligned} \tag{3.16}$$

Thus instead of determining δE from separate fits to $C_{KK}(t)$ and $C_K(T)$ we can directly fit Equation (3.16) to the ratio Equation (3.15) to circumvent the pollution and obtain δE.

3.3.2 TIME DEPENDENT POLLUTION

In the case of multi particle operators with different single meson operators the pollution gets time dependent which is demonstrated in the following for the interpolator $\mathcal{O}_{\pi K}(t)$:

$$\mathcal{O}_{\pi K}(t) \;=\; \sum_{x,x} \bar{u}(x,t)\, i\gamma_5\, d(x,t)\; \bar{s}^+(x,t)\, i\gamma_5\, d(x,t)\,. \tag{3.17}$$

In the spectral decomposition Equation (3.6) the main contribution is given by the states $\langle n| = \langle \pi K|$ and $\langle m| = \langle \Omega|$ and vice versa. Another contribution with non-zero overlap to the composite particle operator comes from setting $\langle n| = \langle \pi|$ and $\langle m| = \langle K|$ and vice versa. The correlation function

$$C_{\pi K}(t) = \left\langle \mathcal{O}_{\pi K}(t) \mathcal{O}^\dagger_{\pi K}(0) \right\rangle \tag{3.18}$$

then has contributions

$$C^0_{\pi K}(t) \propto \left|\left\langle \pi K \left| \mathcal{O}^\dagger \right| \Omega \right\rangle\right|^2 \left(e^{-E_{\pi K}(T-t)} + e^{-E_{\pi K} t}\right) \tag{3.19}$$

$$C^1_{\pi K}(t) \propto \left|\langle \pi | \mathcal{O}^\dagger | K \rangle\right|^2 \left(e^{-E_\pi t} e^{-E_K (T-t)} + e^{-E_K t} e^{-E_\pi (T-t)}\right) . \tag{3.20}$$

In what follows we will neglect other contributions to the spectral decomposition and work with the sum

$$\begin{aligned} C_{\pi K}(t) &\approx C^0_{\pi K}(t) + C^1_{\pi K}(t) \\ &= A_0^2 \left(e^{E_{\pi K}(t-T/2)} + e^{-E_{\pi K}(t-T/2)}\right) + A_1^2 \left(e^{(E_K - E_\pi)t} e^{-E_K T} + e^{-(E_K - E_\pi)t} e^{-E_\pi T}\right) , \end{aligned} \tag{3.21}$$

with the amplitudes

$$A_0^2 = \frac{1}{Z} \left|\left\langle \pi K \left| \mathcal{O}^\dagger \right| \Omega \right\rangle\right|^2 e^{-E_{\pi K} T/2} , \quad A_1^2 = \frac{1}{Z} \left|\left\langle \pi \left| \mathcal{O}^\dagger \right| K \right\rangle\right|^2 . \tag{3.22}$$

Apart from time independent states in the second term, Equation (3.21) features terms which are time dependent. These time dependent contributions cannot be removed by only shifting the correlation function about a certain amount of timeslices. To extract the wanted contributions $E_{\pi K}$ we may use an ansatz described in Ref. [28]. We first diminish the influence of the pollution by weighting the correlation function with a factor $\exp(\Delta E t)$, where ΔE is either a) $\Delta E = E_K - E_\pi$ or b) $\Delta E = E_\pi - E_K$. For the argument we will choose option a). The weighted correlation function $C^w_{\pi K}(t)$ is given by

$$\begin{aligned} C^w_{\pi K}(t) &= e^{\Delta E t} C_{\pi K}(t) \\ &= A_0^2 e^{\Delta E t} \left(e^{-E_{\pi K}(t-T/2)} + e^{E_{\pi K}(t-T/2)}\right) + A_1^2 \left(e^{2\Delta E t} e^{-E_K} T + e^{-E_\pi T}\right) . \end{aligned} \tag{3.23}$$

We already see the removal of one time dependent pollutional term. The second step consists of shifting $C^w_{\pi K}(t)$ about a fixed number of time slices δt that removes the temporally constant contribution:

$$\begin{aligned} C^{ws}_{\pi K}(t') &= C^w_{\pi K}(t + \delta t) - C^w_{\pi K}(t) \\ &= A_0^2 e^{\Delta E t} \left(e^{E_{\pi K}(t-T/2)} B_0 + e^{-E_{\pi K}(t-T/2)} B_1\right) + \tilde{A}_1^2 \left(e^{2\Delta E t} e^{-E_K T}\right) . \end{aligned} \tag{3.24}$$

The constants B_0, B_1 and $\widetilde{A}_1^2$ collect contributions which are constant in time. They are given by

$$\tilde{A}_1^2 = A_1^2 (e^{2\Delta E \delta t} - 1) , \tag{3.25}$$

$$B_0 = e^{\Delta E \delta t} e^{E_{\pi K} \delta t} - 1 , \tag{3.26}$$

$$B_1 = e^{\Delta E \delta t} e^{-E_{\pi K} \delta t} - 1 . \tag{3.27}$$

ensemble	β	$a\mu_\ell$	$a\mu_\sigma$	$a\mu_\delta$	$(L/a)^3 \times T/a$
A30.32	1.90	0.0030	0.150	0.190	$32^3 \times 64$
A40.20	1.90	0.0040	0.150	0.190	$20^3 \times 48$
A40.24	1.90	0.0040	0.150	0.190	$24^3 \times 48$
A40.32	1.90	0.0040	0.150	0.190	$32^3 \times 64$
A60.24	1.90	0.0060	0.150	0.190	$24^3 \times 48$
A80.24	1.90	0.0080	0.150	0.190	$24^3 \times 48$
A100.24	1.90	0.0100	0.150	0.190	$24^3 \times 48$
B35.32	1.95	0.0035	0.135	0.170	$32^3 \times 64$
B55.32	1.95	0.0055	0.135	0.170	$32^3 \times 64$
B85.24	1.95	0.0085	0.135	0.170	$32^3 \times 64$
D30.48	2.10	0.0030	0.120	0.1385	$48^3 \times 96$
D45.32sc	2.10	0.0045	0.0937	0.1077	$32^3 \times 64$

Table 3.1: The gauge ensembles used in this thesis. For the labeling of the ensembles we adopted the notation in Ref. [32]. In addition to the relevant input parameters we give the lattice volume.

Finally the multiplication with the inverse weight factor $\exp(-\Delta E t)$ reverses the first multiplication with $\exp(\Delta E t)$:

$$\begin{aligned}\widetilde{C}(t) &= e^{-\Delta E t} C^{ws}_{\pi K}(t') \\ &= A_0^2 \left(e^{E_{\pi K}(t-T/2)} B_0 + e^{-E_{\pi K}(t-T/2)} B_1 \right) + \tilde{A}_1^2 \left(e^{\Delta E t} e^{-E_K T} \right) . \end{aligned} \tag{3.28}$$

The desired total energy now can be obtained by fitting Equation (3.28) to the weighted and shifted data of the 4-point correlation function. Applying the weighting and shifting procedure a second time, now with choice b) for ΔE, in principle removes the other contribution to the pollution as well. For the correlation functions under inspection this does not work, because numerical noise spoils the reliable extraction of the energy $E_{\pi K}$ for our statistics.

3.4 DATA ANALYSIS TOOLS

This section is devoted to the tools used in the data analysis of the present work. For our analysis we use the ensembles of gauge configurations generated by the ETMC, cf. Ref. [24, 31, 32], which are listed in Table 3.1. Each ensemble in turn encompasses several thousand measurements of gauge configurations from which we use a subset of about $N_{\text{conf}} \approx 300$ configurations. In the course of the data analysis a thorough statistical treatment of the data is vital for extracting meaningful results from the computations of the various correlation functions. We therefore discuss how to obtain valid functional descriptions of the data using χ^2-minimization in the case of correlated data. Because the gauge configurations for one ensemble were generated following a Markov chain, we also have to take care of possible correlation in the simulation time, so called autocorrelation. In the last part of this section two variants of the Bootstrap method are presented as a means to estimate the standard deviation of observables, the naive

and the stationary bootstrap.

3.4.1 OBSERVABLE ESTIMATION VIA χ^2-MINIMIZATION

A reliable way to obtain estimators of observable values is the minimization of the χ^2-function with respect to the parameters of the fit function. Given a set of N measurements of an observable $Y = \{ \vec{y}_i \mid i = 1, \ldots, N \}$ depending on an explanatory variable $\vec{x}$ and a function $\vec{f}$ describing this dependency via $\vec{y} = \vec{f}(\vec{x}, \vec{\beta})$ the objective is to minimize the function

$$\chi^2 = \left(\vec{y} - \vec{f}(\vec{x}, \vec{\beta})\right) C^{-1} \left(\vec{y} - \vec{f}(\vec{x}, \vec{\beta})\right) , \tag{3.29}$$

with respect to the vector of parameters $\vec{\beta}$. In the ideal case the weight matrix C^{-1} is the exact inverse of the variance-covariance matrix. If the full variance-covariance matrix is used during the minimization of Equation (3.29) the fit is fully correlated, whereas on usage of solely the diagonal entries C_{ii}^{-1} the fit is uncorrelated. A measurement of the goodness of a fit is the χ^2 value divided by the degrees of freedom of the fit denoted by χ^2/dof. According to this a fit is said to optimally describe the data when $\chi^2/\mathrm{dof} = 1$, as discussed in Ref. [33]. In an uncorrelated fit the reduced χ^2 is not as reliable because possible correlation in the data is not taken into account properly.

To incorporate prior knowledge into a χ^2-minimization the vectors $\vec{y}$ and $\vec{f}$, and the matrix C^{-1} get extended. This prior knowledge often is a subset of the parameters $\vec{\beta}$ whose values are known a priori, for example from a preceding fit. To this end let $\vec{p}$ denote the part of $\vec{\beta}$ whose values are known to be $\vec{p}_{\mathrm{meas}}$. The vector of data points now gets augmented $\vec{y}' = (\vec{y}, \vec{p}_{\mathrm{meas}})$ while the vector of function values is changed to $\vec{f}'(\vec{x}, \vec{\beta}, \vec{p}) = (\vec{f}(\vec{x}, \vec{\beta}), \vec{p})$. The new variance-covariance matrix C' then is estimated accordingly to incorporate the new datapoints $\vec{p}_{\mathrm{meas.}}$. The χ^2 function to minimize now is then given by

$$\chi^2 = \left(\vec{y}' - f'(\vec{x}, \vec{\beta}, \vec{p})\right) C'^{-1} \left(\vec{y}' - f'(\vec{x}, \vec{\beta}, \vec{p})\right) . \tag{3.30}$$

3.4.2 AUTOCORRELATION

The data used in this work stem from Markov Chain simulations as will be detailed in Chapter 4. Consequently statistical errors of observables estimated from these data are affected by autocorrelation. As stated in Ref. [34] this distortion can lead to underestimation of the statistical error. For a better understanding of how to assess the autocorrelation of data from Markov Chain simulations we follow the line of argument in Ref. [34]. The method is called Γ-method. All our data analysis is based on one replicum of a Monte Carlo run for each ensemble of gauge configurations. Thus we have N measurements available. The key quantity for error estimation is the autocorrelation function defined as

$$\Gamma_{\alpha\beta}(n) = \left\langle (a_\alpha^i - A_\alpha)(a_\beta^{i+n} - A_\beta) \right\rangle , \tag{3.31}$$

which correlates the deviation of the i-th measurement a_α^i from the true value A_α of the observable with the deviation of the $i+n$-th measurement a_β^i from the true value of another

observable A_β. An example for primary observables A_γ are the values of correlation functions whereas the effective mass is an observable derived from the values of correlation functions. Derived quantities are functions of primary observables $f(A_\alpha)$. The true value of a derived quantity is given by the evaluation of a function f at the true observable values A_α:

$$F = f(A_1, A_2, \ldots) = f(A_\alpha)\,. \tag{3.32}$$

An estimator for A_α is given by

$$\hat{a}_\alpha = \frac{1}{N}\sum_{i=1}^{N} a_{\alpha,i}\,, \tag{3.33}$$

which deviates from the true value:

$$\hat{\delta}_\alpha = \hat{a}_\alpha - A_\alpha\,. \tag{3.34}$$

The derived observable F can be estimated by evaluating the function f at the estimators $\hat{a}_\alpha$:

$$\widehat{F} = f(\hat{a}_\alpha)\,. \tag{3.35}$$

Expanding $f(\hat{a}_\alpha)$ in a Taylor series leads to

$$\widehat{F} = F + \sum_\alpha f_\alpha \hat{\delta}_\alpha + \frac{1}{2}\sum_{\alpha\beta} f_{\alpha\beta}\hat{\delta}_\alpha\hat{\delta}_\beta + \ldots\,, \tag{3.36}$$

where the coefficients f_α are given by the partial derivatives of f with respect to the true mean values A_α at A_α

$$f_\alpha = \left.\frac{\partial f}{\partial A_\alpha}\right|_{A_\alpha}\,, \quad f_{\alpha\beta} = \left.\frac{\partial^2 f}{\partial A_\alpha \partial A_\beta}\right|_{A_\alpha, A_\beta}\,. \tag{3.37}$$

For the estimator $\widehat{F}$ of a derived observable the error σ_F is approximately given by

$$\sigma_F^2 = \left\langle (\widehat{F} - F)^2 \right\rangle \approx \frac{C_F}{N}\,, \tag{3.38}$$

with

$$C_F = \sum_{\alpha\beta}\sum_{t=-\infty}^{\infty} f_\alpha f_\beta \Gamma_{\alpha\beta}(t)\,, \tag{3.39}$$

defining the projection of the integrated autocorrelation function onto the derived function. The naive variance is recovered when evaluating $\Gamma_{\alpha\beta}(t)$ at $t = 0$. Separating the naive variance $v_F = \sum_{\alpha,\beta} f_\alpha f_\beta \Gamma_{\alpha\beta}(0)$ from Equation (3.38) leads to

$$\sigma_F^2 = \frac{2\tau_{\mathrm{int},F}}{N} v_F\,. \tag{3.40}$$

Here the integrated autocorrelation time $\tau_{\mathrm{int},F}$

$$\tau_{\mathrm{int},F} = \frac{1}{2v_F} \sum_{\alpha\beta} \sum_{t=-\infty}^{\infty} f_\alpha f_\beta \Gamma_{\alpha\beta}(t)\,, \tag{3.41}$$

has been introduced. From Equation (3.40) it can be seen that the true error σ_F^2 is enhanced by a factor $2\tau_{\mathrm{int},F}$ in comparison to the simple variance v_F.

In what follows we will introduce estimators of $\tau_{\mathrm{int},F}$ as was done in Ref. [34] and present the procedure [34] with which we check the analysis data for autocorrelation. To this end estimators for the autocorrelation function $\Gamma_{\alpha\beta}(t)$, the variance v_F, and the partial derivatives f_α are needed. The first estimator reads

$$\widehat{\Gamma}_{\alpha\beta}(t) = \frac{1}{N-t} \sum_{i=1}^{N-t} (a_\alpha^i - \hat{a}_\alpha)(a_\beta^i - \hat{a}_\beta)\,. \tag{3.42}$$

With an estimator of the gradients f_α

$$\hat{f}_\alpha = \frac{\partial f}{\partial \hat{a}_\alpha}\,, \tag{3.43}$$

an estimator for the autocorrelation function of a derived quantity reads

$$\widehat{\Gamma}_F(t) = \sum_{\alpha\beta} \hat{f}_\alpha \hat{f}_\beta \widehat{\Gamma}_{\alpha\beta}(t) \tag{3.44}$$

Numerically the integrated projected autocorrelation function C_F can be estimated via

$$\widehat{C}_F(W) = \left(\widehat{\Gamma}_F(0) + 2 \sum_{t=1}^{W} \widehat{\Gamma}_F(t) \right)\,, \tag{3.45}$$

with W being an integer cutoff and the factor 2 takes into account the symmetry of the autocorrelation function. In the current notation an estimator for the variance is simply given by evaluating Equation (3.44) at $t = 0$. Thus $\tau_{\mathrm{int},F}$ can be estimated with

$$\hat{\tau}_{\mathrm{int},F}(W) = \frac{\widehat{C}_F(W)}{2\hat{v}_F}\,. \tag{3.46}$$

In practical analyses of the autocorrelation the width W of the window in which the autocorrelation function is estimated plays a crucial role. As detailed in Ref. [34] the error of $\widehat{C}_F(W)$ receives a systematic contribution due to the truncation at W and a statistical one. Hence an optimal value for W is given when the total relative error of the final error $\hat{\sigma}_F$ estimate is minimal

$$\frac{\delta_{\mathrm{tot}}(\hat{\sigma}_F)}{\hat{\sigma}_F} \approx \frac{1}{2} \min_W \left(\exp(-W/\tau) + 2\sqrt{W/N} \right)\,. \tag{3.47}$$

Thus the integrated autocorrelation time can be estimated in dependence of the width W

and $\hat{\tau}_{\text{int},F}(W)$ reaches a plateau at optimal W. In this way the integrated autocorrelation time can reliably be assessed, revealing whether the data under consideration suffers from autocorrelation.

3.4.3 BOOTSTRAPPING

The statistical bootstrap, introduced in Ref. [35], is a method to infer properties of the true distribution of an observable from a finite number of measurements. The bootstrap is built on resampling the data randomly with replacement. The underlying probability density function (pdf) f of an observable x often is unknown such that variances of estimators of x cannot be determined by conventional statistical methods. A cure comes with approximating f by its empirical estimator $\hat{f}$. If $\hat{f} \approx f$ the estimated distribution of estimators $\hat{x}$ allows to infer properties, such as the standard deviation, of the true distribution from the distribution of $\hat{x}$. One of the big advantages of the bootstrap is its applicability to any statistical observable. We start with a set of N measurements of an observable x denoted

$$X = \{ x_1, x_2 \ldots, x_N \} \, . \tag{3.48}$$

In order to generate R bootstrap samples we take the following steps:

1. Calculate the estimator $\hat{x}$ of the original measurements X which defines the 1st bootstrap sample
2. From the original dataset X randomly draw N measurements x_i with replacement
3. Compute estimator $\hat{x}$
4. Repeat Items 2 and 3 $R - 1$ times

For this thesis we apply the bootstrap with $\hat{x}$ being the sample mean. The sample mean of the original sample is quoted as the central value and its variance is calculated from the bootstrap sample estimates with the central value as mean value. Another advantage of using the statistical bootstrap is that it automatically maintains correlation in the data. By keeping the bootstrap samples throughout the analysis until the end the error is propagated automatically. There exist different varieties of bootstrap resampling of which we shortly discuss its stationary and parametric form in the following.

PARAMETERIC BOOTSTRAP When no measurements of an observable are available but only the mean μ and standard deviation σ, e.g. from a previous analysis, are known it is not straightforward to incorporate these observables in a bootstrap analysis. One possibility is the parametric bootstrap. A parametric bootstrap starts from the assumption that values of the measurements follow a certain, unknown distribution. In our cases we assume that the input observable has Gaussian distributed values. We thus sample from the Gaussian distribution with mean μ and width σ R times in order to generate our bootstrap samples as before. In this work this variant of the bootstrap is used for physical input data like for example meson masses or decay constants.

DATA BLOCKING AND STATIONARY BOOTSTRAP As described above, autocorrelation in Monte Carlo time enhances the true variance of an estimator. In the naive bootstrap the autocorrelation is destroyed by randomly resampling the data of Correlation functions. For data with measurable autocorrelation this leads to an underestimation of the standard deviation. A possible way out is to bin the measurements into blocks of size of the estimated autocorrelation time and then bootstrap the per bin means of the data. Unfortunately this blocking reduces the size of the original sample and sometimes the autocorrelation times are so large that proper statistical inference is no longer possible. In this work instead we take care of autocorrelation by using the stationary bootstrap described in Ref. [36].

In contrast to blocking the data the stationary bootstrap has a variable block-length and allows for the same samplesize as the ordinary bootstrap. The resampling starts from the set of original measurements $X = X_i, i \in [1, N]$ and is implemented by constructing blocks of measurement indices. The resampling amounts to a 5-step procedure

1. Generate same length arrays of start values I and block-lengths L. Elements of I are taken from the uniform distribution over the interval $[1, N]$. The block-lengths L are drawn from the geometric distribution with mean $1/l$, where b is the average block-length.

2. Build blocks of indices from pairs of $(i, l) \in (I, L)$ according to

$$B_i = \{\, i \bmod N, (i+1) \bmod N, \ldots, (i+l-1) \bmod N \,\} \,.$$

3. Concatenate the blocks B_i to form an index array $n = \{\, B_1, B_2, \ldots, B_m \,\}$. If necessary B_m is truncated such that n has N entries. joining the m blocks, where the number of entries in n is N.

4. From the original measurements construct a new sample X^r by choosing measurements with indices n from the original measurements and calculate the estimator $\hat{x}$ on X^r.

5. Repeat Items 1 to 4 $R - 1$ times

After this resampling procedure one ends up with R samples of the data, as in the naive bootstrap. This variant of the bootstrap takes care of autocorrelation in the same way as blocking but allows for the same sample size.

CHAPTER 4

SIMULATING LATTICE QCD

With the theoretical grounds prepared in the previous chapters we are now ready to describe how to simulate Lattice QCD gauge fields and propagators. To this end we here give an overview of the algorithms used for the generation of gauge fields and propagators. The Markov chain Monte Carlo algorithm most commonly used today is the Hybrid Monte Carlo (HMC) algorithm or variants thereof. The HMC algorithm was initially introduced in Ref. [37]. In addition we present methods to improve the short range behavior of gauge fields and propagators, which go by the names of Hypercubic (HYP) blocking and stochastic Laplacian-Heaviside (sLapH) smearing.

4.1 HYBRID MONTE CARLO ALGORITHM

To evaluate n-point functions we need a numerical evaluation of their path integral representation, given in Equation (2.15). Following Equation (2.67) we can generate N gauge field configurations Y, provided the gauge degrees of freedom follow the distribution

$$P(\mathrm{Y}) = \frac{1}{Z}\det(D)\exp(-S_G[\mathrm{Y}])\,, \tag{4.1}$$

where Z is the partition function and $\det(D)$ denotes the fermion determinant after integrating out the Grassmann valued fermion fields ψ. With the N realizations of Y at hand the expectation value $\langle O\rangle$ of an observable O is given by the statistical average over the gauge field configurations as

$$\langle O\rangle = \sum_{i=1}^{N} O[\mathrm{Y}_i] + \mathcal{O}\left(\frac{1}{\sqrt{N}}\right)\,, \tag{4.2}$$

where the observable still needs to be evaluated on the background of each configuration and the statistical error of O scales with the inverse of $\sqrt{N}$. The sampling method used for the Y used in this thesis is the Hybrid Monte Carlo algorithm. Details of its implementation are written up in Ref. [38]. We briefly demonstrate the basic steps of the algorithm for the case of a mass degenerate doublet of two twisted mass fermions. The extension to non degenerate

doublets is a bit more involved but follows the same principles. It is detailed in Ref. [38].

Regarding two mass degenerate fermions in a doublet we can rewrite the fermion determinant $\det(Q^\dagger Q)$ as an integral over pseudofermionic fields $\phi^\dagger$ and ϕ, with bosonic statistics.

$$\det(Q^\dagger Q) \propto \int \mathrm{D}\phi\ \mathrm{D}\phi^\dagger\ \exp\left(-(Q^{-1}\phi, Q^{-1}\phi)\right)\,, \tag{4.3}$$

with the scalar product (a, b) and the one flavor operator

$$Q = \gamma_5(D_W + m_0) + i\mu_\ell\,. \tag{4.4}$$

The integral to sample then takes the form

$$\begin{aligned}\mathcal{I} &= \int \mathrm{D}\phi^\dagger\ \mathrm{D}\phi\ \mathrm{D}U\ \exp(-S_G[U] - \phi^\dagger(Q^\dagger Q)^{-1}\phi) \\ &= \int \mathrm{D}\phi^\dagger\ \mathrm{D}\phi\ \mathrm{D}U\ \exp(-S_{\text{eff}}[\phi^\dagger, \phi, U])\,.\end{aligned} \tag{4.5}$$

The HMC algorithm is based on guiding the sampling process through the configuration space via integrating the equations of motion of a Hamilton operator $\mathcal{H}$

$$\mathcal{H}[P, U, \phi^\dagger, \phi] = \frac{1}{2}\sum_{x,\mu} \mathrm{tr}\left(P_{x,\mu}^2\right) + S_{\text{eff}}[\phi^\dagger, \phi, U]\,. \tag{4.6}$$

The kinetic part consists of the traceless momenta $P(x, \mu)$ which are conjugate to U, and generated in an initial heat-bath step, alongside the initial pseudofermionic fields $\phi^\dagger$ and ϕ. They are generated as

$$\phi = Qr\,, \quad \left\langle r^\dagger r \right\rangle = 1\,, \tag{4.7}$$

with complex random numbers r following a Gaussian distribution. One then proceeds to suggest a new configuration (U', P') via integrating the equations of motion of Equation (4.6) along a fictitious computer time τ_{MC}.

To account for numerical errors in the molecular dynamics integration the new proposal (U', P') is accepted with the probability

$$p = \min\left\{1, \exp(\mathcal{H}[P', U', \phi^\dagger, \phi] - \mathcal{H}[P, U, \phi^\dagger, \phi])\right\} \tag{4.8}$$

Summarizing, one step of the HMC algorithm is composed of three different parts:

1. Choose conjugate momenta and pseudofermion fields ϕ
2. Integrate Hamiltonian equations of motion $(U, P) \to (U', P')$ along a fictitious computer time τ_{MC}.
3. Accept (U', P') with probability $\min(1, \exp(-\Delta\mathcal{H}))$

The HMC can be shown to fulfill the detailed balance condition. The algorithm can be accelerated substantially by several methods as mass and even-odd preconditioning or integration on

multiple scales of the computer time τ'. Since these topics are out of scope for this work we refer to Ref. [38, 39], which also serve as a reference to the implementation used for the gauge configurations in this work: tmLQCD.

4.2 SMEARING METHODS

This section is devoted to the description of improvements that can be applied to gauge fields and propagators stemming from QCD simulations in order to improve on the signal of correlation functions obtained from contractions. The methods go by the name of smearing and affect either the gauge fields, generated in Monte Carlo simulations, or the quark fields, constructed for the evaluation of correlation functions. Smearing the gauge field corresponds to averaging out short distance fluctuations in the SU(3) color matrices. Thus the influence of the long distance behavior of the gauge field on the correlation functions is increased. As explained before the lattice wave functions only have a certain overlap with the continuum wave functions. Smearing out the lattice wave functions results in a spatial extension of the wave function. Thus the overlap with the continuum wave functions can be increased. In the remainder of this section we introduce the smearing schemes used in this work for the gauge fields and the quark propagators. We start with hypercubic blocking or HYP-smearing of the quark fields and then move on to Distillation or Laplacian-Heaviside (LapH) smearing. A description of how to improve LapH with diluted stochastic sources concludes this section.

4.2.1 SMOOTHING THE GAUGE FIELD USING HYPERCUBIC BLOCKING

Hypercubic blocking is one of several ways to average gauge link matrices. It was first described in Ref. [40] and is an extension of APE-smearing [41]. In our analysis we will only use a three-dimensional version of HYP-smearing which makes it a two step procedure. The process is depicted in Figure 4.1. Each original link variable is decorated with its surrounding staples (dashed lines in Figure 4.1(a)) in the same plane as the original link to produce the solid decorated links $V_\mu(x)$. Staples of $V_\mu(x)$ are then used to obtain the blocked links $W_\mu(x)$ (thick central line in Figure 4.1(b)). Mathematically the procedure is expressed in Equations (4.9) and (4.10)

$$V_\mu(x) = \mathcal{P}_{\mathrm{SU(3)}}\left((1-\alpha_2)U_\mu(x) + \frac{\alpha_2}{2}\sum_{\pm\eta\neq\rho,\mu} U_\eta(x)U_\mu(x+\eta)U_{-\eta}(x+\eta+\mu)\right) \tag{4.9}$$

$$W_\mu(x) = \mathcal{P}_{\mathrm{SU(3)}}\left((1-\alpha_1)V_\mu(x) + \frac{\alpha_1}{4}\sum_{\pm\eta\neq\mu} V_\eta(x)V_\mu(x+\eta)V_{-\eta}(x+\mu+\eta)\right). \tag{4.10}$$

the parameters $\alpha_i\, i = 1,2$ control the strength of the smearing with $\alpha_i = 0$ meaning no smearing at all. The operators $\mathcal{P}_{\mathrm{SU(3)}}$ project the smeared object back to elements of SU(3). Their application to 3×3 color gauge matrices U is defined in the following way

$$\mathcal{P}_{\mathrm{SU(3)}}(U) = \frac{M}{\sqrt[3]{\det M}}, \quad M = \frac{U}{\sqrt{U^\dagger U}}.$$

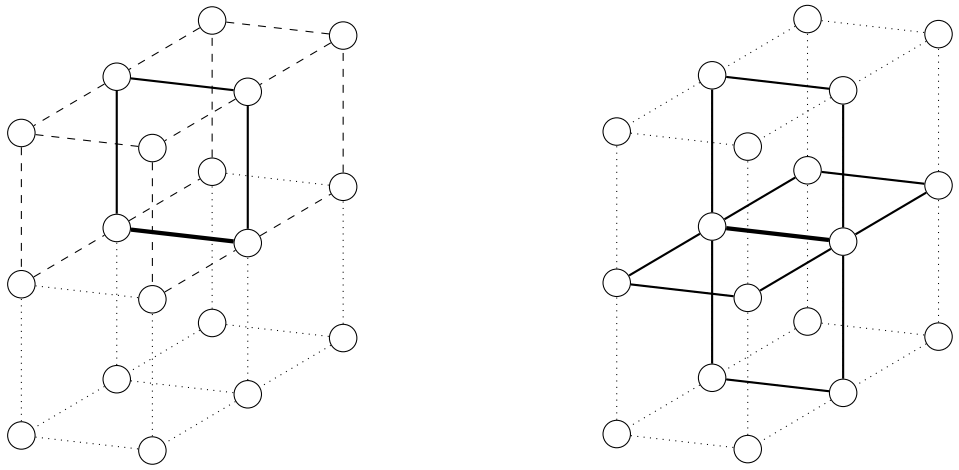

(a) Decorating the links $U_\kappa(x)$ (b) APE-smearing the decorated links $V_\mu(x)$

Figure 4.1: The two steps of one application of hypercubic blocking. Figure 4.1(a) depicts the staples involved in the decoration process as dashed lines. Each solid line link variable is constructed by the dashed staples lying in the same plane as the original link. Figure 4.1(b) shows the staples used for constructing the central hypercubic blocked link as solid lines.

The procedure of hypercubic blocking can be repeated to successively smear the gauge field. This introduces the number of iterations n_{iter} as an additional parameter.

4.2.2 SMEARING QUARK FIELDS WITH DISTILLATION

Laplacian-Heaviside smearing is one possibility of improving the overlap of lattice operators with physical operators. Morningstar et al. described it in Ref. [3]. The main advantages of this approach are reduced excited states contamination in correlation functions and efficient storage of quark propagators. Thanks to a certain decomposition of the quark propagators they can be reused in calculations involving different operator quantum numbers without redoing costly inversions of the Dirac operator. The smearing of the quark fields is done by applying a smearing kernel $\mathcal{S}$ to the original quark fields ψ to get the resulting smeared quark fields as a matrix-vector product $\psi_{i\beta}(x)$:

$$\widetilde{\psi}_{a\alpha}(x) = \mathcal{S}_{ab}(x,y)\psi_{b\alpha}(y).$$

Here Greek indices are indices in Dirac-space whereas Latin indices correspond to color. The Arguments x and y are taken to denote spatial lattice sites. The smearing kernel, as defined in Ref. [42], is composed of a real cutoff parameter σ_s for the eigenvalue spectrum of the discrete 3-dimensional gauge covariant Laplace operator $\widetilde{\Delta}$, and the Heaviside step function Θ:

$$\mathcal{S} = \Theta(\sigma_s^2 + \tilde{\Delta})\,. \tag{4.11}$$

The Laplace operator is defined in terms of the gauge field links $U_k^{ab}(x)$ in the following way:

$$\tilde{\Delta}^{ab}(x,y;U) = \sum_{k=1}^{3} \left\{ U_k^{ab}(x)\delta(y,x+k) + U_k^{ba}(y)^*\delta(x,y-k) - 2\delta(x,y)\delta_{ab} \right\}. \tag{4.12}$$

The Laplace operator is block diagonal in time and Dirac space. As before the index k indicates the direction in which the link variable is to be taken. The operator of Equation (4.12) is gauge covariant and preserves all relevant symmetries of the lattice.

It can be decomposed into a diagonal matrix Λ_Δ of eigenvalues and a matrix V_Δ containing the eigenvectors of the Laplace operator as columns. Using the decomposition

$$\tilde{\Delta} = V_\Delta \Lambda_\Delta {V_\Delta}^\dagger \tag{4.13}$$

we can realize this cutoff implied by the Heaviside function in Equation (4.11) by taking only the N lowest eigenvalues into account. The eigenvalue of the N-th eigenvector then is the cutoff σ_s. Having available V_Δ the distillation operator $\square$ can be defined for every time slice t as the matrix product

$$\square(t) = V_N(t) V_N^\dagger(t)$$

which is a projection operator ($\square^2 = \square$) onto the subspace of all calculated eigenvectors. The matrix V_N can be ordered by increasing eigenvalues in its columns where N is the number of eigenvectors taken into account. Considering all eigenvectors N_E of $\widetilde{\Delta}$ causes $\square$ to become the identity and so no smearing takes place at all when acting on quark fields. If $v_x^{(k)}$ describes the element x of the k-th eigenvector of the time slice then $\square(t)$ can be expressed by its elements

$$\square_{x,y}(t) = \sum_{k=1}^{N} \left(v_x^{(k)} v_y^{(k)\dagger} \right). \tag{4.14}$$

correlation functions constructed with help of this operator retain their symmetries because of the symmetry preserving property of Equation (4.12) By construction the projector $\square(t)$ and the operator $\tilde{\Delta}(t)$ share the same transformation behavior under local $SU(3)$ gauge transformations G

$$\Delta \to \Delta' = G \Delta G^\dagger \tag{4.15}$$

$$\square \to \square' = G \square G^\dagger . \tag{4.16}$$

Thus $\square(t)$ is the numerical representation of the smearing operator $\mathcal{S}$ defined in Equation (4.11).

4.2.3 PROPAGATORS WITH DISTILLATION

A closer look at hadron correlation functions expressed in terms of so called quark lines reveals the reusability of the propagators. A usual correlation function $C(t)$ can be expressed by the trace over quark propagators D^{-1} multiplied with according gamma structures Γ_a, as discussed in Section 3.1. On the application of quark field smearing the quark fields are multiplied by the smearing matrix S and the correlation function now reads

$$\begin{aligned} C(t) &= \left\langle \bar{\psi}_f(n,t) S^\dagger \Gamma_a S \psi_{f'}(n,t) \bar{\psi}_{f'}(m,t') S^\dagger \Gamma_b S \psi_f(m,t') \right\rangle \\ &= -\mathrm{tr} \left(\Gamma_a \mathcal{S} D^{-1}(n|m)_f \mathcal{S} \Gamma_b \mathcal{S} D^{-1}(m|n)_{f'} \mathcal{S} \right) , \end{aligned} \tag{4.17}$$

where we have used the hermiticity of the LapH-smearing operator $\mathcal{S}$. The quark line $\mathcal{Q}$ is the object $\mathcal{S}D_f^{-1}\mathcal{S}$ which in our case can be also written as

$$\mathcal{Q} = V_s(V_s^\dagger D_f^{-1} V_s)V_s^\dagger = V_s \tau V_s \,. \tag{4.18}$$

The propagator is a square matrix connecting every 2 sites of the lattice thus being of size $(L^3 \cdot T \cdot N_c \cdot N_d)^2$. The object in parentheses, called perambulator τ, is much smaller in size than the original propagator D_f^{-1}. such that inverting and storing it is more efficient than storing the original propagator.

4.2.4 IMPROVING DISTILLATION WITH DILUTED STOCHASTIC SOURCES

When applying Laplacian-Heaviside smearing to calculate quark propagators an exact treatment of those propagators, even with only few eigenvectors, still is prohibitively costly. Typical lattices in the present work have dimensions $N_\mathrm{T} \times N_\mathrm{S}^3 = 64 \times 32^3$ and need $N_\mathrm{EV} = 220$ eigenvectors for a proper sampling of the eigenspectrum of $\widetilde{\Delta}$. The number of inversions needed for an exact solution of τ is $N_\mathrm{I} = N_\mathrm{EV} \cdot N_\mathrm{T} \cdot N_\mathrm{D} > 50000$ which is not feasible for the number of configurations and ensembles we are dealing with. The number of inversions needed can be decreased by not looking at the exact solution but instead estimate the perambulator stochastically. To this end we introduce complex random noise vectors η with properties

$$\begin{aligned} \langle \eta_i \rangle &= 0 \,, \\ \langle \eta_i \eta_j^* \rangle &= \delta_{ij} \,. \end{aligned}$$

Specifically we employed Z_2 noise for the perambulator generation in this thesis. The smeared propagator is then given by solving

$$DX^r = \eta^r \tag{4.19}$$

for X or equivalently by calculating

$$D_{ij}^{-1} \approx \frac{1}{N_R} \sum_{r=1}^{N_R} X_i^r \eta_j^{r*} \,,$$

where N_R is the total number of employed random vectors. According to Ref.[43], the variance $\mathrm{var}(D_{ij}^{-1})$ can be decomposed into

$$\mathrm{var}\left(D_{ij}^{-1}\right) = \frac{1}{N_R}\left(\left[D_{ij}^{-1}\right]^2 K^2 + \sum_{k\neq j}\left[D_{ik}^{-1}\right]^2\right) = \frac{1}{N_R}\left(\sum_{k\neq j}\left[D_{ik}^{-1}\right]^2\right) \,.$$

Despite we still have off-diagonal elements in $\eta\eta^\dagger$ which are non-zero and thus spoil the behavior of the correlation function's variance. A cure for that was introduced by C. Morningstar et al. in Ref. [3]. First the random vectors η_i are full vectors in the spin, spatial, and color space. Due to the application of $\mathcal{S}$ it is sufficient to calculate on the LapH-subspace, which is comprised of the spin, color and eigenvector space. We denote the Z_2 random vectors on

this subspace by ρ. They get diluted such that some of the off-diagonal elements in $\rho\rho^\dagger$ vanish completely. The dilution is realized by introducing complete sets of projection operators $\{ P^{(b)} \}$. Each element $P^{(b)}$ is then a matrix in the LapH-subspace. The multi-index b denotes a certain scheme of cancelling entries of each ρ_i. The quark line from Equation (4.18) now changes to :

$$\begin{aligned} \mathcal{Q} &= V_s V_s^\dagger D^{-1} V_s V_s^\dagger \\ &= \sum_b \left\langle V_s V_s^\dagger D^{-1} V_s P^{(b)} \rho \left(V_s P^{(b)} \rho \right)^\dagger \right\rangle , \end{aligned} \tag{4.20}$$

where we have used the projector property $\langle \rho\rho^\dagger \rangle = \mathbb{1}$. The error of correlation functions calculated with diluted quark lines now behaves like

$$\Delta C(t) \propto \frac{1}{\sqrt{N_R}} . \tag{4.21}$$

The original perambulator now gets altered to its diluted form τ_d

$$\tau \to \tau_d = V_s^\dagger D^{-1} V_s P^{(b)} \rho . \tag{4.22}$$

This quantity is even smaller in disk space usage than τ but in order to regenerate quark lines also the initial random vectors ρ and their seeds have to be stored. A further observation is that neither τ_d nor ρ depend on the Γ structures, necessary for Correlation functions. Their only dependency is the quark flavor such that interpolators with different quantum numbers can be composed easily from the stored quantities, as long as the eigenvectors V_s are still available. Thus the sLapH approach allows to calculate reusable all-to-all propagators with an acceptable number of inversions and reduced variance compared to the stochastic case.

CHAPTER 5

$I_3 = 1$ KAON KAON SCATTERING LENGTH

5.1 INTRODUCTION

In this chapter we present our analysis of the elastic scattering process $K^+K^+ \to K^+K^+$ in the s-wave at maximal isospin. This work was published in Ref. [1].

The calculation is carried out in a mixed action approach. The quark sea is discretized with the $N_f = 2 + 1 + 1$ Wilson twisted mass (Wtm) action, whereas the light valence quarks are implemented as a doublet of $N_f = 2$ Wtm quarks. The strange valence quarks are implemented using unitarity breaking Osterwalder-Seiler fermions. In total we use 12 ensembles of gauge configurations with different pion masses, denoted by the bare light quark mass $a\mu_\ell$. For the bare valence strange quark mass $a\mu_s$ we have three values available on each of the three lattice spacings β. We calculate the two-point function C_K of a single meson and the four-point function C_{KK} for a system of two kaons.

As has already been done in Ref. [30], we strive to improve the behavior of our correlation functions with the sLapH method. It is worthwhile noting that we here reuse the light quark perambulators which originally were calculated in Ref. [30]. In order to determine the energy shift $\delta E = E_{KK} - 2M_K$ of the interacting system in comparison to the non-interacting case, we make use of a ratio of shifted correlation functions, also used in Refs. [29, 44] which allows us to determine δE directly. Time independent states distorting the late time behavior of C_{KK} and C_K^2 are removed by the shift occurring in this ratio. We then proceed to solve Lüscher's finite size formula, cf. eq. (2.88), relating the energy shift and the elastic scattering length, for the scattering length a_0. To fix the strange quark mass we employ 2 methods. The first one is based on the leading order GMOR relations of the pseudoscalar masses in Chiral Perturbation Theory (ChPT), whereas the second uses the physical value of the Kaon mass, described by ChPT. Within these two approaches the $a\mu_s$ dependent values of M_K and $M_K a_0$ are fixed to the physical strange quark mass dictated by the two aforementioned methods. As a last step the chiral and continuum extrapolations of $M_K a_0$ are carried out as a combined fit. $M_K a_0$ is assumed to behave linearly as a function of the light quark mass m_ℓ and quadratically as a function of the squared lattice spacing a^2.

In addition we investigate the volume dependence of δE via the ensemble A40 at 3 different lattice volumes and give an estimate of the effective range of the interaction $K^+K^+ \to K^+K^+$.

5.2 SUMMARY

The main result of this chapter is the continuum and chirally extrapolated value of the scattering length, which we quote to be

$$M_K a_0 = -0.385(16)_{\text{stat}}(^{+0}_{-12})_{m_s}(^{+0}_{-5})_{Z_P}(4)_{r_f}\,. \tag{5.1}$$

Systematic effects include the fixing procedure of the strange quark mass, m_s, two different values of renormalization constants, Z_P and neglect of higher order terms in the extraction of the scattering length. When using a linear dependence on the light quark mass only, we observe a roughly 20% discrepancy between the coarsest lattice spacing and the value extrapolated to the continuum. We therefore conclude that taking the continuum limit is important when treating the data as linearly dependent on the light quark mass. Along the chiral and continuum extrapolation we found out that a proper interpolation of the kaon decay constant to the physical strange quark mass is important when extrapolating $M_K a_0$ with its appropriate ChPT formula.

Another finding of this study is that the scattering length is only weakly depending on the valence strange quark mass. Regarding the volume dependence of δE, we conclude that box sizes of $L \leq 2\,\text{fm}$ at a pion mass of $M_\pi \approx 330\,\text{MeV}$ are too small for a reliable extraction of the energy shift.

PHYSICAL REVIEW D **96,** 034510 (2017)

Hadron-Hadron Interactions from $N_f = 2+1+1$ lattice QCD: Isospin-1 *KK* scattering length

C. Helmes,* C. Jost, B. Knippschild, B. Kostrzewa, L. Liu, C. Urbach, and M. Werner
(ETM Collaboration)

Helmholtz Institut für Strahlen- und Kernphysik, University of Bonn, Bonn D-53115, Germany
(Received 30 May 2017; published 10 August 2017)

We present results for the interaction of two kaons at maximal isospin. The calculation is based on $N_f = 2+1+1$ flavor gauge configurations generated by the European Twisted Mass Collaboration with pion masses ranging from about 230 MeV to 450 MeV at three values of the lattice spacing. The elastic scattering length $a_0^{I=1}$ is calculated at several values of the bare strange and light quark masses. We find $M_K a_0 = -0.385(16)_{\mathrm{stat}}(^{+0}_{-12})_{m_s}(^{+0}_{-5})_{Z_P}(4)_{r_f}$ as the result of a combined extrapolation to the continuum and to the physical point, where the first error is statistical, and the three following are systematical. This translates to $a_0 = -0.154(6)_{\mathrm{stat}}(^{+0}_{-5})_{m_s}(^{+0}_{-2})_{Z_P}(2)_{r_f}$ fm.

DOI: 10.1103/PhysRevD.96.034510

I. INTRODUCTION

Shortly after the big bang, the Universe is believed to have been in a quark-gluon plasma state of matter. Apart from the inside of neutron stars, the only places where this state of matter appears and can be studied are detectors investigating heavy ion or proton-proton collisions like the STAR detector at the Relativistic Heavy Ion Collider (RHIC) at BNL [1] or the ALICE experiment at the LHC at CERN [2]. The collisions taking place at such sites yield in their final states numerous light hadrons like pions and kaons. Due to the mass difference between kaons and pions, the produced kaons carry much lower momenta than the pions, therefore being much more likely to interact elastically. The interaction of two kaons is determined by quantum chromodynamics (QCD), which is nonperturbative at low energies. The understanding and interpretation of the results of the aforementioned experiments make a nonperturbative investigation of kaon-kaon interactions highly desirable. While this can be formulated in chiral perturbation theory (ChPT), it is theoretically interesting to check if the effective approach is able to properly describe kaon-kaon scattering. Lattice QCD provides a nonperturbative *ab initio* method to perform such a study.

Hadron-hadron scattering has become more and more accessible to lattice QCD simulations over the last several years. This is on the one hand due to Lüscher's finite-volume formalism, and on the other hand due to lattice QCD ensembles becoming ever more realistic. For kaon-kaon scattering in the isospin-1 channel, only a few lattice QCD calculations have been performed [3,4], where the result of the former calculation has been used in Ref. [2] for the ALICE results. In the maximal isospin channel, kaon-kaon scattering resembles the well-studied pion-pion case [4–10]: there are no fermionic disconnected diagrams, and only one light quark is replaced by a strange quark. Since we already investigated pion-pion scattering in the isospin-2 channel [11], a lot of our analysis tools can be carried over to the present investigation.

In this paper we present the first study of K^+K^+ scattering from lattice QCD based on $N_f = 2+1+1$ ensembles of the European Twisted Mass Collaboration (ETMC) [12,13] covering three values of the lattice spacing. These ensembles, which employ up to five values of the light quark mass per lattice-spacing value, allow us to perform reliable chiral and continuum extrapolations of our results.

For the strange quark, we employ a mixed action approach with so-called Osterwalder-Seiler valence quarks on the Wilson twisted mass sea [14]. This allows us to tune the valence strange quark mass value to its physical value without spoiling the automatic $\mathcal{O}(a)$ improvement guaranteed by Wilson twisted mass lattice QCD at maximal twist [15]. However, while unitarity-breaking effects vanish in the continuum limit, this ansatz also introduces partial quenching effects, which we cannot control in the present calculation. However, in previous calculations with this setup, no sizable effects were found; see e.g. Refs. [16,17]. The mixed-action approach for the strange quark also allows us to avoid the parity-flavor mixing present in the $1+1$ (strange-charm) sea sector of Wilson twisted mass lattice QCD at maximal twist with $N_f = 2+1+1$ flavors.

Our final result differs by about 2σ from the determinations by NPLQCD [3] and about 4σ from the determination of PACS-CS [4]. This deviation can likely be attributed to lattice artifacts: NPLQCD works mainly at a single lattice spacing, with the exception of one ensemble

*Corresponding author.
helmes@hiskp.uni-bonn.de

at a second lattice-spacing value. PACS-CS works at a single lattice spacing only. However, we can also not exclude residual unitarity-breaking effects in our calculation. Interestingly, our result is actually equal to the leading-order ChPT prediction for $M_K a_0$.

II. LATTICE ACTION

We use gauge configurations generated by the ETM Collaboration with $N_f = 2 + 1 + 1$ dynamical quark flavors [12]. The Iwasaki gauge action [18] is used in combination with the Wilson twisted mass fermion discretization. There are three values of the lattice spacing available, with $\beta = 1.90$, $\beta = 1.95$, and $\beta = 2.10$ corresponding to $a \sim 0.089$ fm, $a \sim 0.082$ fm, and $a = 0.062$ fm, respectively. The lattice scale for the ensembles has been determined in Ref. [17] using f_π. Also in Ref. [17], the pseudoscalar renormalization constant Z_P, the inverse of which is the quark mass renormalization constant in the twisted mass approach, has been determined for each lattice spacing and then converted to the $\overline{\text{MS}}$ scheme at a scale of 2 GeV.

The computation of Z_P employs the RI-MOM renormalization scheme and further makes use of two different methods, which are labeled **M1** and **M2** by the authors. The two methods **M1** and **M2** give results which differ by lattice artifacts. As an intermediate length scale, we use the Sommer parameter r_0/a determined in Ref. [12] for each value of the light quark mass m_ℓ and extrapolate to the chiral limit in Ref. [17], assuming either a linear or quadratic dependence on the light quark mass. The value of r_0 in fm was determined in Ref. [17] using chiral perturbation theory (ChPT) employing methods **M1** and **M2** for Z_P, reading

$$\begin{aligned} r_0 &= 0.470(12)\ \text{fm} \qquad (\mathbf{M1}), \\ r_0 &= 0.471(11)\ \text{fm} \qquad (\mathbf{M2}). \end{aligned} \tag{1}$$

We keep the two values separate here, because we will use them to estimate systematic uncertainties. The values for Z_P, the lattice spacing a, and r_0/a are summarized in Table I for the three β values. For details, we refer to Ref. [17]. Note that μ_σ and μ_δ are kept fixed for all μ_ℓ values at $\beta = 1.90$ and $\beta = 1.95$. Between the two ensembles D30.48 and D45.32sc, they differ slightly.

TABLE I. Compilation of values for the Sommer parameter r_0/a, the lattice spacing a, and Z_P at 2 GeV in the $\overline{\text{MS}}$ scheme determined with methods **M1** and **M2** for three values of the lattice spacing. See Ref. [17] for details.

β	Z_P (**M1**)	Z_P (**M2**)	a [fm]	r_0/a
1.90	0.529(07)	0.574(04)	0.0885(36)	5.31(8)
1.95	0.509(04)	0.546(02)	0.0815(30)	5.77(6)
2.10	0.516(02)	0.545(02)	0.0619(18)	7.60(8)

In order to set the strange quark mass, we use M_K in physical units as input. We use $M_K^{\text{phys}} = 494.2(3)$ MeV, corrected for electromagnetic and isospin breaking effects [19].

As further inputs, we use the average up/down quark mass, $m_\ell^{\text{phys}} = 3.70(17)$ MeV, from Ref. [17], as well as the neutral pion mass, $M_{\pi^0}^{\text{phys}} = 134.98$ MeV [20].

In more detail, for the sea quarks we use the Wilson twisted mass action with $N_f = 2 + 1 + 1$ dynamical quark flavors. The Dirac operator for the light quark doublet reads [21]

$$D_\ell = D_{\text{W}} + m_0 + i\mu_\ell \gamma_5 \tau^3, \tag{2}$$

where D_{W} denotes the standard Wilson Dirac operator and μ_ℓ is the bare light twisted mass parameter. τ^3 and in general τ^i, $i = 1, 2, 3$ represent the Pauli matrices acting in flavor space. D_ℓ acts on a spinor $\chi_\ell = (u, d)^T$, and hence, the u (d) quark has twisted mass $+\mu_\ell$ ($-\mu_\ell$).

For the heavy doublet of c and s quarks [14], the Dirac operator is given by

$$D_{\text{h}} = D_{\text{W}} + m_0 + i\mu_\sigma \gamma_5 \tau^1 + \mu_\delta \tau^3. \tag{3}$$

The bare Wilson quark mass m_0 has been tuned to its critical value m_{crit} [12,22]. This guarantees automatic order-$\mathcal{O}(a)$ improvement [15], which is one of the main advantages of the Wilson twisted mass formulation of lattice QCD. For a discussion on how to tune to m_{crit}, we refer to Refs. [12,22].

The splitting term in the heavy doublet [Eq. (3)] introduces parity and flavor mixing between strange and charm quarks which would render the present analysis very complicated. For this reason, we rely in this paper on a mixed-action approach for the strange quark: in the valence sector, we use the so-called Osterwalder-Seiler (OS) discretization [23] with the Dirac operator

$$D_s^\pm = D_{\text{W}} + m_0 \pm i\mu_s \gamma_5, \tag{4}$$

with bare strange quark mass μ_s. Formally, this introduces two valence strange quarks with $\pm\mu_s$ as the bare quark mass. We will denote these two as $s^\pm$, and they will coincide in the continuum limit. Hence, observables computed using one or the other will differ by $\mathcal{O}(a^2)$ lattice artifacts. It was shown in Ref. [23] that $\mathcal{O}(a)$ improvement stays intact when m_0 is set to the same value m_{crit} as used in the unitary sector. For each β value, we choose a set of three bare strange quark masses $a\mu_s$, as listed in Table II. The mass values are chosen such as to bracket the physical strange quark mass independently of the light quark mass.

We remark here that in twisted mass lattice QCD, the quark masses renormalize multiplicatively with $1/Z_P$ [21]. Since OS and unitary actions agree in the chiral limit, the

TABLE II. Values of the bare strange quark mass $a\mu_s$ used for the three β values. The lightest strange quark mass on the ensemble D30.48 is $a\mu_s = 0.0115$ instead of $a\mu_s = 0.013$.

β	1.90	1.95	2.10
$a\mu_s$	0.0185	0.0160	0.013/0.0115
	0.0225	0.0186	0.015
	0.0246	0.0210	0.018

OS strange quark mass also renormalizes multiplicatively with $1/Z_P$.

A. Lattice operators and correlation functions

For the charged pion, we use the interpolating operator

$$\mathcal{O}_\pi(t) = \sum_{\mathbf{x}} \bar{u}(\mathbf{x}, t) i\gamma_5 d(\mathbf{x}, t) \tag{5}$$

projected to zero momentum. As an interpolating operator with the quantum numbers of the kaon, we use

$$\mathcal{O}_K(t) = \sum_{\mathbf{x}} \bar{s}^+(\mathbf{x}, t) i\gamma_5 d(\mathbf{x}, t) \tag{6}$$

projected to zero momentum. We use the combination of a strange quark with $+|\mu_s|$ and the down quark with $-|\mu_\ell|$, because it is known that observables employing this combination are subject to milder lattice artifacts compared to the combination with same signs. The corresponding two-point function reads

$$C_K(t - t') = \langle \mathcal{O}_K(t) \mathcal{O}_K^\dagger(t') \rangle, \tag{7}$$

and likewise the pseudoscalar two-point function C_π, with $\mathcal{O}_K$ replaced by $\mathcal{O}_\pi$. From the behavior of C_K (C_π) at large Euclidean time

$$C_K \propto \frac{1}{2}(e^{-M_K t} + e^{-M_K(T-t)}), \tag{8}$$

the kaon mass aM_K (aM_π) can be extracted. In order to compute the finite-volume energy shift $\delta E = E_{KK} - 2M_K$, needed in Lüscher's formula to obtain the scattering length a_0, we have to determine the energy of the two-kaon system in the interacting case. Using the isospin $I = 1$ operator

$$\mathcal{O}_{KK}(t) = \sum_{\mathbf{x},\mathbf{x}'} \bar{s}^+(\mathbf{x}, t) i\gamma_5 d(\mathbf{x}, t) \bar{s}^+(\mathbf{x}', t) i\gamma_5 d(\mathbf{x}', t), \tag{9}$$

one defines the correlation function

$$C_{KK}(t - t') = \langle \mathcal{O}_{KK}(t) \mathcal{O}_{KK}^\dagger(t') \rangle. \tag{10}$$

It shows a dependence on Euclidean time similar to C_K with the addition of a time-independent piece, the so-called thermal pollution:

$$C_{KK} \propto \frac{1}{2}(e^{-E_{KK} t} + e^{-E_{KK}(T-t)}) + \text{const.} \tag{11}$$

To determine δE from C_{KK}, we use a method which was devised in Ref. [8] for the $\pi\pi$ system with $I = 2$. In this method, we consider the ratio

$$R(t + 1/2) = \frac{C_{KK}(t) - C_{KK}(t+1)}{C_K^2(t) - C_K^2(t+1)}, \tag{12}$$

which can be shown to have the large Euclidean time dependence

$$R(t + 1/2) = A(\cosh(\delta E t') + \sinh(\delta E t') \coth(2E_K t')), \tag{13}$$

with $t' = t + 1/2 - T/2$ and amplitude A.

The kaon and pion masses are affected by (exponentially suppressed) finite size effects. The corresponding ChPT corrections $K_{M_\pi} = M_\pi(L)/M_\pi(L = \infty)$ and $K_{M_K} = M_K(L)/M_K(L = \infty)$ were determined from the data in Ref. [17], and we reuse these values, which are collected in Table IX. From here on, we only work with finite-size-corrected hadron masses:

$$aM_H^* := \frac{aM_H}{K_{M_H}},$$

for $H = \pi, K$, and we drop the asterisk to ease the notation.

B. Stochastic LapH

As a smearing scheme, we employ the so-called stochastic Laplacian-Heaviside (sLapH) method [24,25]. In this approach, the quark field under consideration is smeared with the so-called smearing matrix

$$S = V_S V_S^\dagger.$$

The matrices V_S are matrices obtained by stacking the eigenvectors of the lattice Laplacian,

$$\tilde{\Delta}^{ab}(x, y; U) = \sum_{k=1}^{3} \{\tilde{U}_k^{ab}(x)\delta(y, x + \hat{k}) + \tilde{U}_k^{ba}(y)^\dagger \delta(y, x - \hat{k}) - 2\delta(x, y)\delta^{ab}\}, \tag{14}$$

columnwise. The complete set of eigenvectors spans the so-called LapH space. The indices a,b denote different colors; the variables x,y space-time points; and $\tilde{U}$ (possibly smeared) $SU(3)$ gauge link matrices. The index S on V_S denotes a truncation of the eigenspectrum of $\tilde{\Delta}$ such that excited-state contaminations of the quark field are maximally suppressed. In addition, we smear the gauge fields appearing in Eq. (14) with three iterations of two-level

HYP smearing [26], with parameters $\alpha_1 = \alpha_2 = 0.62$. To build correlation functions, we denote quark lines connecting the source and sink time slices with

$$\mathcal{Q} = \mathcal{S}\Omega^{-1}\mathcal{S} = V_s(V_s^\dagger \Omega^{-1} V_s)V_s^\dagger, \tag{15}$$

where Ω^{-1} denotes the quark propagator and $\mathcal{P} = (V_s^\dagger \Omega^{-1} V_s)$ is called the perambulator. We use all-to-all propagators to calculate the correlation functions, which can get prohibitively expensive when done exactly. Therefore, we employ a stochastic method with random vectors diluted in time, Dirac space, and LapH subspace. Using the same notation as in Ref. [11], the all-to-all propagator then reads

$$\Omega^{-1} \approx \frac{1}{N_R}\sum_{r=1}^{N_R}\sum_b X^{r[b]}\rho^{r[b]\dagger}, \tag{16}$$

with the number of random vectors N_R and the compound index $r[b]$, counting the total number of random vectors and the total number of dilution vectors N_D. For the kaon correlation functions, we reuse the light quark propagators already calculated for the $\pi\pi$ paper, Ref. [11]. The number of dilution vectors for the light quark propagators, therefore, is the same. An exception is ensemble D30.48, which was not included in the $\pi\pi$ paper. For this volume of $L/a = 48$, the values for the several N_D are collected in Table III together with the values of N_D for the other lattice sizes. Concerning the newly calculated strange quark propagators, we adopted the same dilution scheme.

An investigation of the number of random vectors N_R yielded no further error reduction for the energy shift δE when increasing N_R from four to five random vectors for each strange quark perambulator. Thus, we decided to take four random vectors per strange quark perambulator into account for the current analysis.

III. ANALYSIS METHODS

A. Lüscher method

We are interested in the limit of small scattering momenta for the kaon-kaon system with $I = 1$ below the inelastic threshold. Very much like in the case of $\pi\pi$ scattering with $I = 2$, the scattering length a_0 can be related in the finite range expansion to the energy shift δE by an expansion in $1/L$ as follows [27]:

TABLE III. Summary of the number of dilution vectors, N_D, used in each index. We use a block scheme in time and an interlace scheme in eigenvector space.

$(L/a)^3 \times T/a$	N_D (time)	N_D (Dirac)	N_D (LapH)
$24^3 \times 48$	24	4	6
$32^3 \times 64$	32	4	4
$48^3 \times 96$	32	4	4

$$\delta E = -\frac{4\pi a_0}{M_K L^3}\left(1 + c_1\frac{a_0}{L} + c_2\frac{a_0^2}{L^2} + c_3\frac{a_0^3}{L^3}\right) - \frac{8\pi^2 a_0^3}{M_K L^6} r_f + \mathcal{O}(L^{-7}), \tag{17}$$

with coefficients [27,28]

$$c_1 = -2.837297, \quad c_2 = 6.375183, \quad c_3 = -8.311951.$$

Here, r_f is the effective range parameter. Equation (17) can be solved for the scattering length a_0/a given L/a, $a\delta E$, and aM_K if the terms up to $\mathcal{O}(1/L^5)$ are taken into account. This approach is valid only if the residual exponentially suppressed finite-volume effects are negligible compared to the ones related for δE. Moreover, by truncating Eq. (17) at $\mathcal{O}(1/L^5)$, one assumes that the effective range has no sizable contribution. We estimate the effect of this truncation in Appendix A and find it to be negligible.

B. Chiral and continuum extrapolations

The values of δE and a_0 are calculated for each combination of $a\mu_s$ and $a\mu_\ell$. In order to arrive at our final values for the scattering length, we need to perform interpolations in the strange quark mass, extrapolations in the light quark mass, and the continuum extrapolation. We adopt the following strategy: we will first tune the renormalized strange quark to its physical value for all β values and light quark masses. Next, we interpolate $M_K a_0$ in the strange quark mass for all ensembles to this value. The value for $M_K a_0$ obtained from this interpolation is finally extrapolated to the physical point and the continuum limit in a combined fit.

We use two different strategies, from here on denoted by **A** and **B**, to tune the renormalized strange quark mass to its physical value.

(A) As a strange quark mass proxy, we use

$$M_s^2 = M_K^2 - M_\pi^2/2, \tag{18}$$

which is directly proportional to the strange quark mass at leading order in ChPT. We interpolate $M_K a_0$ linearly in $(aM_s)^2$ to the value where M_s^2 assumes its physical value for each ensemble separately. This requires the physical value of M_K and M_π and the lattice spacing as an input. The bare strange quark mass is not explicitly used in this case.

(B) Here, we use the bare strange quark mass parameter μ_s explicitly. To determine the renormalized, physical value of the strange quark mass, we first perform a global fit of the NLO $SU(2)$ ChPT prediction for M_K^2

$$(aM_K)^2 = \frac{P_0}{P_r P_Z}(a\mu_\ell + a\mu_s)\left[1 + P_1\frac{P_r}{P_Z}a\mu_\ell + \frac{P_2}{P_r^2}\right]a \tag{19}$$

to all our data for aM_K simultaneously. Note that in $SU(2)$ ChPT, there are no chiral logarithms in M_K^2 predicted at NLO. Here we have three global fit parameters P_0, P_1, and P_2. In addition, we have β-dependent fit parameters $P_r(\beta)$ and $P_Z(\beta)$ for r_0/a and Z_P, respectively, which we constrain using Gaussian priors based on the determinations of these from Ref. [17].

Hence, we have in total nine fit parameters, for which we define the augmented χ^2 function:

$$\chi^2_{\text{aug}} = \chi^2 + \sum_\beta \left[\left(\frac{(r_0/a)(\beta) - P_r(\beta)}{\Delta r_0/a(\beta)} \right)^2 + \left(\frac{Z_P(\beta) - P_Z(\beta)}{\Delta Z_P(\beta)} \right)^2 \right]. \tag{20}$$

Using the best-fit parameters, $a\mu_s^{\text{ref}}$ can be determined from

$$a\mu_s^{\text{ref}} = \frac{(r_0 M_K^{\text{phys}})^2 P_Z}{P_r P_0 [1 + P_1 r_0 m_\ell^{\text{phys}} + P_2 P_r^{-2}]} - \frac{P_Z}{P_r}(r_0 m_\ell^{\text{phys}}) \tag{21}$$

using the input values specified before.

This allows us to interpolate $M_K a_0$ in $a\mu_s$ to the reference value $a\mu_s^{\text{ref}}$ for each ensemble separately. In the continuum limit, the physical value of the renormalized strange quark mass, $r_0 m_s^{\text{phys}}$, is then given by

$$r_0 m_s^{\text{phys}} = \frac{(r_0 M_K^{\text{phys}})^2}{P_0 [1 + P_1 r_0 m_\ell^{\text{phys}}]} - (r_0 m_\ell^{\text{phys}}). \tag{22}$$

In the following, we will denote the combination of **M1** with strategy **A** as **M1A** and likewise **M1B**, **M2A**, and **M2B**.

The values of $M_K a_0$ interpolated as explained above are now to be understood at fixed renormalized strange quark mass. The quark mass dependence of $M_K a_0$ is known from ChPT and is given at NLO [29–31] by

$$M_K a_0 = \frac{M_K^2}{8\pi f_K^2} \left[-1 + \frac{16}{f_K^2} \left(M_K^2 L' - \frac{M_K^2}{2} L_5 + \zeta \right) \right]. \tag{23}$$

Here, L_5 is a low-energy constant (LEC) and L' is a combination of LECs. ζ is a known function with chiral logarithms, which can be found in the references above. We can rewrite Eq. (23) in terms of the quark masses by replacing M_K^2 and f_K with their corresponding LO ChPT expressions. Note that we use the convention with $f_\pi = 130$ MeV.

As we will see later, our data for $M_K a_0$ are not sufficiently precise to resolve terms beyond leading order, in contrast to M_K^2. Including lattice artifacts of order a^2, we therefore resort to the following effective fit ansatz for $M_K a_0$ linear in μ_ℓ and a^2:

$$M_K a_0 = Q_0 \frac{P_r}{P_Z} a\mu_\ell + Q_1 \frac{1}{P_r^2} + Q_2, \tag{24}$$

with three free fit parameters Q_0, Q_1, and Q_2. The continuum and chiral limit for $M_K a_0$ is then given by

$$(M_K a_0)^{\text{phys}} = Q_0 r_0 m_\ell^{\text{phys}} + Q_2.$$

For the fit, we use again an augmented χ^2 like in Eq. (20) to take the errors on r_0/a and Z_P into account.

All errors are computed using the (chained) bootstrap with 1500 bootstrap samples. Values not determined by ourselves—e.g., for r_0/a or Z_P—are included in the bootstrap analysis using the parametric bootstrap. Where relevant, fits are fully correlated. The configurations used are well separated in HMC trajectories, and we have checked explicitly for autocorrelation using a blocked bootstrap.

IV. RESULTS

In this section, we present the results for the energy shift δE, the scattering length a_0, and the chiral and continuum extrapolations of $M_K a_0$. From the four approaches **M1A**, **M1B**, **M2A**, and **M1B** we obtain four values for $M_K a_0$, which we combine into our final result. The spread between the four values is used to estimate the systematic uncertainty.

A. Energy shift δE

The energy shift is calculated by fitting Eq. (13) to the data of the ratio defined in Eq. (12). Because of the cosh-like behavior of C_K and C_{KK}, we symmetrize the correlation functions. For the kaon masses we use the results of fully correlated fits to the two-point correlation function [Eq. (8)]. We repeat our fits for multiple fit ranges for each correlation function. The systematic uncertainties of the fitting procedures are then estimated using the approach introduced in Ref. [11]. The energy value is determined as the median of the weighted distribution over the fit ranges. The weight assigned to each fit reads

$$w_X = [(1 - 2|p_X - 0.5|^2) \cdot \min(\Delta X)/\Delta X]^2, \tag{25}$$

where $X = E_K, \delta E$. p_X is the p value of the fit and ΔX denotes the statistical uncertainty of the considered quantity $\langle X \rangle$. An estimate of the systematic uncertainty is then calculated from the 68.54% confidence interval of the weighted distribution of X. The statistical error comes from bootstrapping this procedure.

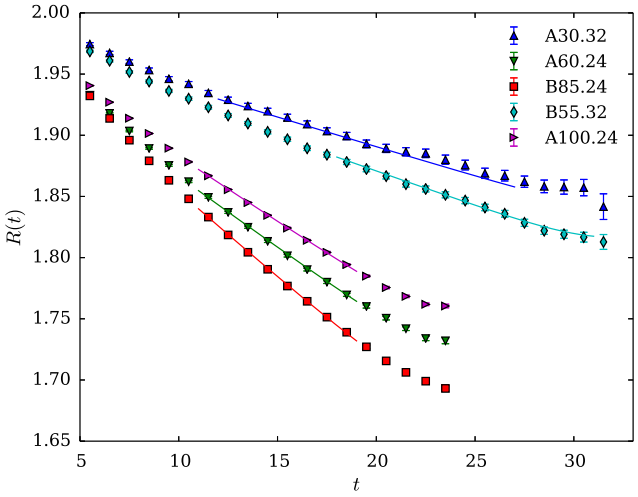

FIG. 1. Representative fits of Eq. (13) to the ratio data for different ensembles at the lowest value of $a\mu_s$.

In order to choose the fit ranges for obtaining M_K from C_K and δE from R, we require several criteria to be fulfilled. Concerning the initial time slice t_i, we demand that the excited states in both C_K and R be sufficiently decayed away. For C_K, we visually inspect the effective mass. Since C_K does not suffer from exponential error growth at late times, we set $t_f = T/2$. Thus, we vary t_i and t_f within the constraints above. In the case of the ratio, t_f is set to the time slice where R starts to deviate significantly from the behavior suggested by Eq. (13). The minimal number of time slices for a fit range is chosen with the same criterion as for C_K. The values of t_i, t_f, and t_{min} for C_K and R are compiled in Tables X–XII for each value of $a\mu_s$ in Appendix B.

In Fig. 1, we show exemplary fits of the ratio in Eq. (13) to the data for several ensembles and selected fit ranges. At least for the ensembles with $L = 24$, the tendency of an upward bend of the data at late times can be seen clearly.

As mentioned before, for Eq. (17) to be valid, residual exponentially suppressed finite-volume effects must be negligible. Moreover, the terms in Eq. (17) of order $1/L^6$ and higher must be negligible. We can test the latter for ensembles A40.20, A40.24, and A40.32, which differ only in volume. In Fig. 2, we plot δE as a function of $1/L$ for these three ensembles and $a\mu_s = 0.0185$. The other two μ_s values give similar results. We have solved Eq. (17) including all terms up to order $1/L^6$ for a_0 and r_f using A40.24 and A40.32 only, the result of which is shown as the solid line with error band in the left panel of the figure. It leads to $M_K a_0 = -0.292(20)$. Including also A40.20, we perform a two-parameter fit with three data points, finding $M_K a_0 = -0.318(9)$. The corresponding fit is shown in the right panel of the figure. Leaving out the effective range term at order $1/L^6$ results in unreasonably large χ^2 values.

Noting that solving Eq. (17) up to order $1/L^5$ for a_0 for ensemble A40.32 gives $M_K a_0 = -0.315(11)$, which agrees within error with the two estimates from above, we conclude that $L/a = 32$ is sufficiently large, while $L/a = 24$ is at the border. $L/a = 20$ is certainly too small to extract $M_K a_0$ from a single volume neglecting the effective range term.

We check the impact of the inclusion of r_f on the extraction of $M_K a_0$ in Appendix A. With a LO ChPT estimation of r_f included in the extraction of a_0, the values for $M_K a_0$ vary by about 1 standard deviation. The central values for the $L/a = 24$ lattices change by about 1% on the inclusion of the order-$1/L^6$ terms (cf. Table VIII). Thus, we quote as our chiral and continuum extrapolated result $M_K a_0$ at $\mathcal{O}(1/L^5)$ and attribute to it a conservatively estimated systematic uncertainty of 1%.

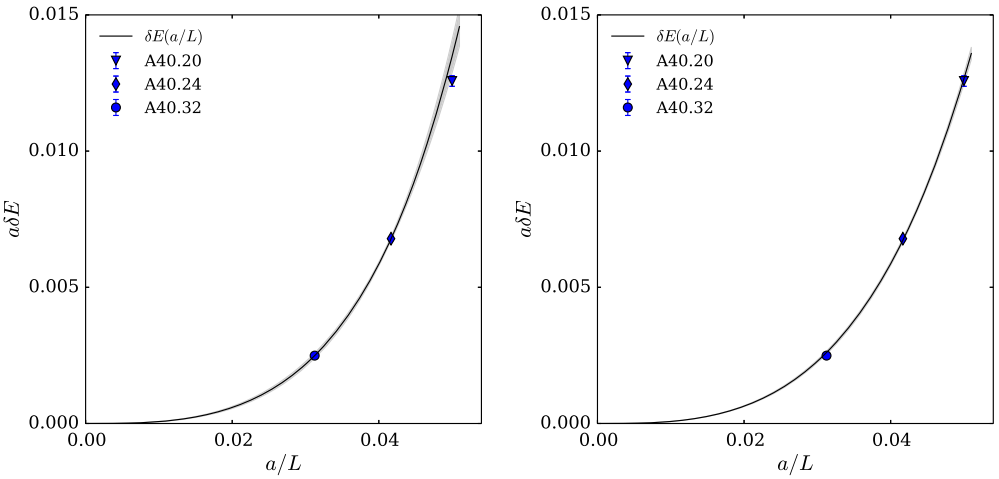

FIG. 2. δE as a function of $1/L$ for ensemble A40.32 with $a\mu_s = 0.0185$. In the left panel, we show as the solid line the solution of Eq. (17) for a_0 and r_f given the two data points with the largest L. In the right panel, the solid line represents a fit of Eq. (17) to all three data points.

TABLE IV. Physical values of M_s^2 for the three β values. The stated values correspond to the continuum values of $(r_0 M_s^{\rm phys})^2$ equal to 1.33(7) and 1.34(6) for Z_P from **M1** and **M2**, respectively.

β	$(aM_s^{\rm phys})^2$ (**M1**)	$(aM_s^{\rm phys})^2$ (**M2**)
1.90	0.0473(28)	0.0475(26)
1.95	0.0400(22)	0.0402(20)
2.10	0.0231(12)	0.0232(11)

B. Scattering length

Given the values of $a\delta E$ and aM_K, the scattering length a_0 is determined using Eq. (17).

The number of fit ranges for extracting $a\delta E$ is low, compared to the $\pi\pi$ case of Ref. [11]. Thus, an estimate of the systematic effects stemming from the fitting procedure is likely to be incorrect. Therefore, instead of estimating the systematic uncertainty introduced by the fitting procedure after the chiral extrapolations, we consider the p-value weighted median over the fit ranges. This procedure is further supported by the fact that the statistical uncertainties of $M_K a_0$ do not essentially differ from the uncertainties obtained by adding statistical and systematic uncertainties in quadrature. The final results for aM_K, $a\delta E$, a_0/a, and $M_K a_0$ are compiled in Tables XV–XVII for all ensembles. The chiral and continuum extrapolations are carried out using only the largest of the A40 ensembles, A40.32, because it has the smallest finite-volume effects.

C. Strategies M1A and M2A: $M_K a_0$ from fixed M_s^2

To evaluate $M_K a_0$ at the physical strange quark mass, we convert M_s^2 to lattice units using r_0/a listed in Table I. First, we express M_s^2 in units of r_0 using the estimates in Eq. (1), which gives $(r_0^{\rm M1} M_s^{\rm phys})^2 = 1.33(7)$ with Z_P from **M1** and $(r_0^{\rm M2} M_s^{\rm phys})^2 = 1.34(6)$ with Z_P from **M2**. In lattice units at our three lattice spacings, these correspond to the values given in Table IV.

For each ensemble, we then interpolate $M_K a_0$ by performing a correlated linear fit to the data at the three values of $a\mu_s$ (the independent variable being $a^2 M_s^2$). An example of this is given in Fig. 6 in Appendix B.

Having interpolated $M_K a_0$ on all ensembles, the data is extrapolated to the physical point and to the continuum in a global fit using Eq. (24). In Fig. 3, the dimensionless product $M_K a_0$ is shown as a function of $r_0 m_\ell$ together with the global fit for each value of β for **M1A** in the left panel and for **M2B** in the right panel. Note that we take into account all correlation between data which enters through the procedure for fixing the strange quark mass at each value of the lattice spacing. The results of the fits can be found in Table V.

D. Strategies M1B and M2B: $M_K a_0$ from fixed m_s^R

Analysis B involves as a first step a global fit of Eq. (19) to the values of aM_K. As an example, the fits to the data of the A ensembles are shown in Appendix B in Fig. 7 for Z_P from **M1** (left panel) and **M2** (right panel).

The fit takes into account the correlation between data at different values of $a\mu_s$ but the same $a\mu_\ell$ value. The results of the global fits are compiled in Tables XIII and XIV. The fitted parameters allow us to calculate the renormalized strange quark mass, $m_s^{\rm phys}$, from Eq. (22). As input, we use r_0 from Eq. (1), Z_P from Table I, $m_\ell^{\rm phys}$, and $M_K^{\rm phys}$.

For the physical values of the strange quark mass at 2 GeV in the $\overline{\rm MS}$ scheme, we find

$$m_s^{\rm phys} = 101.3(4.7)\ \text{MeV3} \qquad (\textbf{M1B}),$$
$$m_s^{\rm phys} = 99.4(4.4)\ \text{MeV} \qquad (\textbf{M2B}). \tag{26}$$

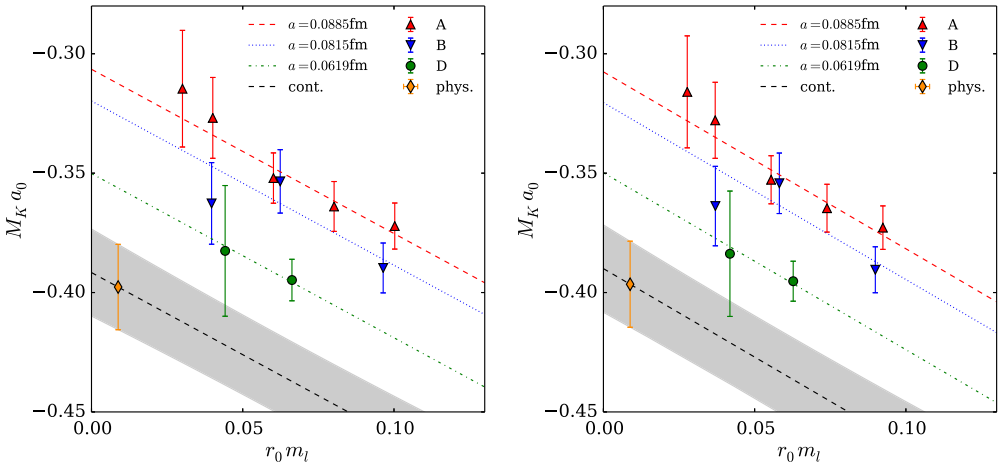

FIG. 3. Chiral and continuum extrapolation of $M_K a_0$ to the physical point as a function of the light quark mass for **M1A** in the left panel and **M2A** in the right panel. The three lattice spacings and the best-fit curves are color-encoded. The black dashed line shows the continuum curve with the physical point result indicated by the diamond.

TABLE V. Physical values for $M_K a_0$ obtained from the global fit of Eq. (24) to the data from the different approaches. We also give the χ^2 and p values of the fit together with the best-fit parameters Q_0–Q_2.

	M1A	**M2A**	**M1B**	**M2B**
$(M_K a_0)^{\text{phys}}$	−0.398(18)	−0.397(18)	−0.389(18)	−0.384(16)
χ^2/d.o.f.	2.23/7	2.43/7	3.07/7	4.94/7
p value	0.95	0.93	0.88	0.67
Q_0	−0.69(12)	−0.74(12)	−0.67(12)	−0.70(12)
Q_1	2.4(6)	2.3(7)	2.0(6)	1.7(6)
Q_2	−0.39(2)	−0.39(2)	−0.38(2)	−0.38(2)

TABLE VI. Values of $a\mu_s$ corresponding to the renormalized physical strange quark mass in lattice units for the three values of β calculated from Eq. (21).

β	$a\mu_s^{\text{ref}}$ (**M1**)	$a\mu_s^{\text{ref}}$ (**M2**)
1.90	0.0202(12)	0.0204(11)
1.95	0.0182(10)	0.0181(9)
2.10	0.0150(8)	0.0151(8)

These values compare well to the corresponding results from Ref. [17]:

$$m_s^{\text{ETMC}} = 101.6(4.4)\ \text{MeV} \qquad (\textbf{M1}),$$
$$m_s^{\text{ETMC}} = 99.0(4.4)\ \text{MeV} \qquad (\textbf{M2}).$$

We can convert the values from Eq. (26) to lattice units for the three β values, which we compiled in Table VI. Next, we interpolate $M_K a_0$ in $a\mu_s$ to these values for all ensembles. As an example, we show the linear correlated fit for ensemble B55.32 in Appendix B in Fig. 8 for **M1B** in the left panel and for **M2B** in the right panel.

Interpolated to the reference strange quark mass, the values of $M_K a_0$ are shown as a function of the renormalized light quark mass in Fig. 4 in units of r_0. We also show the best-fit function for each β value and the continuum extrapolation. The continuum-extrapolated values at the physical point $(M_K a_0)^{\text{phys}}$ are indicated by the diamonds. Note again that due to the strange quark mass fixing procedure, all points for a single lattice spacing are correlated.

In Table V, we give our final results for $(M_K a_0)^{\text{phys}}$ for the four different approaches **M1A**, **M2A**, **M1B**, and **M2B** together with the best-fit parameters $Q_{1,2,3}$, the χ^2/d.o.f., and the p value of the fit.

As the final result, we quote the p-value weighted median over the four determinations:

$$M_K a_0 = -0.385(16)_{\text{stat}}\binom{+0}{-12}_{m_s}\binom{+0}{-5}_{Z_P}(4)_{r_f}. \qquad (27)$$

The statistical uncertainty comes from the bootstrap procedure. The systematic uncertainty coming from the two methods to estimate Z_P is estimated as follows: we first compute the weighted average of only **M1A** and **M1B**, and also that of only **M2A** and **M2B**. The systematic uncertainty is then taken as the deviation between these two weighted averages and the final result, Eq. (27). For the systematic uncertainty from setting the strange quark mass we proceed in the same way, except that we first compute the weighted average of only **M1A** and **M2A**, and also that of only **M1B** and **M2B**. As the last error, we quote the systematic uncertainty from neglecting higher-order terms in the calculation of the scattering length. Using M_K^{phys}, we obtain for the scattering length

$$a_0 = -0.154(6)_{\text{stat}}\binom{+0}{-5}_{m_s}\binom{+0}{-2}_{Z_P}(2)_{r_f}\ \text{fm}. \qquad (28)$$

V. DISCUSSION

We have used four methods to determine $M_K a_0$ at the physical light and strange quark mass value in the continuum limit. The differences between these methods are

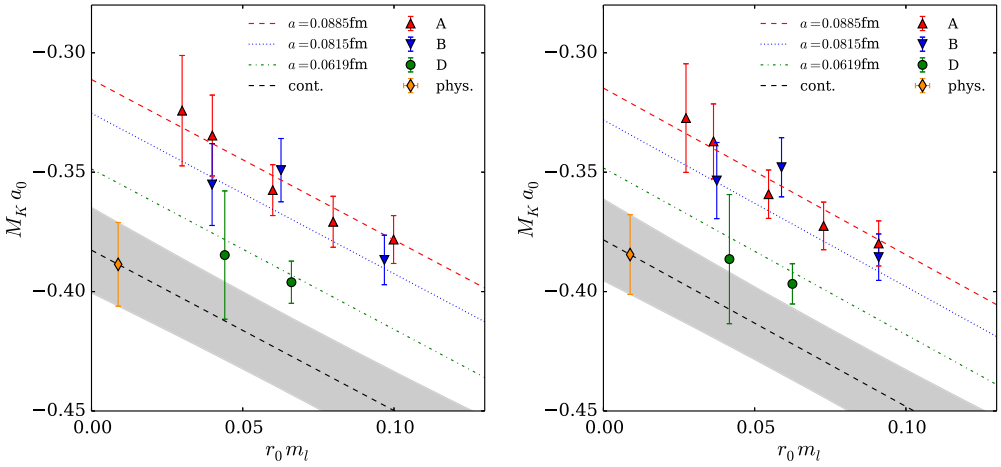

FIG. 4. Same as Fig. 3, but for **M1B** (left panel) and **M2B** (right panel).

lattice artifacts. From Table V, it becomes clear that all four methods give results which are well compatible within statistical uncertainties. This gives us confidence in our procedure and in our final result [Eq. (27)]. The four different estimates can still serve as an estimate of systematic effects, which are, however, smaller than the statistical uncertainty of about 4%. The largest fraction of this statistical uncertainty stems from the uncertainty in the scale.

It turns out that lattice artifacts are not negligible in $M_K a_0$: from $\beta = 1.90$ to the continuum, a roughly 20% relative change in the result is observed. From our finest lattice spacing we still see a change of about 8%. It is interesting to note that our central value equals, within errors, the LO ChPT estimate

$$(M_K a_0)^{\mathrm{LOChPT}} = -\frac{M_K^2}{8\pi f_K^2} = -0.385.$$

A possibly still uncontrolled systematic uncertainty could come from our chiral and continuum extrapolation. In lattice ChPT, usually the a^2 term is taken to be of higher order than the term linear in μ_ℓ. For this we would need to include higher orders in the quark mass as well. However, the precision in our data is not sufficient to resolve such terms. But the need for the a^2 term is evident. Therefore, we decided to stick to a power counting with $a^2 \propto \mu_\ell$. An alternative and probably better chiral representation of $M_K a_0$ in terms of M_K/f_K was used in Ref. [3]. This representation turned out to be not feasible for us, because we have only very little spread in M_K/f_K. Smaller uncertainties on $M_K a_0$ might enable the investigation of the light and strange quark mass dependence using mixed-action ChPT at NLO.

We also cannot estimate the effects from partial quenching of the strange quark. However, it should be noted that the kaon masses that we obtain in the OS valence sector at the physical strange quark mass, as set via either method **A** or **B**, deviate from those of the unitary kaon mass published in Ref. [32] by a few percent at most. Partial quenching effects in analyses using OS valence fermions on a $N_f = 2 + 1 + 1$ twisted mass sea have been shown to be small for other observables in the past. Moreover, we would like to remark that the dependence of $M_K a_0$ on μ_s is not very pronounced. Finally, our estimate in Appendix A indicates that the $\mathcal{O}(L^{-6})$ terms in the Lüscher formula [Eq. (17)] are indeed negligible for our case. Nevertheless, we do not have a sufficient number of volumes available to determine it from the data.

Two other lattice calculations of $M_K a_0$ are available. The NPLQCD Collaboration used three-flavor mixed action ChPT to obtain $M_K a_0 = -0.352(16)$, with statistical and systematic uncertainties combined in quadrature [3]. They worked with domain-wall valence quarks on a sea of $N_f = 2 + 1$ asqtad-improved rooted staggered quarks. A second calculation was performed by the authors of Ref. [4] with $N_f = 2 + 1$ dynamical flavors of nonperturbatively $O(a)$-improved Wilson quarks. Their result reads $M_K a_0 = -0.310(17)(32)$. The discrepancy between these determinations and our final result, Eq. (27), is quite substantial. In the NPLQCD determination, predominantly one lattice spacing of $a = 0.125$ fm was considered in the chiral extrapolation. One ensemble with a finer lattice spacing was included in the analysis to attempt a quantification of discretization errors, but it should be noted that the uncertainty on this point was about a factor of 3 larger than on all other points in the analysis. The PACS-CS Collaboration used only one lattice spacing value with $a \sim 0.09$ fm, very close to our coarsest lattice spacing value. PACS-CS included one ensemble with $M_\pi = 170$ MeV in their analysis, which is, however, giving very noisy results. Both collaborations use one strange quark mass value which was tuned to be close to physical.

In Fig. 5, we compare our result at the coarsest lattice spacing—i.e., the A ensembles, interpolated to the physical strange quark mass with method **M1A**—to the results of the other two collaborations. There is no obvious conclusion from this comparison. But the errors of the PACS-CS results appear to be large enough to explain the observed differences, given the fact that the PACS-CS result is at one lattice spacing value only. The comparison to the NPLQCD data points is more difficult, in particular since the one NPLQCD point with a finer lattice spacing points towards an even smaller absolute value for $M_K a_0$, though with a large statistical uncertainty. This can only be resolved with continuum extrapolations for the other formulations. However, the NPLQCD and our result agree within 2 standard deviations.

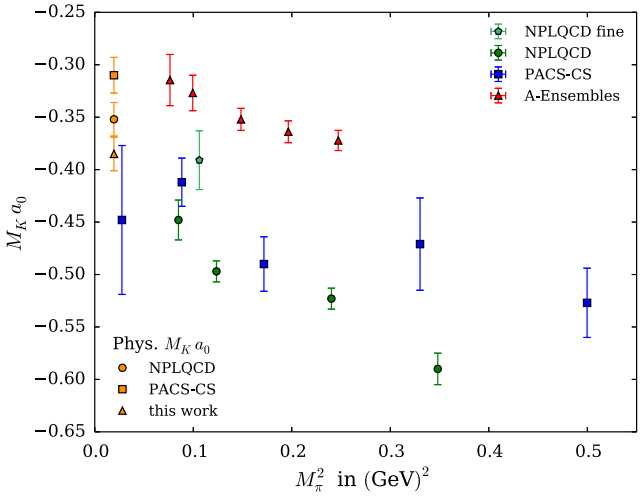

FIG. 5. $M_K a_0$ as a function of M_π^2. We show our results at the coarsest lattice spacing value for method **M1A** together with the results of NPLQCD [3] and PACS-CS [4], with the orange circle and square indicating the respective final results. The orange triangle shows our final result.

VI. SUMMARY

We investigated the scattering length of the $K^+ - K^+$ system by means of finite-volume methods for lattice QCD devised by M. Lüscher. The lattice formulation is Wilson twisted mass lattice QCD at maximal twist and $N_f = 2 + 1 + 1$ dynamical quark flavors. The gauge configurations, involving 11 pion masses at three different lattice spacings, were generated by the ETMC. To the author's knowledge, our result represents the first study of the $K^+ - K^+$ system controlling lattice artifacts using three lattice spacing values and up/down, strange, and charm dynamical quarks. For the strange quark, we used a mixed action approach with so-called Osterwalder-Seiler valence strange quarks to be able to correct for a slight mistuning of the sea strange quark mass value.

In total, we followed four different strategies to arrive at the continuum-extrapolated value for $M_K a_0$ at physical light and strange quark masses. All four show very good agreement, indicating that the corresponding extrapolations are well controlled. Our final result for the scattering length is

$$M_K a_0 = -0.385(16)_{\text{stat}} \binom{+0}{-12}_{m_s} \binom{+0}{-5}_{Z_P} (4)_{r_f}$$

from the weighted median over the four strategies. In our calculation, we find that the continuum extrapolation is vital in obtaining the final number: from the coarsest to the continuum result, we observe a roughly 20% difference. We think that this is also the reason for the discrepancy we observe when comparing to the two previous lattice calculations of $M_K a_0$, because for the other two results a continuum extrapolation could not be performed.

In the near future, we will extend the analysis performed here to the pion-kaon case.

ACKNOWLEDGMENTS

We thank the members of ETMC for their most enjoyable collaboration. The computer time for this project was made available to us by the John von Neumann Institute for Computing (NIC) on the Jureca and Juqueen systems in Jülich. We thank A. Rusetsky for very useful discussions. We thank S. Simula for the estimates of the finite size corrections to M_π and M_K. This project was funded by the Deutsche Forschungsgemeinschaft as a project in the Sino-German CRC110. The open source software packages tmLQCD [33–35], LEMON [36], Eigen [37], Boost [38], SciPy [39] and R [40] have been used. In addition, we employed QUDA [41,42] for calculating propagators on GPUs.

APPENDIX A: EFFECTIVE RANGE FROM CHPT

We start from the partial wave expansion for the scattering amplitude $T^I(s,t,u)$ [43]:

$$T^I(s,t,u) = 32\pi \sum_{\ell=0}^{\infty} (2\ell+1) P_\ell(\cos\vartheta) t_\ell^I(s), \tag{A1}$$

which depends on the Legendre polynomials $P_\ell(\cos\vartheta)$ and the partial wave amplitudes $t_\ell^I(s)$. The amplitudes $t_\ell^I(s)$ can be expanded in terms of the scattering momentum q and the slope parameters:

$$\text{Re}t_\ell^I = q^{2\ell}(a_\ell^I + q^2 b_\ell^I + \mathcal{O}(q^4)). \tag{A2}$$

Since we are interested in maximal isospin and the s wave, we take $I = 1$ and $\ell = 0$. This yields

$$t_0^1(s) = \frac{T^1(s,t,u)}{32\pi}. \tag{A3}$$

In Ref. [43], $T(s,t,u)$ for $K^+K^- \to K^+K^-$ is given to leading order by

$$T(s,t,u) = \frac{2M_K^2 - u}{f_\pi^2}. \tag{A4}$$

To turn this into an amplitude valid for K^+K^+ scattering, we employ crossing symmetry, which interchanges the Mandelstam variables s and u. With that, the partial wave amplitude becomes

$$t_0^I(s) = \frac{1}{32\pi}\frac{2M_K^2 - s}{f_\pi^2} = \frac{1}{32\pi}\frac{-2M_K^2 - 4q^2}{f_\pi^2}, \tag{A5}$$

where we express s with the momentum transfer q: $s = 4(M_K^2 + q^2)$. Expanding Eq. (A5) in a Taylor series gives

$$\text{Re}t_0^1(q) = -\frac{M_K^2}{16\pi f_\pi^2} - \frac{q^2}{8\pi f_\pi^2}. \tag{A6}$$

Comparing Eq. (A6) with Eq. (A2), we can extract b_0^1 and use $r_f = -2M_K b_0^1$ to get

$$r_f = \frac{M_K}{4\pi f_\pi^2}. \tag{A7}$$

To estimate the effective range, we use the physical value of the kaon mass $M_K = 494.2$ MeV and the ChPT value $f_\pi = 94.2$ MeV. Converting to a length unit with $\hbar c = 197.37$ MeV fm gives

$$r_f = 0.91 \text{ fm}.$$

We can use this to estimate the influence of the $\mathcal{O}(L^{-6})$ terms on the determination of the scattering length a_0 from Lüscher's formula. To this end, we compare the results for the scattering length up to order $\mathcal{O}(L^{-5})$ to the ones of up to order $\mathcal{O}(L^{-6})$ with and without the term involving the effective range. Table VII gives an overview of these differences. For converting r_f back to lattice units,

TABLE VII. Comparison of the scattering lengths of ensembles with different volumes and light quark masses determined from Lüscher's formula to $\mathcal{O}(L^{-7})$ and $\mathcal{O}(L^{-6})$ without the effective range term, at the lowest value of $a\mu_s$.

Ensemble	a_0 at $\mathcal{O}(L^{-6})$	a_0 at $\mathcal{O}(L^{-5})$
A60.24	−1.405(18)	−1.393(18)
A80.24	−1.412(14)	−1.400(14)
A100.24	−1.390(12)	−1.379(12)
B85.24	−1.592(20)	−1.572(19)
A40.32	−1.350(46)	−1.346(46)
D30.48	−2.143(13)	−2.130(12)

TABLE VIII. Comparison of $M_K a_0$ with different orders of L taken into account for determining a_0. The data shown are the p-value weighted medians over all fit ranges for δE at the lowest value of $a\mu_s$.

Ensemble	$M_K a_0$ to $\mathcal{O}(L^{-6})$	$M_K a_0$ to $\mathcal{O}(L^{-5})$
A60.24	−0.344(5)	−0.341(4)
A80.24	−0.360(4)	−0.357(3)
A100.24	−0.367(3)	−0.364(3)
B85.24	−0.368(5)	−0.363(4)
A40.32	−0.316(11)	−0.315(11)
D30.48	−0.322(19)	−0.320(18)

we use parametric bootstrap samples of the lattice spacing a. In Table VIII, the results for $M_K a_0$ for a_0 up to $\mathcal{O}(L^{-6})$ and a_0 truncated at $\mathcal{O}(L^{-5})$ are compared. As is visible from the table, the inclusion of the terms to order $\mathcal{O}(L^{-6})$ in the determination of the scattering length does not change the values of $M_K a_0$ beyond 1 standard deviation.

APPENDIX B: DATA TABLES AND PLOTS

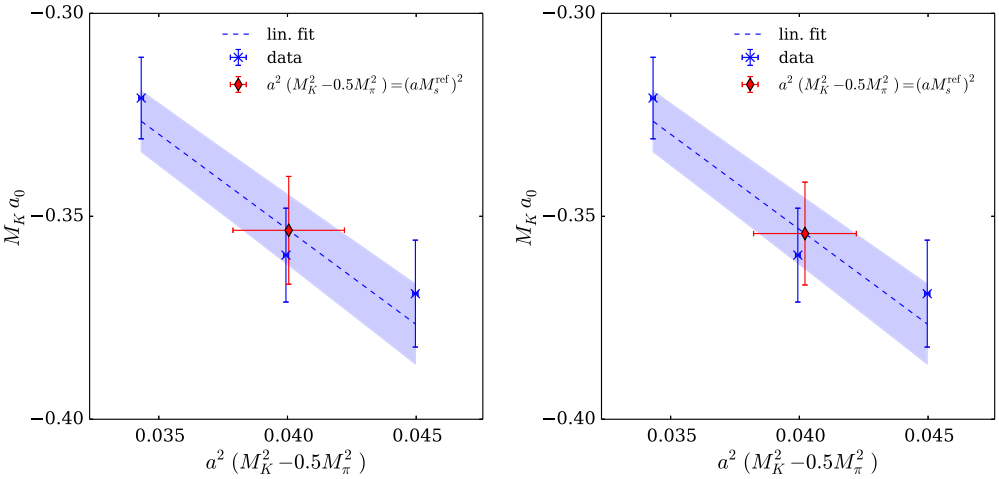

FIG. 6. $M_K a_0$ as a function of M_s^2 for ensemble B55.32 for **M1A** in the left and **M2A** in the right panel. The data are shown as crosses. The dashed line with the error band represents the linear fit. The interpolated value is indicated by the diamond.

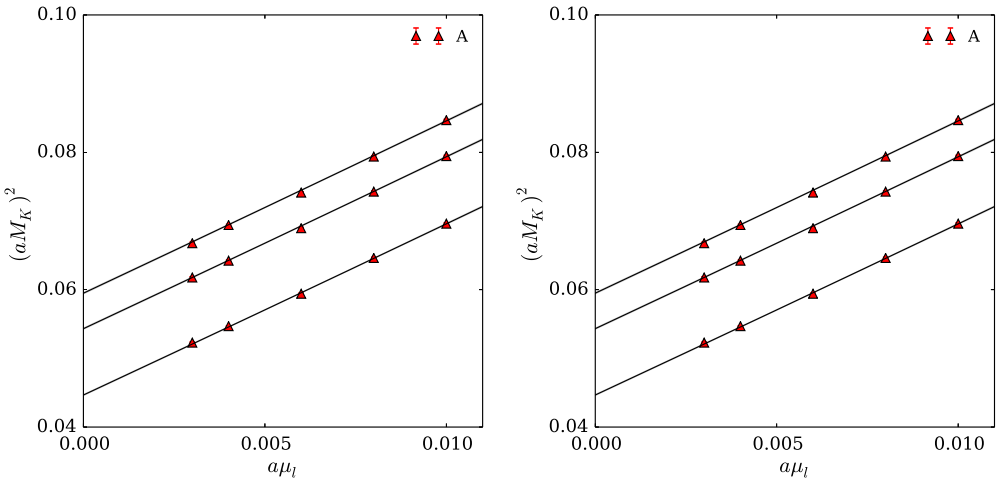

FIG. 7. M_K^2 as a function of $a\mu_\ell$ for **M1B** (left panel) and **M2B** (right panel) for all ensembles at $\beta = 1.90$. The lines represent the best fit of Eq. (19) to the data. The three lines in each plot correspond to the three values of $a\mu_s$.

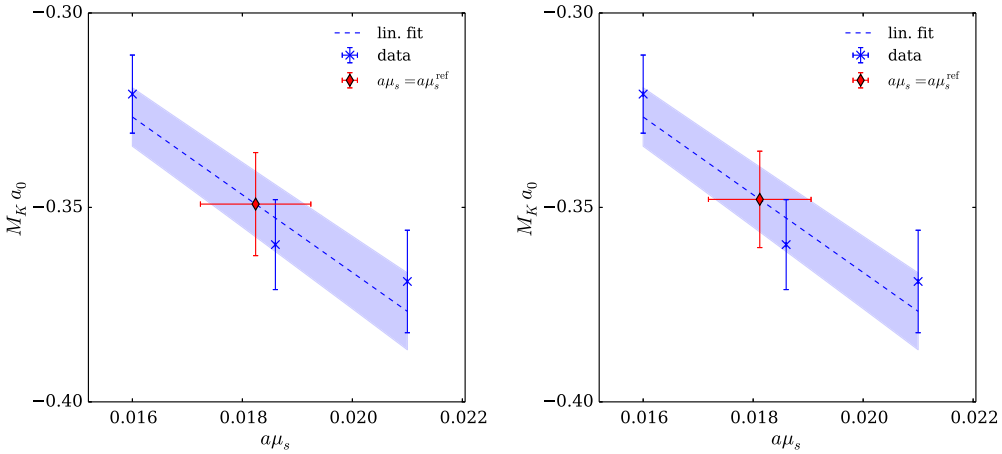

FIG. 8. $M_K a_0$ as a function of $a\mu_s$ for ensemble B55.32 for **M1B** in the left and **M2B** in the right panel. The line with the error band represents the best fit, and the interpolated result is indicated by the diamond.

TABLE IX. Single-pion energy levels from Refs. [12,13] and the finite size correction factors K_{M_π} and K_{M_K} computed in Ref. [17] for M_π and M_K, respectively. The statistical uncertainty of K_{M_K} is only estimated. Where not given, K_{M_K} is set to 1.

Ensemble	aM_π	K_{M_π}	K_{M_K}
A30.32	0.12395(36)(14)	1.0081(52)	0.9954(1)
A40.32	0.14142(27)(42)	1.0039(28)	0.9974(1)
A60.24	0.17275(45)(23)	1.0099(49)	0.9907(1)
A80.24	0.19875(41)(35)	1.0057(29)	0.9950(1)
A100.24	0.22293(35)(38)	1.0037(19)	0.9970(1)
B35.32	0.12602(30)(30)	1.0069(32)	0.9951(1)
B55.32	0.15518(21)(33)	1.0027(14)	0.9982(1)
B85.24	0.19396(38)(54)	1.0083(28)	0.9937(1)
D30.48	0.09780(16)(32)	1.0021(7)	0.9986(1)
D45.32	0.12070(30)(10)	1.0047(14)	1.0000(1)

TABLE X. Fit ranges for the lowest value of $a\mu_s$ for the kaon correlation function C_K and the ratio R. The interval $[t_i, t_f]$ denotes the lowest and largest time slice considered in the fits; t_{min} is the minimal extent of each fit range.

		C_K		R	
Ensemble	$a\mu_s$	$[t_i, t_f]$	t_{min}	$[t_i, t_f]$	t_{min}
A30.32	0.0185	[12, 32]	7	[12, 32]	10
A40.24	0.0185	[12, 24]	5	[11, 24]	7
A40.32	0.0185	[15, 32]	7	[12, 32]	10
A60.24	0.0185	[12, 24]	5	[11, 24]	7
A80.24	0.0185	[12, 24]	5	[11, 24]	7
A100.24	0.0185	[12, 24]	5	[11, 24]	7
B35.32	0.0160	[15, 32]	7	[12, 32]	10
B55.32	0.0160	[15, 32]	7	[14, 32]	10
B85.24	0.0160	[12, 24]	5	[11, 24]	7
D30.48	0.0115	[16, 48]	15	[8, 41]	15
D45.32	0.0130	[15, 32]	7	[12, 32]	10

TABLE XI. Same as Table X, but for the medium value of $a\mu_s$.

		C_K		R	
Ensemble	$a\mu_s$	$[t_i, t_f]$	t_{min}	$[t_i, t_f]$	t_{min}
A30.32	0.0225	[12, 32]	5	[12, 29]	10
A40.24	0.0225	[12, 24]	5	[11, 24]	7
A40.32	0.0225	[15, 32]	7	[12, 32]	10
A60.24	0.0225	[12, 24]	5	[11, 24]	7
A80.24	0.0225	[12, 24]	5	[11, 24]	7
A100.24	0.0225	[12, 24]	5	[11, 24]	7
B35.32	0.0186	[15, 32]	7	[12, 32]	10
B55.32	0.0186	[15, 32]	7	[14, 32]	10
B85.24	0.0186	[12, 24]	5	[11, 24]	7
D30.48	0.0150	[16, 48]	15	[8, 41]	15
D45.32	0.0150	[15, 32]	7	[12, 32]	10

TABLE XII. Same as Table X, but for the highest value of $a\mu_s$.

		C_K		R	
Ensemble	$a\mu_s$	$[t_i, t_f]$	t_{min}	$[t_i, t_f]$	t_{min}
A30.32	0.02464	[12, 32]	5	[12, 32]	10
A40.24	0.02464	[12, 24]	5	[11, 24]	7
A40.32	0.02464	[15, 32]	7	[12, 32]	10
A60.24	0.02464	[12, 24]	5	[11, 24]	7
A80.24	0.02464	[12, 24]	5	[11, 24]	7
A100.24	0.02464	[12, 24]	5	[11, 24]	7
B35.32	0.0210	[15, 32]	7	[12, 32]	10
B55.32	0.0210	[15, 32]	7	[14, 32]	10
B85.24	0.0210	[12, 24]	5	[11, 24]	7
D30.48	0.0180	[16, 48]	15	[8, 41]	15
D45.32	0.0180	[15, 32]	7	[12, 32]	10

TABLE XIII. Parameters from the global fit of Eq. (19) to aM_K^2 with parameters from **M1**.

β	P_Z	P_r	$\bar{P}_0$	P_1	P_2	χ^2/d.o.f.
1.90	0.524(7)	5.22(6)				
1.95	0.512(4)	5.84(5)	5.53(20)	0.14(3)	5.21(1.61)	6.82
2.10	0.516(2)	7.57(8)				

TABLE XIV. Parameters from the global fit of Eq. (19) to aM_K^2 with parameters from **M2**.

β	P_Z	P_r	$\bar{P}_0$	P_1	P_2	χ^2/d.o.f.
1.90	0.572(4)	5.19(6)				
1.95	0.547(2)	5.87(5)	5.65(20)	0.16(3)	7.27(1.67)	6.85
2.10	0.545(2)	7.56(8)				

TABLE XV. Lattice results for aM_K, δE, a_0, and $M_K a_0$ for the smallest value of $a\mu_s$ on all ensembles used in this study. The first parentheses states the statistical uncertainty estimated from the bootstrap samples of the quantity, and the second one states the systematic uncertainty estimated from the different fit ranges used for the correlation functions.

Ens	$a\mu_s$	aM_K	$a\delta E$	a_0	$(M_K a_0)$
A30.32	0.0185	$0.2292(2)(^{+0}_{-0})$	$0.0025(1)(^{+1}_{-0})$	$-1.306(82)(^{+29}_{-15})$	$-0.299(19)(^{+7}_{-3})$
A40.20	0.0185	$0.2385(5)(^{+0}_{-0})$	$0.0126(2)(^{+2}_{-1})$	$-1.523(19)(^{+19}_{-15})$	$-0.363(5)(^{+5}_{-3})$
A40.24	0.0185	$0.2364(3)(^{+0}_{-0})$	$0.0065(1)(^{+1}_{-0})$	$-1.423(17)(^{+20}_{-3})$	$-0.336(4)(^{+5}_{-1})$
A40.32	0.0185	$0.2342(2)(^{+0}_{-0})$	$0.0025(1)(^{+0}_{-0})$	$-1.346(46)(^{+9}_{-14})$	$-0.315(11)(^{+2}_{-3})$
A60.24	0.0185	$0.2449(3)(^{+0}_{-0})$	$0.0061(1)(^{+1}_{-0})$	$-1.393(18)(^{+18}_{-7})$	$-0.341(4)(^{+4}_{-2})$
A80.24	0.0185	$0.2548(2)(^{+1}_{-1})$	$0.0059(1)(^{+1}_{-0})$	$-1.400(14)(^{+16}_{-7})$	$-0.357(3)(^{+4}_{-2})$
A100.24	0.0185	$0.2642(2)(^{+1}_{-1})$	$0.0056(1)(^{+0}_{-0})$	$-1.379(12)(^{+2}_{-2})$	$-0.364(3)(^{+1}_{-1})$
B35.32	0.0160	$0.2053(2)(^{+0}_{-0})$	$0.0035(1)(^{+0}_{-0})$	$-1.606(58)(^{+20}_{-16})$	$-0.330(12)(^{+4}_{-3})$
B55.32	0.0160	$0.2153(2)(^{+0}_{-0})$	$0.0030(1)(^{+0}_{-0})$	$-1.491(47)(^{+18}_{-21})$	$-0.321(10)(^{+4}_{-4})$
B85.24	0.0160	$0.2312(3)(^{+0}_{-0})$	$0.0075(1)(^{+1}_{-1})$	$-1.572(19)(^{+16}_{-17})$	$-0.363(4)(^{+4}_{-4})$
D30.48	0.0115	$0.1504(1)(^{+0}_{-0})$	$0.0018(1)(^{+1}_{-1})$	$-2.130(123)(^{+94}_{-97})$	$-0.320(18)(^{+14}_{-15})$
D45.32	0.0130	$0.1657(3)(^{+0}_{-0})$	$0.0066(2)(^{+0}_{-2})$	$-2.307(51)(^{+12}_{-51})$	$-0.382(9)(^{+2}_{-9})$

TABLE XVI. Same as Table XV, but for the medium value of $a\mu_s$.

Ens	$a\mu_s$	aM_K	$a\delta E$	a_0	$(M_K a_0)$
A30.32	0.0225	$0.2491(3)(^{+2}_{-2})$	$0.0025(2)(^{+1}_{-2})$	$-1.436(97)(^{+45}_{-104})$	$-0.358(24)(^{+11}_{-26})$
A40.20	0.0225	$0.2577(5)(^{+0}_{-0})$	$0.0120(2)(^{+0}_{-1})$	$-1.565(19)(^{+4}_{-11})$	$-0.403(5)(^{+1}_{-3})$
A40.24	0.0225	$0.2560(3)(^{+0}_{-0})$	$0.0062(1)(^{+0}_{-1})$	$-1.454(18)(^{+9}_{-21})$	$-0.372(5)(^{+2}_{-5})$
A40.32	0.0225	$0.2538(2)(^{+0}_{-0})$	$0.0024(2)(^{+1}_{-0})$	$-1.391(86)(^{+46}_{-23})$	$-0.353(22)(^{+12}_{-6})$
A60.24	0.0225	$0.2638(3)(^{+1}_{-1})$	$0.0060(1)(^{+1}_{-1})$	$-1.459(16)(^{+14}_{-28})$	$-0.385(4)(^{+4}_{-7})$
A80.24	0.0225	$0.2732(2)(^{+1}_{-1})$	$0.0057(1)(^{+1}_{-0})$	$-1.435(14)(^{+13}_{-7})$	$-0.392(4)(^{+4}_{-2})$
A100.24	0.0225	$0.2823(2)(^{+0}_{-0})$	$0.0054(1)(^{+0}_{-0})$	$-1.412(12)(^{+8}_{-10})$	$-0.398(3)(^{+2}_{-3})$
B35.32	0.0186	$0.2185(2)(^{+1}_{-1})$	$0.0032(1)(^{+1}_{-1})$	$-1.589(62)(^{+37}_{-47})$	$-0.347(14)(^{+8}_{-10})$
B55.32	0.0186	$0.2281(2)(^{+0}_{-0})$	$0.0031(1)(^{+0}_{-0})$	$-1.578(51)(^{+12}_{-9})$	$-0.360(12)(^{+3}_{-2})$
B85.24	0.0186	$0.2429(3)(^{+1}_{-1})$	$0.0074(1)(^{+1}_{-0})$	$-1.619(14)(^{+13}_{-9})$	$-0.393(3)(^{+3}_{-2})$
D30.48	0.0150	$0.1674(1)(^{+0}_{-0})$	$0.0018(1)(^{+1}_{-1})$	$-2.318(135)(^{+126}_{-59})$	$-0.388(23)(^{+21}_{-10})$
D45.32	0.0150	$0.1748(2)(^{+3}_{-3})$	$0.0061(2)(^{+3}_{-3})$	$-2.250(49)(^{+80}_{-77})$	$-0.393(9)(^{+14}_{-13})$

TABLE XVII. Same as Table XV, but for the highest value of $a\mu_s$.

Ens	$a\mu_s$	aM_K	$a\delta E$	a_0	$(M_K a_0)$
A30.32	0.0246	$0.2590(3)(^{+2}_{-2})$	$0.0025(2)(^{+2}_{-1})$	$-1.535(126)(^{+54}_{-26})$	$-0.398(33)(^{+14}_{-7})$
A40.20	0.0246	$0.2679(5)(^{+0}_{-0})$	$0.0117(2)(^{+3}_{-0})$	$-1.584(19)(^{+33}_{-5})$	$-0.424(5)(^{+9}_{-1})$
A40.24	0.0246	$0.2660(3)(^{+1}_{-1})$	$0.0060(1)(^{+1}_{-1})$	$-1.476(18)(^{+18}_{-23})$	$-0.393(5)(^{+5}_{-6})$
A40.32	0.0246	$0.2638(2)(^{+0}_{-0})$	$0.0025(1)(^{+1}_{-0})$	$-1.484(49)(^{+40}_{-20})$	$-0.391(13)(^{+10}_{-5})$
A60.24	0.0246	$0.2736(3)(^{+0}_{-0})$	$0.0056(1)(^{+1}_{-0})$	$-1.425(20)(^{+27}_{-3})$	$-0.390(5)(^{+7}_{-1})$
A80.24	0.0246	$0.2825(2)(^{+2}_{-2})$	$0.0056(1)(^{+1}_{-1})$	$-1.451(15)(^{+18}_{-18})$	$-0.410(4)(^{+5}_{-5})$
A100.24	0.0246	$0.2914(2)(^{+1}_{-1})$	$0.0053(1)(^{+1}_{-0})$	$-1.421(12)(^{+14}_{-8})$	$-0.414(4)(^{+4}_{-2})$
B35.32	0.0210	$0.2298(2)(^{+0}_{-0})$	$0.0035(2)(^{+1}_{-1})$	$-1.778(87)(^{+35}_{-27})$	$-0.409(20)(^{+8}_{-6})$
B55.32	0.0210	$0.2388(2)(^{+0}_{-0})$	$0.0029(1)(^{+0}_{-1})$	$-1.547(55)(^{+21}_{-25})$	$-0.369(13)(^{+5}_{-6})$
B85.24	0.0210	$0.2535(3)(^{+0}_{-0})$	$0.0071(1)(^{+0}_{-1})$	$-1.624(16)(^{+2}_{-12})$	$-0.412(4)(^{+0}_{-3})$
D30.48	0.0180	$0.1807(1)(^{+0}_{-0})$	$0.0018(1)(^{+1}_{-0})$	$-2.449(147)(^{+122}_{-43})$	$-0.443(27)(^{+22}_{-8})$
D45.32	0.0180	$0.1875(2)(^{+1}_{-1})$	$0.0057(2)(^{+2}_{-1})$	$-2.245(54)(^{+79}_{-36})$	$-0.421(10)(^{+15}_{-7})$

[1] L. Adamczyk *et al.* (STAR Collaboration), Phys. Rev. C **88**, 034906 (2013).
[2] J. Adam *et al.* (ALICE Collaboration), Phys. Rev. C **92**, 054908 (2015).
[3] S. R. Beane, T. C. Luu, K. Orginos, A. Parreño, M. J. Savage, A. Torok, and A. Walker-Loud (NPLQCD Collaboration), Phys. Rev. D **77**, 094507 (2008).
[4] K. Sasaki, N. Ishizuka, M. Oka, and T. Yamazaki (PACS-CS Collaboration), Phys. Rev. D **89**, 054502 (2014).
[5] T. Yamazaki *et al.* (CP-PACS Collaboration), Phys. Rev. D **70**, 074513 (2004).
[6] S. R. Beane, P. F. Bedaque, K. Orginos, and M. J. Savage (NPLQCD Collaboration), Phys. Rev. D **73**, 054503 (2006).
[7] S. R. Beane, T. C. Luu, K. Orginos, A. Parreño, M. J. Savage, A. Torok, and A. Walker-Loud, Phys. Rev. D **77**, 014505 (2008).
[8] X. Feng, K. Jansen, and D. B. Renner, Phys. Lett. B **684**, 268 (2010).
[9] T. Yagi, S. Hashimoto, O. Morimatsu, and M. Ohtani, arXiv:1108.2970.
[10] Z. Fu, Phys. Rev. D **87**, 074501 (2013).
[11] C. Helmes, C. Jost, B. Knippschild, L. Liu, C. Urbach, M. Ueding, M. Werner, C. Liu, J. Liu, and Z. Wang (ETM Collaboration), J. High Energy Phys. 09 (2015) 109.
[12] R. Baron *et al.* (ETM Collaboration), J. High Energy Phys. 06 (2010) 111.
[13] R. Baron *et al.* (ETM Collaboration), Comput. Phys. Commun. **182**, 299 (2011).
[14] R. Frezzotti and G. C. Rossi, Nucl. Phys. B, Proc. Suppl. **128**, 193 (2004).
[15] R. Frezzotti and G. C. Rossi, J. High Energy Phys. 08 (2004) 007.
[16] F. Farchioni *et al.*, *Proc. Sci.*, LATTICE2010 (2010) 128.
[17] N. Carrasco *et al.* (ETM Collaboration), Nucl. Phys. **B887**, 19 (2014).
[18] Y. Iwasaki, Report No. UTHEP-118, 1983.
[19] S. Aoki *et al.*, Eur. Phys. J. C **77**, 112 (2017).
[20] C. Patrignani *et al.* (Particle Data Group Collaboration), Chin. Phys. C **40**, 100001 (2016).
[21] R. Frezzotti, P. A. Grassi, S. Sint, and P. Weisz (ALPHA Collaboration), J. High Energy Phys. 08 (2001) 058.
[22] T. Chiarappa, F. Farchioni, K. Jansen, I. Montvay, E. E. Scholz, L. Scorzato, T. Sudmann, and C. Urbach, Eur. Phys. J. C **50**, 373 (2007).
[23] R. Frezzotti and G. C. Rossi, J. High Energy Phys. 10 (2004) 070.
[24] M. Peardon, J. Bulava, J. Foley, C. Morningstar, J. Dudek, R. G. Edwards, B. Joó, H.-W. Lin, D. G. Richards, and K. J. Juge (Hadron Spectrum Collaboration), Phys. Rev. D **80**, 054506 (2009).
[25] C. Morningstar, J. Bulava, J. Foley, K. J. Juge, D. Lenkner, M. Peardon, and C. H. Wong, Phys. Rev. D **83**, 114505 (2011).
[26] A. Hasenfratz and F. Knechtli, Phys. Rev. D **64**, 034504 (2001).
[27] M. Lüscher, Commun. Math. Phys. **105**, 153 (1986).
[28] S. R. Beane, W. Detmold, and M. J. Savage, Phys. Rev. D **76**, 074507 (2007).
[29] J. Gasser and H. Leutwyler, Nucl. Phys. **B250**, 517 (1985).
[30] V. Bernard, N. Kaiser, and U. G. Meissner, Nucl. Phys. **B357**, 129 (1991).
[31] J.-W. Chen, D. O'Connell, and A. Walker-Loud, Phys. Rev. D **75**, 054501 (2007).
[32] K. Ottnad, Ph. D. thesis, University of Bonn.
[33] K. Jansen and C. Urbach, Comput. Phys. Commun. **180**, 2717 (2009).

[34] A. Abdel-Rehim *et al.*, *Proc. Sci.*, LATTICE2013 (2014) 414.
[35] A. Deuzeman, K. Jansen, B. Kostrzewa, and C. Urbach, *Proc. Sci.*, LATTICE2013 (2013) 416.
[36] A. Deuzeman, S. Reker, and C. Urbach (ETM Collaboration), Comput. Phys. Commun. **183**, 1321 (2012).
[37] G. Guennebaud *et al.*, Eigen v3, http://eigen.tuxfamily.org, 2010.
[38] A. Gurtovoy and D. Abrahams, The boost C++ metaprogramming library, 2002.
[39] E. Jones *et al.*, SciPy: Open source scientific tools for Python, http://www.scipy.org/, 2001.
[40] R Development Core Team, *R: A language and environment for statistical computing* (R Foundation for Statistical Computing, Vienna, Austria, 2005).
[41] M. A. Clark, R. Babich, K. Barros, R. C. Brower, and C. Rebbi, Comput. Phys. Commun. **181**, 1517 (2010).
[42] R. Babich *et al.*, Scaling lattice QCD beyond 100 GPUs, in *SC11 International Conference for High Performance Computing, Networking, Storage and Analysis Seattle, Washington, 2011*, arXiv:1109.2935.
[43] A. G. Nicola and J. R. Pelaez, Phys. Rev. D **65**, 054009 (2002).

CHAPTER 6

$I_3 = 3/2$ PION KAON SCATTERING

6.1 INTRODUCTION

The elastic scattering process $\pi^+K^+ \to \pi^+K^+$ completes our investigation program of maximal isospin scattering including light and strange quarks. This work is in press [2]. Due to the different Mesons interacting with each other it is less straightforward than the case of equal meson scattering and additional thought needs to be put in the analysis procedure, when e.g. removing pollutional states. The computational setup is the same as in chapter 5 we start with a suitable choice of interpolating operators, in this case being the pseudoscalars K^+, π^+ and their composite operator, π^+K^+. The set of these interpolators leads to the three correlation functions C_K, C_π and $C_{\pi K}$. Because of the different mesons participating in the interaction the pollutional states are now time dependent in contrast to the case of same meson scattering. We investigate two different methods to cancel these pollutional states. The first method, weighting and shifting (**E1**), is an established method, cf. Ref. [28], to remove one time dependent pollution with a slight modification. It is described in detail in section 3.3.2. The second method (**E2**) aims at a complete removal of both contributions to the pollution. The determination of the energy shift now involves the reduced mass of the π-K system in the determination of the scattering length. As in chapter 5 we fix the strange quark mass to its physical value via the GMOR-relations. Other than in chapter 5 we use continuum SU(3) ChPT via 2 approaches to extrapolate the data to the physical point. Again, having available values at 3 lattice spacings allows for a thorough investigation of possible lattice spacing dependencies of the scattering length. The first approach fits the continuum SU(3) formula for the dimensionless product $\mu_{\pi K}\, a_0$ directly, whereas the second one uses an intermediate observable Γ to enable a straight line fit, as was already done in Ref. [45].

6.2 SUMMARY

The final result of the elastic s-wave scattering length in the Isospin channel $I_3 = 3/2$ is given by

$$\mu_{\pi K}\, a_0^{3/2,\text{phys}} = -0.0463(17)\,. \tag{6.1}$$

This translates to

$$M_\pi\, a_0^{3/2,\text{phys}} = -0.059(2)\,, \quad M_\pi\, a_0^{1/2,\text{phys}} = 0.163(3)\,. \tag{6.2}$$

The error is a combination of statistical and systematic uncertainties as detailed below. Comparing the two methods to remove thermal states (**E1** and **E2**) reveals that our approach (**E2**) performs better in terms of the estimated statistical error on the energy shift. The mixed action approach used in this publication has significant influence on the evaluation of $\mu_{\pi K}\, a_0^{3/2} = -0.0463(17)$. The sea strange quark mass calculated from the twisted mass parameters does not exactly match the physical strange quark mass owing to the a priori unknown renormalization constants Z_P and Z_S appearing in Equation (2.117). In general it is desirable to simulate as close to the physical situation as possible. This involves tuning the twisted mass parameters μ_σ and μ_δ such that the resulting renormalized sea strange quark mass m_s^{sea} assumes its physical value. In the tuning procedure several assumptions have to be made. Firstly the renormalization constants Z_P and Z_S are not known a priori such that a direct calculation of m_s^{sea} is not feasible. Secondly the tuning procedure depends on the observable used as a proxy for m_s^{phys} and assumptions on parameters entering this proxy, as for instance the lattice spacing. Thus m_s^{sea} turns out different from the m_s^{phys} for the different ensembles in this work. In an ongoing investigation we observed that varying m_s^{sea} has significant influence on the dimensionless scattering length $\mu_{\pi K}\, a_0^{3/2} = -0.0463(17)$. Fitting NLO ChPT to our data suggests that no order $\mathcal{O}\left(M_X^2 a^2\right)$ lattice artifacts, where M_X denotes a pseudoscalar meson mass, are resolvable with the current precision of our data. Here we only investigated the direct fit of NLO ChPT for a possible lattice artifact because a plot of Γ vs. M_K/M_π did not suggest any lattice spacing dependence at all. Because the fitted values of the LECs, L_5 and $L_{\pi K}$, vary a lot when varying the fit ranges in our chiral extrapolations, we fix L_5 with a prior stemming from the most recent calculation available, cf. Ref. [46].

Hadron-Hadron Interactions from $N_f = 2 + 1 + 1$ Lattice QCD: $I = 3/2$ πK Scattering Length

C. Helmes,[1,*] C. Jost,[1] B. Knippschild,[1] B. Kostrzewa,[1]
L. Liu,[2] F. Pittler,[1] C. Urbach,[1] and M. Werner[1]

(**ETM Collaboration**)

[1] *Helmholtz Institut für Strahlen- und Kernphysik, University of Bonn, 53115 Bonn, Germany*
[2] *Institute of Modern Physics, Chinese Academy of Sciences, Lanzhou 730000, China*

Abstract

In this paper we report on results for the s-wave scattering length of the π-K system in the $I = 3/2$ channel from $N_f = 2+1+1$ Lattice QCD. The calculation is based on gauge configurations generated by the European Twisted Mass Collaboration with pion masses ranging from about 230 MeV to 450 MeV at three values of the lattice spacing. Our main result reads $M_\pi\, a_0^{3/2,\mathrm{phys}} = -0.059(2)$. Using chiral perturbation theory we are also able to estimate $M_\pi\, a_0^{1/2,\mathrm{phys}} = 0.163(3)$. The error includes statistical and systematic uncertainties, and for the latter in particular errors from the extrapolation to the physical point.

* Corresponding author: helmes@hiskp.uni-bonn.de

I. INTRODUCTION

For understanding the strong interaction sector of the standard model (SM) it is not sufficient to compute masses of stable particles. Gaining insight into interactions of two or more hadrons and resonances is a must. Due to the non-perturbative nature of low energy quantum chromodynamics (QCD), computations of interaction properties from lattice QCD are highly desirable. While ultimately the phase shift in a given partial wave is to be computed, also the scattering length is in many cases a useful quantity, in particular when the two-particle interaction is weak.

Due to the importance of chiral symmetry in QCD the investigation of systems with two pseudoscalar mesons is of particular interest. Here, chiral perturbation theory (ChPT) is able to provide a description of the pion mass dependence. And any non-perturbative computation in turn allows to check this dependence. Naturally, ChPT works best for two pion systems, while convergence is unclear for pion-kaon or two kaon systems.

The two pion system is studied well experimentally, also in the different isospin channels. However, as soon as one or both pions are replaced by kaons, experimental results become sparse. On the other hand, this gap starts to be filled by lattice QCD calculations. For the pion-kaon system with isospin $I = 3/2$ there are by now a few lattice results available focusing on the scattering length [1–5]. The most recent computation in Ref. [4] uses one lattice at physical pion and kaon masses and lattice spacing $a \approx 0.114\,\text{fm}$. For the sea and valence sector they use $N_f = 2 + 1$ Möbius domain wall fermions and an Iwasaki gauge action. In Ref. [2] a systematic study of the elastic scattering lengths for the light pseudoscalar mesons was carried out with $N_f = 2+1$ $\mathcal{O}(a)$-improved Wilson quarks at pion masses ranging from 170 MeV to 710 MeV and a lattice spacing $a \approx 0.09\,\text{fm}$. Furthermore Refs. [1, 3] use $N_f = 2 + 1$ flavors on the MILC configurations with a rooted staggered sea quark action. Whereas Ref. [3] calculates the scattering length at a lattice spacing $a \approx 0.15\,\text{fm}$, a slightly smaller lattice spacing $a \approx 0.125\,\text{fm}$ has been used in Ref. [1]. The pion masses in Ref. [1] range from 290 MeV to 600 MeV using domain wall valence quarks with a chiral extrapolation done in mixed-action chiral perturbation theory (MAChPT) [6, 7]. The range of pion masses, 330 MeV to 466 MeV, for the Asqtad improved staggered fermions of Ref. [3] is a bit smaller compared to Ref. [1]. In Ref. [5] the phaseshifts and scattering lengths for π-K-scattering in $I = 3/2$ and $I = 1/2$ in the s-wave and the p-wave has been determined. The gauge action is a $N_f = 2$ tree level improved Wilson-Clover action. The authors include the strange quark as a valence quark only which then corresponds to pion and kaon masses of $M_\pi = 266\,\text{MeV}$ and $M_K = 522\,\text{MeV}$, respectively.

In this paper we are going to present results for the s-wave scattering length of the pion-kaon system in the elastic region with isospin $I = 3/2$. The investigation is based on gauge configurations produced by the European Twisted Mass Collaboration (ETMC) with $N_f = 2 + 1 + 1$ dynamical quark flavors [8]. In contrast to previous computations, we are able to investigate discretization effects and to extrapolate to physical quark masses owing to 11 ensembles with M_π ranging from 230 MeV to 450 MeV distributed over 3 different lattice spacing values. We employ in total 4 different extrapolation methods to also estimate systematic uncertainties associated with our computation.

Finally, since this paper is the fourth in a series of publications [9–11] concerning elastic scattering of two pions in different channels and kaon-kaon with $I = 1$, we are able to compare results of two pseudoscalar mesons at maximal isospin involving different amounts of strangeness. The leading order ChPT predictions for the dependence on the reduced mass

ensemble	β	$a\mu_\ell$	$a\mu_\sigma$	$a\mu_\delta$	$(L/a)^3 \times T/a$	$N_{\rm conf}$
A30.32	1.90	0.0030	0.150	0.190	$32^3 \times 64$	259
A40.24	1.90	0.0040	0.150	0.190	$24^3 \times 48$	376
A40.32	1.90	0.0040	0.150	0.190	$32^3 \times 64$	246
A60.24	1.90	0.0060	0.150	0.190	$24^3 \times 48$	303
A80.24	1.90	0.0080	0.150	0.190	$24^3 \times 48$	300
A100.24	1.90	0.0100	0.150	0.190	$24^3 \times 48$	304
B35.32	1.95	0.0035	0.135	0.170	$32^3 \times 64$	241
B55.32	1.95	0.0055	0.135	0.170	$32^3 \times 64$	251
B85.24	1.95	0.0085	0.135	0.170	$32^3 \times 64$	288
D30.48	2.10	0.0030	0.120	0.1385	$48^3 \times 96$	364
D45.32sc	2.10	0.0045	0.0937	0.1077	$32^3 \times 64$	289

Table I: The gauge ensembles used in this study. For the labeling of the ensembles we adopted the notation in Ref. [13]. In addition to the relevant input parameters we give the lattice volume and the number of evaluated configurations, $N_{\rm conf}$.

divided by the relevant decay constant are identical for the three systems and differences appear only at NLO.

This paper is organized as follows: We first introduce the lattice details of our calculation. After the discussion of the analysis methods we present the main result, followed by a detailed discussion of the analysis details. We close with a discussion and summary. Technical details can be found in the appendix.

II. LATTICE ACTION AND OPERATORS

A. Action

The lattice details for the investigation presented here are very similar to the ones we used to study the kaon-kaon scattering length [11]. We use $N_f = 2 + 1 + 1$ flavor lattice QCD ensembles generated by the ETM Collaboration, for which details can be found in Refs. [8, 12, 13]. The parameters relevant for this paper are compiled in Table I: we give for each ensemble the inverse gauge coupling $\beta = 6/g_0^2$, the bare quark mass parameters μ_ℓ, μ_σ and μ_δ, the lattice volume and the number of configurations on which we estimated the relevant quantities.

The ensembles were generated using the Iwasaki gauge action and employ the $N_f = 2 + 1 + 1$ twisted mass fermion action [14–16]. For orientation, the β-values 1.90, 1.95 and 2.10 correspond to lattice spacing values of $a \sim 0.089\,\text{fm}$, $0.082\,\text{fm}$ and $0.062\,\text{fm}$, respectively, see also Table II.

The ensembles were generated at so-called maximal twist, which guarantees automatic $\mathcal{O}(a)$ improvement for almost all physical quantities [14]. The renormalized light quark mass m_ℓ is directly proportional to the light twisted quark mass via

$$m_\ell \;=\; \frac{1}{Z_P}\mu_\ell\,, \tag{1}$$

β	a [fm]	r_0/a
1.90	0.0885(36)	5.31(8)
1.95	0.0815(30)	5.77(6)
2.10	0.0619(18)	7.60(8)

Table II: Values of the Sommer parameter r_0/a and the lattice spacing a at the three values of β. See Ref. [17] for details.

β	1.90	1.95	2.10
$a\mu_s$	0.0185	0.0160	0.013/0.0115
	0.0225	0.0186	0.015
	0.0246	0.0210	0.018

Table III: Values of the bare strange quark mass $a\mu_s$ used for the three β-values. The lightest strange quark mass on the ensemble D30.48 is $a\mu_s = 0.0115$ instead of $a\mu_s = 0.013$.

with Z_P the pseudoscalar renormalization constant. The relation of the bare parameters μ_σ and μ_δ to the renormalized charm and strange quark masses reads

$$m_{c,s} \;=\; \frac{1}{Z_P}\mu_\sigma \;\pm\; \frac{1}{Z_S}\mu_\delta\,, \tag{2}$$

with Z_S the non-singlet scalar renormalization constant.

As noted in Refs. [13, 17], the renormalized sea strange quark masses across the "A", "B" and "D" ensembles vary by up to about 20% and in a few cases differ from the physical strange quark mass to the same extent. For D30.48 and D45.32sc at the finest lattice spacing, the sea strange quark mass on the former ensemble overshoots the physical strange quark mass while it is consistent on the latter ensemble. In order to correct for these mis-tunings and to avoid the complicated flavor-parity mixing in the unitary non-degenerate strange-charm sector [8], we adopt a mixed action ansatz with so-called Osterwalder-Seiler (OS) [16] valence quarks, while keeping $\mathcal{O}(a)$ improvement intact. We denote the OS bare strange quark parameter with μ_s. It is related to the renormalized strange quark mass by

$$m_s \;=\; \frac{1}{Z_P}\mu_s\,. \tag{3}$$

For each ensemble we investigate three values of μ_s which are compiled in Table III. More details on the mixed action approach can be found in Ref. [11].

As a smearing and contraction scheme we employ the stochastic Laplacian-Heaviside approach, described in Ref. [18]. Details of our parameter choices can be found in Refs. [9, 11].

B. Lattice Operators and Correlation Functions

For reasons which will become clear later we need to estimate the masses of the pion, the kaon and the η meson on our ensembles. The masses for the pion and kaon are obtained

from the large Euclidean time dependence of two point functions of the form

$$C_X(t-t') = \langle \mathcal{O}(X)(t)\, \mathcal{O}(X)^\dagger(t') \rangle \,, \tag{4}$$

where $X \in \{\pi, K\}$. The operators for the charged pion and kaon projected to zero momentum read

$$\mathcal{O}(X)(t) \;=\; \sum_{\mathbf{x}} O_X(\mathbf{x},t) \tag{5}$$

with

$$O_\pi(\mathbf{x},t) \;=\; i\bar{d}(\mathbf{x},t)\,\gamma_5\, u(\mathbf{x},t)\,, \tag{6}$$
$$O_K(\mathbf{x},t) \;=\; i\bar{s}(\mathbf{x},t)\,\gamma_5\, u(\mathbf{x},t)\,. \tag{7}$$

For the η (and η') meson we use the two operators

$$O_\ell(\mathbf{x},t) \;=\; \frac{i}{\sqrt{2}}(\bar{u}(\mathbf{x},t)\,\gamma_5\, u(\mathbf{x},t) + \bar{d}(\mathbf{x},t)\,\gamma_5\, d(\mathbf{x},t))\,, \tag{8}$$
$$O_s(\mathbf{x},t) \;=\; i\bar{s}(\mathbf{x},t)\,\gamma_5\, s(\mathbf{x},t)\,. \tag{9}$$

From these we build a two-by-two correlator matrix by taking the disconnected diagrams into account. The η (principal) correlator is determined by solving a generalized eigenvalue problem as described in detail in Ref. [19]. A complete discussion of the analysis of the η (and η') meson is beyond the scope of this paper and the full analysis will be presented in a future publication [20]. In addition to the aforementioned meson masses, we also need to estimate the energy $E_{\pi K}$ of the interacting pion-kaon two particle system. For the case of maximal isospin, i.e. $I = 3/2$, the corresponding two particle operator reads

$$\mathcal{O}(\pi K)(t) = -\sum_{\mathbf{x},\mathbf{x}'} \bar{d}(\mathbf{x},t)\,\gamma_5\, u(\mathbf{x},t)\bar{s}(\mathbf{x}',t)\,\gamma_5\, u(\mathbf{x}',t)\,. \tag{10}$$

It is used to construct the two-particle correlation function

$$C_{\pi K}(t-t') = \langle \mathcal{O}(\pi K)(t)\mathcal{O}(\pi K)^\dagger(t') \rangle \,. \tag{11}$$

$E_{\pi K}$ can then be determined from the large Euclidean time dependence of $C_{\pi K}$.

III. ANALYSIS METHODS

We focus in this work on pion-kaon scattering in the elastic region. For small enough squared scattering momentum p^2 one can perform the effective range expansion for partial wave ℓ:

$$p^{2\ell+1}\cot(\delta_\ell) \;=\; -\frac{1}{a_\ell} + \mathcal{O}(p^2)\,, \tag{12}$$

with phase shift δ_ℓ and scattering length a_ℓ. For the pion-kaon system it is, to a very good approximation, sufficient to study the s-wave, i.e. $\ell = 0$.

In lattice QCD the phase shift or the scattering length can only be computed from finite volume induced energy shifts. The relevant energy shift here is given by

$$\delta E = E_{\pi K} - M_\pi - M_K \,. \tag{13}$$

Using again the effective range expansion, one arrives at the Lüscher formula [21]

$$\delta E = -\frac{2\pi a_0}{\mu_{\pi K} L^3}\left(1 + c_1\frac{a_0}{L} + c_2\frac{a_0^2}{L^2}\right) + \mathcal{O}(L^{-6})\,, \tag{14}$$

relating δE directly to the scattering length a_0, the reduced mass of the pion-kaon system

$$\mu_{\pi K} = \frac{M_\pi M_K}{M_\pi + M_K}\,, \tag{15}$$

and the spatial extent of the finite volume L. The coefficients read [21]

$$c_1 = -2.837297\,, \quad c_2 = 6.375183\,.$$

Given δE, $\mu_{\pi K}$ and L, Lüscher's formula allows one to determine the scattering length a_0 by solving Equation (14) for a_0. In what follows, we will describe how we extract δE and the other relevant bare quantities from correlation functions. Then we will give details on our approach to inter- or extrapolate the results to physical conditions and the investigation of discretization artifacts.

In order to gain some understanding of systematic uncertainties, we perform the analysis in two different ways once the bare data has been extracted. Combined chiral and continuum extrapolations are performed at fixed strange quark mass using next to leading order ChPT (NLO ChPT) and a variant thereof referred to as the Γ method, as described in Ref. [1]. In addition we explore possible discretization effects of $\mathcal{O}\,(a^2)$.

A. Physical Inputs

For the analysis presented below, we require physical inputs for the pion, the kaon and η-meson masses as well as the pion decay constant. To this end, we employ the values in the isospin symmetric limit, $\overline{M}_\pi$ and $\overline{M}_K$, as determined in chiral perturbation theory [22] and given in Ref. [23] as

$$\begin{aligned} \overline{M}_\pi &= 134.8(3)\,\mathrm{MeV}\,, \\ \overline{M}_K &= 494.2(3)\,\mathrm{MeV}\,. \end{aligned} \tag{16}$$

For the η meson mass we use the average obtained by the Particle Data Group [24]:

$$\overline{M}_\eta = 547.86(2)\,\mathrm{MeV}\,. \tag{17}$$

For the decay constant, we use the phenomenological average determined by the Particle Data Group given in Ref. [25] as

$$f_{\pi^-}^{(\mathrm{PDG})} = 130.50(13)\,\mathrm{MeV}\,. \tag{18}$$

As an intermediate lattice scale, we employ the Sommer parameter r_0 [26]. It was determined in Ref. [17] from the ensembles we use here to be

$$r_0 = 0.474(11)\,\mathrm{fm}\,. \tag{19}$$

In the parts of the analysis which require r_0, we use parametric bootstrap samples with central value and width given in Equation (19). Where r_0/a values enter as fit parameters, we constrain the corresponding fit parameters using Gaussian priors in the augmented χ^2 function given as

$$\chi^2_{\mathrm{aug}} \;=\; \chi^2 + \sum_\beta \left(\frac{(r_0/a)(\beta) - P_r(\beta)}{\Delta r_0/a(\beta)}\right)^2\,. \tag{20}$$

B. Energy Values from Correlation Functions

The energies of the two point correlation functions as given in Equation (4) are extracted from fits of the form

$$C_X(t) = A_0^2(e^{-E_X t} + e^{-E_X(T-t)})\,, \tag{21}$$

to the data. While for M_K and M_π the signal extends up to $T/2$, for the η we have to face more noise . We deal with this by applying the excited state subtraction method used and described in Refs. [19, 27].

In the determination of the energy shift δE, the total energy $E_{\pi K}$ of the interacting π-K system must be computed. However, in the spectral decomposition of the two-particle correlation function, unwanted time dependent contributions, so-called thermal pollution, appear. Taking into account that our π-K correlation function is symmetric around the $T/2$ point, the leading contributions in the spectral decomposition can be cast into the form

$$\begin{aligned} C_{\pi K}(t) = A_0^2 \left(e^{-E_{\pi K} t} + e^{-E_{\pi K}(T-t)}\right) \\ + A_1 \left(e^{-E_\pi T} e^{(E_\pi - E_K)t} + e^{-E_K T} e^{(E_K - E_\pi)t}\right)\,, \end{aligned} \tag{22}$$

where

$$A_0^2 = \langle \Omega | \pi^+ K^+ | \pi K \rangle \, \langle \pi K | (\pi^+ K^+)^\dagger | \Omega \rangle \,, \tag{23}$$

is the overlap of the two particle operator $\mathcal{O}(\pi K)$ of Equation (10) with the vacuum Ω and only the first line corresponds to the energy level we are interested in. However, at finite T-values, the second contribution might be sizable, in particular at times close to $T/2$. Moreover, the thermal pollution cannot be separated easily from the signal we are interested in. We have studied two different methods, labeled **E1** and **E2**, to extract $E_{\pi K}$ from $C_{\pi K}(t)$, where **E1** has already been discussed in Ref. [28].

- **E1**: weighting and shifting:
  To render one of the polluting terms in Equation (22) time independent, the correlation function first gets weighted by a factor $\exp((E_K - E_\pi)t)$. We chose this factor, because $\exp(-E_\pi T)$ is significantly larger than $\exp(-E_K T)$. The resulting constant term can then be removed by the shifting procedure, which thus replaces $C_{\pi K}(t)$ by

  $$\begin{aligned} C^w_{\pi K}(t) &= e^{(E_K - E_\pi)t} C_{\pi K}(t)\,, \\ \widetilde{C}^w_{\pi K}(t) &= C^w_{\pi K}(t) - C^w_{\pi K}(t + \delta t)\,, \end{aligned} \tag{24}$$

  where δt is a fixed number of time slices.

  Subsequently, we multiply $\widetilde{C}^w_{\pi K}(t)$ by $\exp(-(E_K - E_\pi)t)$, which (mostly) recovers the original time dependence in the contribution of interest

  $$C^{\mathrm{E1}}_{\pi K}(t) = e^{-(E_K - E_\pi)t} \widetilde{C}^w_{\pi K}(t)\,. \tag{25}$$

  We now extract the total energy of the π-K system, $E_{\pi K}$. To this end we apply Equations (24) and (25) to the data at hand and then fit

  $$\begin{aligned} C^{\mathrm{E1}}_{\pi K}(t) = A_0^2 \left(e^{-E_{\pi K} t} + e^{-E_{\pi K}(T-t)} - e^{(E_K - E_\pi)\delta t} \left(e^{-E_{\pi K}(t+\delta t)} + e^{-E_{\pi K}(T-(t+\delta t))}\right)\right) \\ + \widetilde{A}_1 e^{(E_K - E_\pi)t}\,. \end{aligned} \tag{26}$$

Note that in contrast to Ref. [28], where correlator matrices with various sources of thermal pollution are considered, we are able to take $\tilde{A}_1$ as an additional fit parameter in order to account for this sub-leading term.

- **E2**: dividing out the pollution:
  To improve on method **E1**, we assume that the decomposition given in Equation (22) allows one to neglect any further thermal pollution. This leads to dividing out the time dependent part

$$p(t) = e^{(E_K - E_\pi)t} e^{-E_K T} + e^{-(E_K - E_\pi)t} e^{-E_\pi T} \,, \tag{27}$$

  explicitly. With

$$C'_{\pi K}(t) \;=\; \frac{C_{\pi K}(t)}{p(t)} \tag{28}$$

  we then proceed to calculate

$$\widetilde{C}_{\pi K}(t) = C'_{\pi K}(t) - C'_{\pi K}(t + \delta t) \,, \tag{29}$$

$$C^{\mathrm{E2}}_{\pi K}(t) = p(t) \widetilde{C}_{\pi K}(t) \,, \tag{30}$$

  from which we extract $E_{\pi K}$ through fitting

$$C^{\mathrm{E2}}_{\pi K}(t) = A_0^2 \left(e^{-E_{\pi K} t} + e^{-E_{\pi K}(T-t)} - \frac{p\,(t)}{p\,(t+1)} \cdot \left(e^{-E_{\pi K}(t+1)} + e^{-E_{\pi K}(T-(t+1))} \right) \right) . \tag{31}$$

We remark that for both methods **E1** and **E2** the energies E_π and E_K, i.e. M_π and M_K for zero momentum, are required as an input. They are determined from the corresponding two-point correlation functions. Please note that in method **E2** we need to fit one amplitude, A_0, while method **E1** requires to take care of two amplitudes, A_0 and $\widetilde{A}_1$. For the error analysis bootstrap samples are used to fully preserve all correlations.

After solving Equation (14) for a_0 up to $\mathcal{O}\left(L^{-5}\right)$ on every ensemble for each strange quark mass of Table III, we have three parameters in which we want to extra- or interpolate: the lattice spacing a, the strange quark mass m_s and the light quark mass m_ℓ. To evaluate a_0 at the physical point we follow a two step procedure. We first fix the strange quark mass to its physical value and subsequently perform a combined chiral and continuum extrapolation, investigating different possible types of discretization artifacts.

C. Fixing the strange quark mass

In order to fix the strange quark mass we adopt the following procedure: we match the quantity

$$M_s^2 = M_K^2 - 0.5 M_\pi^2 \,, \tag{32}$$

which is proportional to the strange quark mass at the leading order of ChPT, to its physical value

$$(M_s^{\mathrm{phys}})^2 \;=\; \overline{M}_K^2 - 0.5 \overline{M}_\pi^2 \,, \tag{33}$$

using our determinations of M_K^2 at three valence strange quark masses on a per-ensemble basis. For each ensemble, we then interpolate all valence strange quark mass dependent observables, i.e. $\mu_{\pi K}\, a_0^{3/2}$, M_K, M_η and $\mu_{\pi K}$, in M_s^2 to this reference value.

D. Chiral extrapolation

With the strange quark mass fixed, the extrapolation to the physical point can be carried out using ChPT. The first NLO calculation of the scattering amplitude and scattering lengths was done in Ref. [29]. From the continuum ChPT formulae for the isospin even (odd) scattering lengths a^+ (a^-) in Ref. [30], the NLO ChPT formulae for $\mu_{\pi K}\, a_0^I\,, I \in \{\, 1/2, 3/2\,\}$, can be derived as sketched in Appendix A, giving

$$\begin{aligned}\mu_{\pi K}\, a_0^{3/2} = \frac{\mu_{\pi K}^2}{4\pi f_\pi^2}\Bigg[\frac{32 M_\pi M_K}{f_\pi^2} L_{\pi K}(\Lambda_\chi) - 1 - \frac{16 M_\pi^2}{f_\pi^2} L_5(\Lambda_\chi) \\ + \frac{1}{16\pi^2 f_\pi^2}\chi_{\mathrm{NLO}}^{3/2}(\Lambda_\chi, M_\pi, M_K, M_\eta)\Bigg] + c\cdot f(a^2)\,.\end{aligned} \tag{34}$$

Equation (34) depends on the masses of the pion and the kaon, their reduced mass as defined in Equation (15), the η mass and the pion decay constant. In addition, the equation depends on the low energy constants (LECs) L_5 and $L_{\pi K}$ while $\chi_{\mathrm{NLO}}^{3/2}$ is a known function, see Appendix A 2.

We express Equation (34) in terms of the meson masses and decay constants as they are determined on the lattice, which has the benefit that their ratios can be computed with high statistical precision without the need for explicit factors of the lattice scale. Hence we fit all lattice data simultaneously. Formally we fix the scale-dependent LECs at the renormalization scale $\Lambda_\chi = f_{\pi^-}^{(\mathrm{PDG})}$. However, in practice we employ $a\Lambda_\chi = a f_\pi(\beta, \mu_\ell)/K_{f_\pi}^{\mathrm{FSE}}$ in all chiral logarithms, where the values for the finite-size correction factor $K_{f_\pi}^{\mathrm{FSE}}$ are given in Section V B. Doing so should only induce higher order corrections in the chiral expansion.

Automatic $\mathcal{O}(a)$ improvement of Wilson twisted mass fermions at maximal twist guarantees that the leading lattice artifacts are of $\mathcal{O}(a^2)$ or better. For instance, for the $I = 2$ $\pi\pi$ s-wave scattering length, discretization effects start only at $\mathcal{O}(a^2 M_\pi^2)$ [31]. A corresponding theoretical result for πK is missing so far. However, our numerical data suggest that also for πK lattice artefacts are very small. Still, we include a term $c\cdot f(a^2)$ accounting for possible discretization effects, with fit parameter c and $f(a^2)$ either equal to a^2/r_0^2 or to $a^2 M_X^2$, with M_X^2 one of the masses or mass combinations $M_\pi^2\,,\ M_K^2, M_K^2 + 0.5 M_\pi^2, \mu_{\pi K}^2$. In the following analysis we will include the term $c\cdot f(a^2)$ into our fit for every choice of $f(a^2)$ and thus investigate a possible dependence of our data on the lattice spacing.

To summarize, our fit parameters are the LECs L_5 and $L_{\pi K}$, and c, where $L_{\pi K}$ is the combination of renormalized LECs

$$L_{\pi K} = 2L_1 + 2L_2 + L_3 - 2L_4 - \frac{L_5}{2} + 2L_6 + L_8\,. \tag{35}$$

Let us mention already here that the fits to the data described in the next section turn out to be not sensitive to L_5. Therefore, we include it as a prior in the fit with the value taken from Ref. [23]. In slight abuse of language we will denote this extrapolation method as NLO ChPT.

E. Extrapolations Using the Γ Method at Fixed m_s

Next, we describe an alternative way to extrapolate our data, first applied in Ref. [1]. In what follows we just shortly introduce the derivation of the fit formula and refer to

Appendix A 2 for a more detailed discussion. To derive the relevant formulae we first plug the expressions for a^+ and a^- (cf. Appendix A 2) into eq. (A4) and reorder such that LECs appear on one side of the equation. The result reads

$$L_5 - 2\frac{M_K}{M_\pi}L_{\pi K} = \frac{f_\pi^2}{16M_\pi^2}\left(\frac{4\pi f_\pi^2}{\mu_{\pi K}^2}[\mu_{\pi K}\, a_0^{3/2}] + 1 + \chi^-_{\mathrm{NLO}}(\Lambda_\chi, M_\pi, M_K, M_\eta)\right.$$
$$\left. -2\frac{M_K M_\pi}{f_\pi^2}\chi^+_{\mathrm{NLO}}(\Lambda_\chi, M_\pi, M_K, M_\eta)\right)\,, \tag{36}$$

with $\chi^\pm_{\mathrm{NLO}}(\Lambda_\chi, M_\pi, M_K, M_\eta)$ given in Appendix A 2. We label the right hand side of Equation (36) $\Gamma\,(M_\pi/f_\pi,\, M_K/f_\pi)$ which comprises only measurable quantities:

$$\Gamma\left(\frac{M_\pi}{f_\pi},\, \frac{M_K}{f_\pi}\right) = L_5 - 2\frac{M_K}{M_\pi}L_{\pi K}\,. \tag{37}$$

Having calculated $\Gamma\,(M_\pi/f_\pi,\, M_K/f_\pi)$ using the interpolated data of $\mu_{\pi K}\, a_0^{3/2}$, M_K, M_η and $\mu_{\pi K}$, and the data of M_π and f_π we fit Equation (37) via L_5 and $L_{\pi K}$ to the data obtained in this way. Please note that also Γ is still dimensionless which enables a fit to all lattice data simultaneously. Given L_5 and $L_{\pi K}$ from the fit one can compute $\mu_{\pi K}\, a_0^{3/2}$ at the physical point using Equation (34). Again, it turns out we are not sensitive to L_5 in our fits. Therefore, we use a prior as discussed before. This extrapolation method we denote as Γ method.

IV. RESULTS

In this section we present our main result for $\mu_{\pi K}\, a_0^{3/2}$ extrapolated to the physical point.

We use two thermal state pollution removal methods, **E1** and **E2**, for $E_{\pi K}$. Next we employ the two (related) ChPT extrapolations, Γ method and NLO ChPT, as discussed before. For reasons that will be detailed on in Section V D 1, we state the NLO ChPT results with $c = 0$. For each of the two ChPT extrapolation methods we use three fit ranges as compiled in Table IV. Hence, we have twelve estimates for each quantity at the physical point available, which we use to estimate systematic uncertainties. We remark that the fit for the Γ method is in terms of M_K/M_π and for NLO ChPT in terms of $\mu_{\pi K}/f_\pi$. Thus, we vary the fit range at the lower end for the Γ method and at the upper end for NLO ChPT.

For $\mu_{\pi K}\, a_0^{3/2}$ the twelve estimates are shown in Figure 1. The final result is obtained as the weighted average over all of these, as shown in the figure as the horizontal bold line. The weight is computed according to

$$w = \frac{(1 - 2\cdot|p - 1/2|)^2}{\Delta^2} \tag{38}$$

with p the p-value of the corresponding ChPT fit and Δ the statistical uncertainty obtained from the fit.

The statistical uncertainty of the final results is determined from the bootstrap procedure. For $\mu_{\pi K}\, a_0^{3/2}$ this is shown in Figure 1 as the inner error band. In addition, we determine three systematic uncertainties: The first is obtained from the difference between using only **E1** or only **E2** results. The second from the difference between using only the Γ method

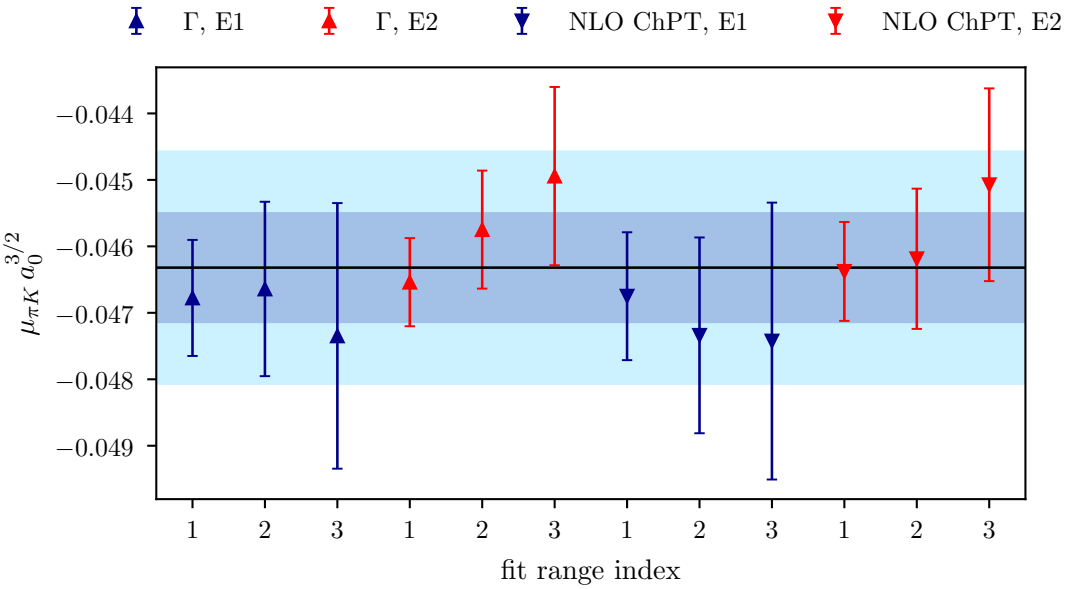

Figure 1: Comparison of values for $\mu_{\pi K}\, a_0^{3/2}$ at the physical point obtained with the different methods used in this paper. The fit ranges decrease with increasing index as described in Table IV. The inner error band represents the statistical error only, while the outer error band represents the statistical and systematic errors added in quadrature.

Method	index	Begin	End
	1	1.2	2.0
Γ	2	1.4	2.0
	3	1.5	2.0
	1	1.2	1.6
NLO	2	1.2	1.41
	3	1.2	1.35

Table IV: Fit ranges used for extrapolations Γ and NLO ChPT. The index column refers to Figure 1.

or only NLO ChPT. Finally, we use the maximal difference of the weighted average to the twelve estimates as a systematic uncertainty coming from the choice of fit ranges.

The results of all twelve fits can be found in Table VIII for the Γ method and Table VII for NLO ChPT fits. The fit range indices used in Figure 1 are resolved in Table IV. The results for all approaches after averaging over the fit ranges are listed in Table XIV.

With this procedure and all errors added in quadrature we quote

$$\mu_{\pi K}\, a_0^{3/2,\mathrm{phys}} = -0.0463(17)\,, \qquad L_{\pi K} = 0.0038(3)\,. \tag{39}$$

This translates to

$$M_\pi\, a_0^{3/2,\mathrm{phys}} = -0.059(2)\,, \qquad M_\pi\, a_0^{1/2,\mathrm{phys}} = 0.163(3) \tag{40}$$

as our final results. The error budget is compiled in Table V. While the dominating contribution to the error for both $\mu_{\pi K}\, a_0^{3/2}$ and $L_{\pi K}$ summed in quadrature is coming from the fit

range and the statistical uncertainty, also the choice of the thermal state removal method contributes significantly. The contribution from the different chiral extrapolation methods is negligible. If the errors were added (not in quadrature), the total error would become a factor ~ 1.7 larger.

We remark that these results have been obtained with L_5 as an input, because the fits are not sufficiently sensitive to determine L_5 directly. We use the most recent determination from a $N_f = 2 + 1 + 1$ lattice calculation by HPQCD [23], which is extrapolated to the continuum limit. At our renormalization scale it reads

$$L_5 \;=\; 5.4(3) \times 10^{-3}\,. \tag{41}$$

	$\mu_{\pi K}\, a_0^{3/2} \cdot 10^5$	$L_{\pi K} \cdot 10^5$
statistical	82 (28%)	15 (32%)
fit range	139 (47%)	19 (41%)
E1 vs. **E2**	64 (22%)	12 (24%)
NLO ChPT v. Γ	9 (3%)	1 (3%)
$\sum$	294 (100%)	47 (100%)
sqrt $\sum$ in quadrature	173	27

Table V: Error budget for the final results of $\mu_{\pi K}\, a_0^{3/2}$ and $L_{\pi K}$.

V. ANALYSIS DETAILS AND DISCUSSION

A. Error Analysis, Thermal Pollution and Choice of Fit Ranges

The error analysis is performed using the stationary blocked bootstrap procedure [32]. In order to determine an appropriate average block length, we compute the integrated autocorrelation time τ_{int} for the correlation functions $C_X(t)$ at all source-sink separations, with X being π, K, η or πK. In the case of πK, $C_X(t)$ is of course first suitably transformed for the extraction of the interaction energy as discussed in section III B. The computation of τ_{int} is detailed in Ref. [33]. The average block length is then chosen to be the ceiling of the maximum integrated autocorrelation time observed over all correlation functions at all source-sink separations

$$b = \lceil \max_{X,t} \left(\tau_{\text{int}}^{(X,t)} \right) \rceil$$

on a per-ensemble basis. We have confirmed explicitly that this method produces a block length at which the estimate of the statistical error plateaus and are thus confident that we properly take into account the effect of autocorrelations on our quoted statistical errors. Using the so-determined block length on a per-ensemble basis, we generate $N = 1500$ samples from which we estimate statistical errors throughout our analysis.

As discussed in Section III B, we employ methods **E1** and **E2** to remove unwanted thermal pollution from the πK two particle correlation function. Both methods allow us to describe the data rather well, but the choice of best fit range depends on the method used to remove the thermal pollution. This in turn affects the value of the extracted $E_{\pi K}$ and, subsequently, the value of $\mu_{\pi K}\, a_0^{3/2}$ obtained from the energy difference.

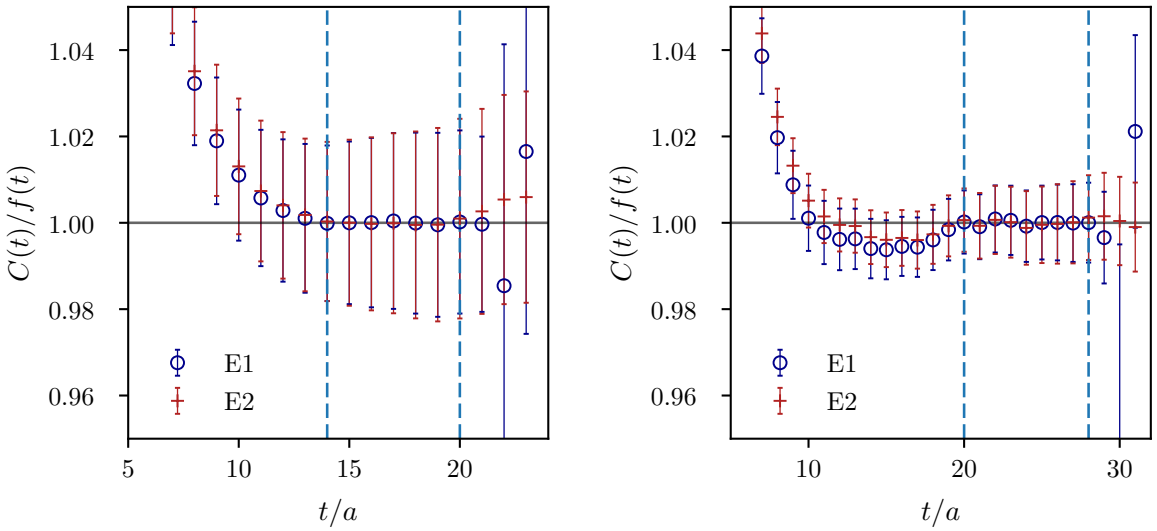

(a) Fit range: $[14, 20]$
$aE_{\pi K} = \{0.389(1)^{\mathrm{E1}}, 0.389(1)^{\mathrm{E2}}\}$

(b) Fit range: $[20, 28]$
$aE_{\pi K} = \{0.3793(6)^{\mathrm{E1}}, 0.3789(5)^{\mathrm{E2}}\}$

Figure 2: Plot of Equation (42) for ensembles A40.24 and A40.32 for the lightest strange quark mass for the fit ranges used for the analysis, comparing the quality of the data description by methods **E1** and **E2**.

To demonstrate the quality of our fits, we look at the ratio

$$\frac{C_{\pi K}^{[\mathrm{E1,E2}]}(t)}{f^{[\mathrm{E1,E2}]}(t)}\,, \tag{42}$$

where $C^{[\mathrm{E1,E2}]}$ are defined in Equations (25) and (30), respectively, and the fit functions $f^{[\mathrm{E1,E2}]}(t)$ are given in Equations (26) and (31), respectively. The ratio is shown in Figure 2 for the two ensembles A40.24 and A40.32 for two fit ranges for which both methods describe the data well.

The choice of the fit ranges to determine energy levels is always difficult. In the past, we have used many fit ranges and weighted them according to their fit qualities [9, 11]. However, this procedure relies on properly estimated variance-covariance matrices, which is notoriously difficult. For the pion-kaon correlation functions needed in this paper we have observed several cases where the fit including the variance-covariance matrix did not properly describe the data after visual inspection. Therefore, we use fits here assuming independent data points with the correlation still taken into account by the bootstrap procedure.

As a consequence, we cannot apply the weighting procedure used in Refs. [9, 11] any longer and have to choose fit ranges. The procedure is as follows: Due to exponential error growth of $C_{\pi K}$ we fix $t_f = T/2 - 4a$ and vary t_i, beginning from a region where excited states do not contribute significantly anymore. From these fits we choose one fit range where the ratio of Equation (42) is best compatible with 1. The statistical error is calculated from the bootstrap samples as discussed before. We then estimate the systematic uncertainty from the remaining fit ranges. To this end we determine the difference of the mean value to the upper and lower bound of values for $E_{\pi K}$. This procedure results in an asymmetric estimate of the systematic uncertainty of $E_{\pi K}$. The results are compiled in Table XI. Since C_K and

	aM_π		aM_K		$aE_{\pi K}$	
Ensemble	t_i	t_f	t_i	t_f	t_i	t_f
A30.32	13	32	13	32	21	28
A40.24	11	24	11	24	14	20
A40.32	13	32	13	32	20	28
A60.24	11	24	11	24	16	20
A80.24	11	24	11	24	16	20
A100.24	11	24	11	24	15	20
B35.32	13	32	13	32	22	28
B55.32	13	32	13	32	19	28
B85.24	11	24	11	24	15	20
D45.32sc	14	32	14	32	22	28
D30.48	22	48	22	48	35	44

Table VI: Typical minimal and maximal values of the starting and end points of fit ranges for the Correlation functions under investigation.

C_π do not suffer from exponential error growth at late times we set $t_f = T/2$. Table VI gives an overview of our chosen values of t_i and t_f for all ensembles.

It is always difficult to include systematic uncertainties in the analysis chain. Since we see systematic uncertainties on extracted energies on the same level as the statistical one, we adopt the following procedure to include this uncertainty: Because $\mu_{\pi K}\, a_0^{3/2}$ is derived from $E_{\pi K}$ we chose to scale the statistical error for $\mu_{\pi K}\, a_0^{3/2}$ on each ensemble after the data have been interpolated in the strange quark mass. To this end we define a scaling factor s via the standard error ΔX and the average of the systematic uncertainties $\overline{Q}_X$ over the 3 strange quark masses for each ensemble:

$$s = \sqrt{\frac{(\Delta X)^2 + \overline{Q}_X^2}{(\Delta X)^2}}\,, \tag{43}$$

where the average $\overline{Q}_X$ is the simple mean over the six systematic errors.

B. Meson Masses, Energy Shift δE and Scattering Length $\mu_{\pi K}\, a_0^{3/2}$

In order to extract δE we first determine M_K and M_π from fitting Equation (21) to our data for $C_\pi(t)$ and $C_K(t)$. We then calculate the reduced mass $\mu_{\pi K}$ via Equation (15) for all combinations of fit ranges. M_π, M_K and $\mu_{\pi K}$ are listed in Table X.

The two methods **E1** and **E2** give us two estimates of $E_{\pi K}$ as outlined in Section III B, from which we determine δE and hence the scattering length using Equation (14). The values for $E_{\pi K}$ and δE are collected in Tables XI and XII.

We introduce factors K_X^{FSE} for $X \in \{M_K,\, M_\pi,\, f_\pi\}$ to correct our lattice data for finite size effects. They have already been calculated in Ref. [17] and are listed in Table IX. We apply these factors for e.g. M_π like

$$M_\pi^* = \frac{M_\pi}{K_{M_\pi}^{\mathrm{FSE}}}\,.$$

We correct every quantity of the set named above and drop the asterisk in what follows to improve legibility. For M_η statistical uncertainties are too big to resolve finite volume effects, see also Ref. [34].

For the two methods **E1** and **E2** we solve Equation (14) for a_0 up to $\mathcal{O}(L^{-5})$ numerically. The values for a_0 and its product with the reduced mass, $\mu_{\pi K}\, a_0^{3/2}$ are collected in Table XIII. Since the finite size behavior of the scattering length is unknown, we do not apply finite size corrections to the reduced mass appearing in $\mu_{\pi K}\, a_0^{3/2}$, either.

C. Strange quark mass fixing

Before we perform a combined continuum and chiral extrapolation, we interpolate all data to reference strange quark masses as discussed before. The data for the three strange quark masses are strongly correlated because the same stochastic light perambulators were used for all light-strange observables. As a consequence, the variance-covariance matrix was sometimes not sufficiently well estimated such that its inverse was unreliable. As a result, we resort to performing these fits using uncorrelated χ^2 which results in best fit parameters which describe the data much better. It should be noted that all statistical covariance is still fully taken into account by the bootstrap procedure and our final statistical errors on all fit parameters are correctly estimated.

As an example, we show in Figure 3 the interpolation of $\mu_{\pi K}\, a_0^{3/2}$ in $M_K^2 - 0.5M_\pi^2$ for ensemble B55.32 comparing methods **E1** and **E2**. The large uncertainty in the interpolation variable stems mainly from the uncertainty in the scaling quantity r_0. Furthermore the errors of the three data points are highly correlated. The interpolation to the reference point is shown as a red diamond. In general, the strange quark mass dependence of $\mu_{\pi K}\, a_0^{3/2}$ is mild and stems mainly from the reduced mass $\mu_{\pi K}$. The values thus determined are compiled in Table XV. They serve as input data for the subsequent chiral extrapolations.

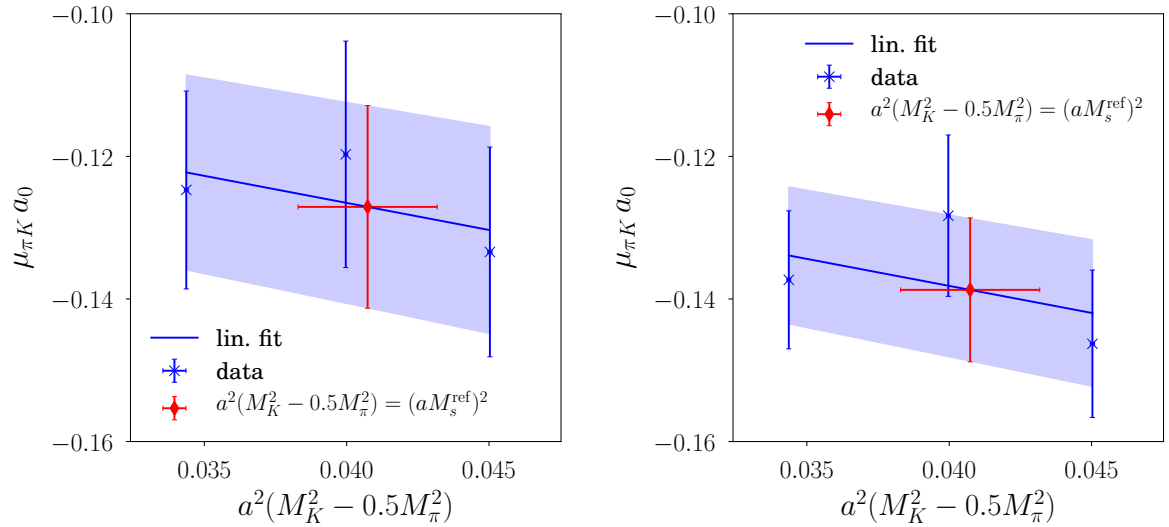

(a) B55.32 for **E1**

(b) B55.32 for **E2**

Figure 3: Interpolations of $\mu_{\pi K}\, a_0^{3/2}$ for the two different methods **E1** and **E2**.

D. Chiral Extrapolations and Discretization Effects

Having interpolated all our lattice data to a fixed reference strange quark mass corresponding to the physical strange quark mass at leading chiral order, we will describe below the results and possible systematic errors in our chiral extrapolations.

1. *Chiral Perturbation Theory at NLO*

To investigate possible discretization effects we first let c in Equation (34) vary freely and fit Equation (34) for the different choices of $f(a^2)$. We are neither able to obtain a statistically significant result for the fit parameter c, nor do we see significant differences in the extracted values of $L_{\pi K}$ and $\mu_{\pi K}\, a_0^{3/2}$. We conclude that within our statistical uncertainties we are not able to resolve lattice artifacts in this quantity. Consequently we are justfied to fit all of our data simultaneously with the continuum ChPT formula Equation (34) and to claim that at this order in the chiral expansion, our results correspond to the physical point in the continuum limit.

In the right column of plots in figure Figure 4, we show the lattice data for $\mu_{\pi K}\, a_0^{3/2}$ interpolated to the reference strange quark mass as a function of $\mu_{\pi K}/f_\pi$ for the two thermal pollution removal methods **E1** and **E2**. The solid line corresponds to the leading order, parameter free ChPT prediction. Plotting our best fit curve with NLO ChPT together with the data is difficult, because $\mu_{\pi K}\, a_0^{3/2}$ depends on meson masses and f_π besides $\mu_{\pi K}/f_\pi$. Therefore, in order to demonstrate that the fit is able to describe our data, we indicate the relative deviation $\delta_r(\mu_{\pi K}\, a_0^{3/2})$ between the fitted points and the original data

$$\delta_r(\mu_{\pi K}\, a_0^{3/2}) = \frac{(\mu_{\pi K}\, a_0^{3/2})^{\text{meas}} - (\mu_{\pi K}\, a_0^{3/2})^{\text{fit}}}{(\mu_{\pi K}\, a_0^{3/2})^{\text{meas}}}\,, \tag{44}$$

in Figures 4b and 4d. The indicated error bars are statistical only and it is clear that within these uncertainties, our data is reasonably well described by the fit.

As in Section V D 2, to investigate the validity of Equation (34) across our entire range of pion masses, we studied three different fit intervals for $\mu_{\pi K}/f_\pi$, namely

$$\frac{\mu_{\pi K}}{f_\pi} \in \{\, (0; 1.35), (0; 1.41), (0; 1.60)\,\}\,, \tag{45}$$

where now the first range corresponds to only using our lightest pion masses and the third range includes all of our ensembles. The resulting trend in the extracted values of $L_{\pi K}$ and $\mu_{\pi K}\, a_0^{3/2}$ is shown in Table VII. Just as in the study of the Γ method, including heavier pion masses leads to smaller values of $L_{\pi K}$ and correspondingly smaller values of $\mu_{\pi K}\, a_0^{3/2}$.

2. $\mathbf{\Gamma}$ *Method*

In this section we present results employing the determination of $L_{\pi K}$ using the linear fit introduced in Section III E. Figure 5 shows the chiral extrapolations in terms of M_K/M_π for pollution removal **E1** and **E2**. Since we work at fixed strange quark mass, the light quark

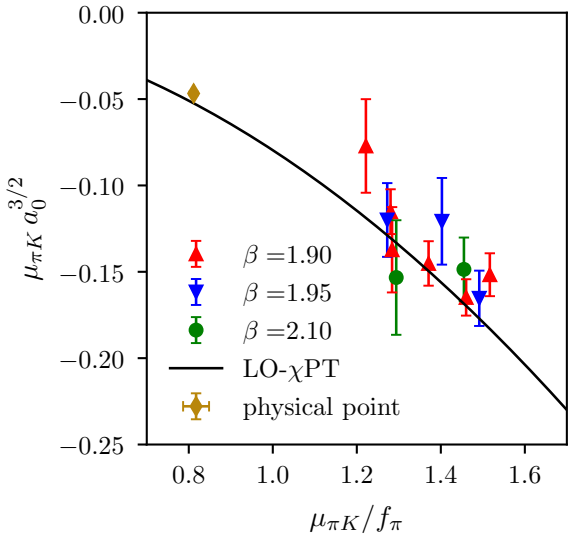

(a) **E1**:$\mu_{\pi K}\, a_0^{3/2}$ in terms of $\mu_{\pi K}/f_\pi$ together with LO ChPT formula.

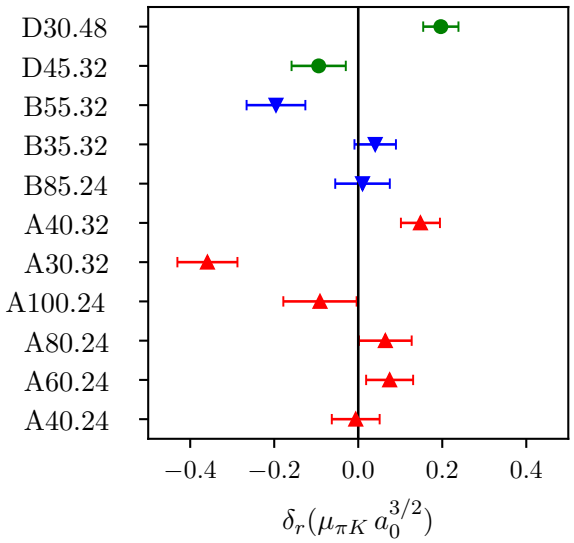

(b) **E1**:Relative deviation between the measured and the fitted values of $\mu_{\pi K}\, a_0^{3/2}$.

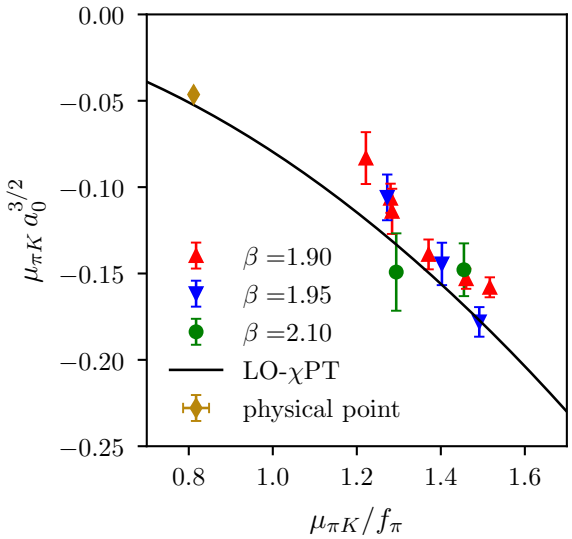

(c) **E2**:$\mu_{\pi K}\, a_0^{3/2}$ in terms of $\mu_{\pi K}/f_\pi$ together with LO ChPT formula.

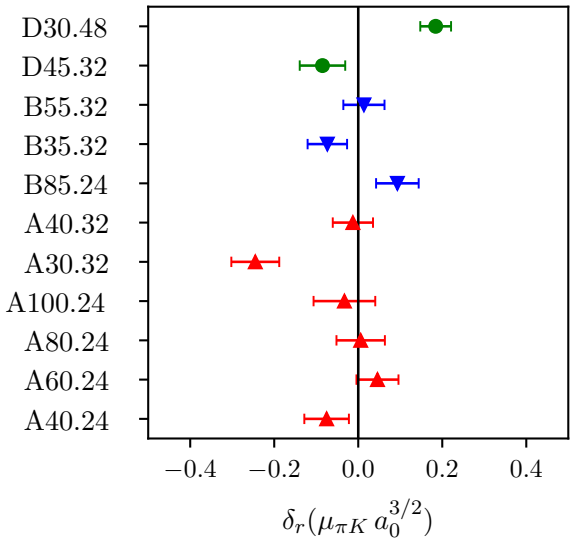

(d) **E2**:Relative deviation between the measured and the fitted values of $\mu_{\pi K}\, a_0^{3/2}$.

Figure 4: Chiral extrapolation of $\mu_{\pi K}\, a_0^{3/2}$ for **E1** and **E2**. Different colors and symbols denote different values of β. In black we plot the LO ChPT formula. The golden diamond gives our final result using the given method at the physical point.

mass decreases from left to right in the figure. In order to check how our extraction of $L_{\pi K}$ is affected by the range of included pion masses we employ three different fit ranges

$$\frac{M_K}{M_\pi} \in \{\, (0; 2.0), (1.5; 2.0), (1.4; 2.0) \,\} \,. \tag{46}$$

In Table VIII we compile the results for the fits corresponding to the data points of Figure 5 for all 3 fit ranges. As the fit range is restricted to our lightest ensembles, the value extracted

Removal	Fit range	p-value	$L_{\pi K} \times 10^3$	$\mu_{\pi K}\, a_0^{3/2} \times 10^2$
	0.0 to 1.35	0.6	3.6(3)	−4.7(2)
E1	0.0 to 1.41	0.7	3.6(2)	−4.7(1)
	0.0 to 1.60	0.7	3.7(2)	−4.7(1)
	0.0 to 1.35	0.5	3.9(2)	−4.5(1)
E2	0.0 to 1.41	0.5	3.8(2)	−4.6(1)
	0.0 to 1.60	0.4	3.7(1)	−4.64(7)

Table VII: Fit results for the NLO ChPT fit. The fits shown in Figure 4 correspond to the largest fit range in the table.

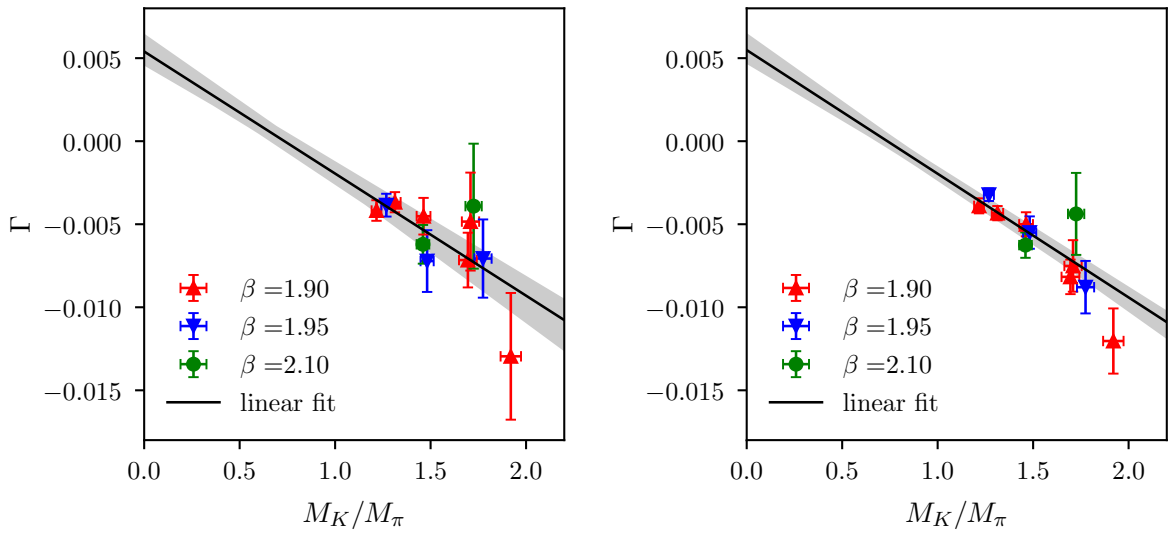

(a) Pollution Removal **E1**

(b) Pollution Removal **E2**

Figure 5: Chiral extrapolation using the Γ method with data interpolated to the reference strange quark mass. The data for different lattice spacings are color encoded. In addition we show the linear fit (solid curve, gray error band)

for $L_{\pi K}$ tends up, while the absolute value of the extracted $\mu_{\pi K}\, a_0^{3/2}$ decreases. It is worth noting that this behavior is only observed for the pollution removal **E2**, whereas for **E1** the values for $L_{\pi K}$ and $\mu_{\pi K}\, a_0^{3/2}$ stay constant within their statistical errors.

VI. DISCUSSION

Let us first discuss the main systematics of our computation: In contrast to the pion-pion or kaon-kaon systems, there is time dependent thermal pollution in the correlation functions relevant for the extraction of the pion-kaon s-wave scattering length. This very fact turns out to represent one of the major systematic uncertainties in the present computation. We have investigated two methods to remove the leading thermal pollution, denoted as **E1** and **E2**. With both we are able to describe the data for the correlation functions. However, there is uncertainty left, because we remove only the leading pollution and the removal procedure

Removal	Fit range	p-value	$L_{\pi K} \times 10^3$	$\mu_{\pi K}\, a_0^{3/2} \times 10^2$
	0.0 to 2.0	0.8	3.7(2)	−4.68(9)
E1	1.4 to 2.0	0.7	3.7(2)	−4.7(1)
	1.5 to 2.0	0.6	3.6(3)	−4.7(2)
	0.0 to 2.0	0.3	3.7(1)	−4.65(7)
E2	1.4 to 2.0	0.5	3.8(2)	−4.57(9)
	1.5 to 2.0	0.4	4.0(2)	−4.5(1)

Table VIII: Fit results of the chiral exptrapolation using the Γ method. The fits shown in Figure 5 correspond to the largest fit range in the table.

requires input estimated from other two point functions. Thus, we eventually decided to use both methods **E1** and **E2** and include the differences in the systematic uncertainty.

Secondly, we perform a mixed action simulation for the strange quark. We use this to correct for small mis-tuning in the sea strange quark mass value used for the gauge configuration generation. This leads — at least in principle — to a small mismatch in the renormalization condition used for the continuum extrapolation. We cannot resolve the corresponding effect on our results quantitatively given our statistical uncertainties. But, since we study quantities which mainly depend on the valence quark properties we expect them to be small.

Thirdly, in the ChPT determination of $L_{\pi K}$ the remaining LEC, L_5, entered as a prior to numerically stabilize our fits. The HPQCD value of Ref. [35] stems from an independent lattice simulation, but is extrapolated to the continuum limit. In Ref. [35] L_5 is given at scale M_η, which we translated to our renormalization scale given by the pion decay constant.

In addition, the extrapolation from our data to the physical point is quite long. Here, a computation directly with physical pion mass would improve our confidence in the result. The final error on our determination is only as small as it is due to the highly constraining ChPT description of $\mu_{\pi K}\, a_0^{3/2}$.

Finally, although we are not able to resolve lattice artefacts in our determination of $\mu_{\pi K}\, a_0^{3/2}$ our statistical errors and limited set of gauge ensembles especially at the finest lattice spacing might make us unable to resolve possible lattice artefacts.

VII. SUMMARY

In this paper we have presented a first lattice computation of the pion-kaon s-wave scattering length for isospin $I = 3/2$ extrapolated to the continuum limit. By varying our methodology we estimate the systematic uncertainties in our results. Our errors cover statistical uncertainties, continuum and chiral extrapolations as well as the removal of thermal pollution.

In the left panel of Figure 6 we compare the results presented in this paper with previous lattice determinations. The inner (darker) error bars show the purely statistical errors whereas the outer (lighter) ones correspond to the statistical and systematic errors added in quadrature. Even though the four other determinations lack the extrapolation to the continuum limit, overall agreement within errors is observed. However, concerning the final uncertainty, our determination improves significantly on the previous determinations by

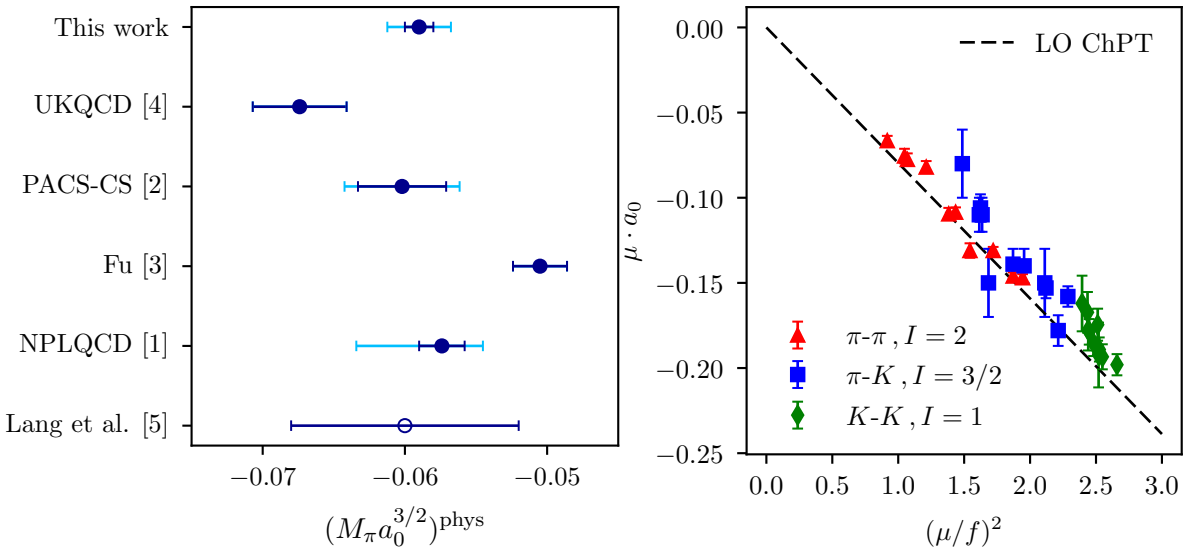

Figure 6: Left: Comparison of physical results for $M_\pi a_0^{I=3/2}$ from various lattice computations [1–5]. The unfilled point denotes the LO extrapolation to the physical point using the data of Ref. [5]. Right: s-wave scattering lengths for the pion-pion, pion-kaon and kaon-kaon maximum isospin channels as a function of the squared reduced mass μ^2 of the system divided by f_π^2 for pion-pion and pion-kaon and by f_K^2 for kaon-kaon.

controlling more sources of uncertainty.

As mentioned in the introduction, the three two particle systems pion-pion, pion-kaon and kaon-kaon are very similar. Therefore, it is interesting to compare the data for pion-pion [9], kaon-kaon [11] and pion-kaon in a single plot. This is done in the right panel of Figure 6 where we show $\mu \cdot a_0$ as a function of $(\mu/f)^2$. Here μ is the reduced mass of the corresponding two particle system and f is the pion decay constant f_π for the pion-pion and pion-kaon and f_K for the kaon-kaon system. The dashed line in the right panel of Figure 6 is the leading order, parameter-free ChPT prediction all three systems share. The three symbols (and colors) represent our data for the three different systems, respectively.

It can be seen that for all three systems, the deviations from LO ChPT are small. For the pion-kaon system, a parametrization in terms of $f_K \cdot f_\pi$ would bring the points even closer to the LO line, while increasing the deviation of the final result from the LO estimate. For the kaon-kaon system, instead, a parametrization in terms of f_π rather than f_K (which is perfectly valid at this order of ChPT) would render the deviation from the LO line more severe.

It is somewhat surprising that ChPT appears to work so well for all three systems, especially for the heavier points in our simulations and even more for the kaon-kaon system, where the expansion parameter becomes large. A possible reason for this finding might be the fact that all three systems are only weakly interacting.

ACKNOWLEDGEMENTS

We thank the members of ETMC for the most enjoyable collaboration. The computer time for this project was made available to us by the John von Neumann-Institute for

Computing (NIC) on the Juqueen and Jureca systems in Jülich. We thank K. Ottnad for providing us with the data for f_π and S. Simula for the estimates of the finite size corrections to M_π, M_K and f_π. This project was funded by the DFG as a project in the Sino-German CRC110. The open source software packages tmLQCD [36], Lemon [37], QUDA [38–40], R [41], python [42] and SciPy [43] have been used.

---

[1] S. R. Beane *et al.*, Phys. Rev. **D74**, 114503 (2006), arXiv:hep-lat/0607036 [hep-lat].
[2] **PACS-CS** Collaboration, K. Sasaki, N. Ishizuka, M. Oka and T. Yamazaki, Phys.Rev. **D89**, 054502 (2014), arXiv:1311.7226 [hep-lat].
[3] Z. Fu, Phys. Rev. **D85**, 074501 (2012), arXiv:1110.1422 [hep-lat].
[4] T. Janowski, P. A. Boyle, A. Jüttner and C. Sachrajda, PoS **LATTICE2014**, 080 (2014).
[5] C. B. Lang, L. Leskovec, D. Mohler and S. Prelovsek, Phys. Rev. **D86**, 054508 (2012), arXiv:1207.3204 [hep-lat].
[6] J.-W. Chen, D. O'Connell, R. Van de Water and A. Walker-Loud, Phys. Rev. D **73**, 074510 (2006), https://link.aps.org/doi/10.1103/PhysRevD.73.074510.
[7] J.-W. Chen, D. O'Connell and A. Walker-Loud, Phys. Rev. D **75**, 054501 (2007), https://link.aps.org/doi/10.1103/PhysRevD.75.054501.
[8] **ETM** Collaboration, R. Baron *et al.*, Comput.Phys.Commun. **182**, 299 (2011), arXiv:1005.2042 [hep-lat].
[9] **ETM** Collaboration, C. Helmes *et al.*, JHEP **09**, 109 (2015), arXiv:1506.00408 [hep-lat].
[10] L. Liu *et al.*, Phys. Rev. **D96**, 054516 (2017), arXiv:1612.02061 [hep-lat].
[11] C. Helmes *et al.*, Phys. Rev. **D96**, 034510 (2017), arXiv:1703.04737 [hep-lat].
[12] T. Chiarappa *et al.*, Eur.Phys.J. **C50**, 373 (2007), arXiv:hep-lat/0606011 [hep-lat].
[13] **ETM** Collaboration, R. Baron *et al.*, JHEP **06**, 111 (2010), arXiv:1004.5284 [hep-lat].
[14] R. Frezzotti and G. C. Rossi, JHEP **08**, 007 (2004), hep-lat/0306014.
[15] R. Frezzotti and G. C. Rossi, Nucl. Phys. Proc. Suppl. **128**, 193 (2004), hep-lat/0311008.
[16] R. Frezzotti and G. C. Rossi, JHEP **10**, 070 (2004), arXiv:hep-lat/0407002.
[17] **ETM** Collaboration, N. Carrasco *et al.*, Nucl.Phys. **B887**, 19 (2014), arXiv:1403.4504 [hep-lat].
[18] C. Morningstar *et al.*, Phys.Rev. **D83**, 114505 (2011), arXiv:1104.3870 [hep-lat].
[19] **ETM** Collaboration, K. Ottnad, C. Urbach and F. Zimmermann, Nucl. Phys. **B896**, 470 (2015), arXiv:1501.02645 [hep-lat].
[20] C. Jost, in preparation.
[21] M. Lüscher, Commun.Math.Phys. **105**, 153 (1986).
[22] J. Gasser and H. Leutwyler, Ann. Phys. **158**, 142 (1984).
[23] S. Aoki *et al.*, Eur. Phys. J. **C77**, 112 (2017), arXiv:1607.00299 [hep-lat].
[24] **Particle Data Group** Collaboration, Tanabashi *et al.*, Phys. Rev. D **98**, 030001 (2018), https://link.aps.org/doi/10.1103/PhysRevD.98.030001.
[25] **Particle Data Group** Collaboration, C. Patrignani *et al.*, Chin. Phys. **C40**, 100001 (2016).
[26] R. Sommer, Nucl.Phys. **B411**, 839 (1994), arXiv:hep-lat/9310022 [hep-lat].
[27] **ETM** Collaboration, C. Michael, K. Ottnad and C. Urbach, Phys.Rev.Lett. **111**, 181602 (2013), arXiv:1310.1207 [hep-lat].
[28] J. J. Dudek, R. G. Edwards and C. E. Thomas, Phys.Rev. **D86**, 034031 (2012), arXiv:1203.6041 [hep-ph].

[29] V. Bernard, N. Kaiser and U.-G. Meißner, Nucl. Phys. **B357**, 129 (1991).
[30] B. Kubis and U.-G. Meissner, Phys. Lett. **B529**, 69 (2002), arXiv:hep-ph/0112154 [hep-ph].
[31] M. I. Buchoff, J.-W. Chen and A. Walker-Loud, Phys.Rev. **D79**, 074503 (2009), arXiv:0810.2464 [hep-lat].
[32] D. N. Politis and J. P. Romano, Journal of the American Statistical Association **89**, 1303 (1994), https://doi.org/10.1080/01621459.1994.10476870, https://doi.org/10.1080/01621459.1994.10476870.
[33] **ALPHA** Collaboration, U. Wolff, Comput. Phys. Commun. **156**, 143 (2004), hep-lat/0306017.
[34] **ETM** Collaboration, K. Ottnad and C. Urbach, Phys. Rev. **D97**, 054508 (2018), arXiv:1710.07986 [hep-lat].
[35] R. J. Dowdall, C. T. H. Davies, G. P. Lepage and C. McNeile, Phys. Rev. **D88**, 074504 (2013), arXiv:1303.1670 [hep-lat].
[36] K. Jansen and C. Urbach, Comput.Phys.Commun. **180**, 2717 (2009), arXiv:0905.3331 [hep-lat].
[37] **ETM** Collaboration, A. Deuzeman, S. Reker and C. Urbach, arXiv:1106.4177 [hep-lat].
[38] M. A. Clark, R. Babich, K. Barros, R. C. Brower and C. Rebbi, Comput. Phys. Commun. **181**, 1517 (2010), arXiv:0911.3191 [hep-lat].
[39] R. Babich *et al.*, Scaling Lattice QCD beyond 100 GPUs, in *SC11 International Conference for High Performance Computing, Networking, Storage and Analysis Seattle, Washington, November 12-18, 2011*, 2011, arXiv:1109.2935 [hep-lat].
[40] M. A. Clark *et al.*, arXiv:1612.07873 [hep-lat].
[41] R Development Core Team, *R: A language and environment for statistical computing*, R Foundation for Statistical Computing, Vienna, Austria, 2005, ISBN 3-900051-07-0.
[42] G. van Rossum and F. L. Drake, *The Python Language Reference Manual* (Network Theory Ltd., 2011).
[43] E. Jones *et al.*, SciPy: Open source scientific tools for Python, 2001–.

Appendix A: π-K Scattering in ChPT

1. Isospin even/odd Scattering Amplitudes

For completeness, we reproduce here the derivation of the Γ method [1] described in Section III E. The scattering amplitudes for all isospin channels of π-K scattering can be noted down using basis elements that are even (odd) under exchange of the Mandelstam variables s and u

$$\begin{aligned}\mathcal{A}^+ &= \frac{1}{3}\left(\mathcal{A}^{1/2}(s,t,u) + 2\mathcal{A}^{3/2}(s,t,u)\right)\\ \mathcal{A}^- &= \frac{1}{3}\left(\mathcal{A}^{1/2}(s,t,u) - \mathcal{A}^{3/2}(s,t,u)\right)\,.\end{aligned} \tag{A1}$$

From Equation (A1) it follows that

$$\mathcal{A}^{1/2} = \mathcal{A}^+ + 2\mathcal{A}^- \tag{A2}$$

$$\mathcal{A}^{3/2} = \mathcal{A}^+ - \mathcal{A}^-\,, \tag{A3}$$

which immediately carries over to the scattering lengths $a^{1/2}$ and $a^{3/2}$ yielding

$$\mu_{\pi K}\, a_0^{1/2} = \mu_{\pi K}(a^+ + 2a^-) \tag{A4}$$
$$\mu_{\pi K}\, a_0^{3/2} = \mu_{\pi K}(a^+ - a^-)\,. \tag{A5}$$

The scattering lengths a^+ and a^- can be derived from the amplitudes of Equation (A1), as was done in Ref. [30]. For convenience we reproduce them here:

$$a^- = \frac{\mu_{\pi K}}{8\pi f_\pi^2}\left\{1 + \frac{M_\pi^2}{f_\pi^2}\left[8L_5 - \frac{1}{2}\chi^-_{\mathrm{NLO}}(\Lambda_\chi, M_\pi, M_K, M_\eta)\right]\right\} \tag{A6}$$
$$a^+ = \frac{\mu_{\pi K} M_K M_\pi}{8\pi f_\pi^4}\left[16L_{\pi K} + \chi^+_{\mathrm{NLO}}(\Lambda_\chi, M_\pi, M_K, M_\eta)\right]\,, \tag{A7}$$

with the renormalization scale Λ_χ and the abbreviations $\chi^\pm(\Lambda_\chi, M_\pi, M_K, M_\eta)$ denoted in Appendix A 2. Please note that a^+ only depends on L_5 while a^- only depends on $L_{\pi K}$. Inserting the ChPT formulae for a^+ and a^- into Equation (A4) one arrives at Equation (36).

2. Next to Leading Order Functions

For convenience we list the chiral functions $\chi^\pm_{\mathrm{NLO}}$ derived in Ref. [30]

$$\begin{aligned}\chi^+_{\mathrm{NLO}}(\Lambda_\chi, M_\pi, M_K, M_\eta) = \frac{1}{16\pi^2}\Bigg[&\nu_\pi \ln\frac{M_\pi}{\Lambda_\chi} + \nu_K \ln\frac{M_K}{\Lambda_\chi} + \nu_\eta \ln\frac{M_\eta}{\Lambda_\chi} \\ &+\nu_{\tan}\arctan\left(\frac{2(M_K+M_\pi)}{M_K-2M_\pi}\sqrt{\frac{M_K-M_\pi}{2M_K+M_\pi}}\right) \\ &+\nu'_{\tan}\arctan\left(\frac{2(M_K-M_\pi)}{M_K+2M_\pi}\sqrt{\frac{M_K+M_\pi}{2M_K-M_\pi}}\right) + \frac{43}{9}\Bigg]\,,\end{aligned} \tag{A8}$$

$$\begin{aligned}\chi^-_{\mathrm{NLO}}(\Lambda_\chi, M_\pi, M_K, M_\eta) = \frac{M_\pi^2}{8f_\pi^2\pi^2}\Bigg[&\nu'_\pi \ln\frac{M_\pi}{\Lambda_\chi} + \nu'_K \ln\frac{M_K}{\Lambda_\chi} + \nu'_\eta \ln\frac{M_\eta}{\Lambda_\chi} \\ &+\frac{M_K}{M_\pi}\nu'_{\tan}\arctan\left(\frac{2(M_K-M_\pi)}{M_K+2M_\pi}\sqrt{\frac{M_K+M_\pi}{2M_K-M_\pi}}\right)\Bigg]\,.\end{aligned} \tag{A9}$$

The functions $\nu_X^{(\prime)}$ are given by

$$\nu_\pi = \frac{11M_\pi^2}{2(M_K^2 - M_\pi^2)} \tag{A10}$$

$$\nu_K = -\frac{67M_K^2 - 8M_\pi^2}{9(M_K^2 - M_\pi^2)} \tag{A11}$$

$$\nu_\eta = +\frac{24M_K^2 - 5M_\pi^2}{18(M_K^2 - M_\pi^2)} \tag{A12}$$

$$\nu_{\tan} = -\frac{4}{9}\frac{\sqrt{2M_K^2 - M_K M_\pi - M_\pi^2}}{M_K + M_\pi} \tag{A13}$$

$$\nu'_\pi = -\frac{8M_\pi^2 - 5M_\pi^2}{2(M_K^2 - M_\pi^2)} \tag{A14}$$

$$\nu'_K = \frac{23M_K^2}{9(M_K^2 - M_\pi^2)} \tag{A15}$$

$$\nu'_\eta = \frac{28M_K^2 - 9M_\pi^2}{18(M_K^2 - M_\pi^2)} \tag{A16}$$

$$\nu'_{\tan} = -\frac{4}{9}\frac{\sqrt{2M_K^2 - M_K M_\pi - M_\pi^2}}{M_K + M_\pi}\,. \tag{A17}$$

From these isospin even/odd functions the definite isospin functions $\chi_{\mathrm{NLO}}^{3/2}$ and $\chi_{\mathrm{NLO}}^{1/2}$ can be derived in the same way as the scattering lengths of Equations (A4) and (A5)

$$\begin{aligned}\chi_{\mathrm{NLO}}^{3/2}(\Lambda_\chi, M_\pi, M_K) =& \kappa_\pi \ln\frac{M_\pi^2}{\Lambda_\chi^2} + \kappa_K \ln\frac{M_K^2}{\Lambda_\chi^2} + \kappa_\eta \ln\frac{M_\eta^2}{\Lambda_\chi^2} + \frac{86}{9}M_K M_\pi \\ &+ \kappa_{\tan} \arctan\left(\frac{2(M_K - M_\pi)}{M_K + 2M_\pi}\sqrt{\frac{M_K + M_\pi}{2M_K - M_\pi}}\right),\end{aligned} \tag{A18}$$

$$\begin{aligned}\chi_{\mathrm{NLO}}^{1/2}(\Lambda_\chi, M_\pi, M_K) =& \kappa'_\pi \ln\frac{M_\pi^2}{\Lambda_\chi^2} + \kappa'_K \ln\frac{M_K^2}{\Lambda_\chi^2} + \kappa'_\eta \ln\frac{M_\eta^2}{\Lambda_\chi^2} + \frac{86}{9}M_K M_\pi \\ &+ \frac{3}{2}\kappa_{\tan} \arctan\left(\frac{2(M_K - M_\pi)}{M_K + 2M_\pi}\sqrt{\frac{M_K + M_\pi}{2M_K - M_\pi}}\right) \\ &+ \kappa'_{\tan} \arctan\left(\frac{2(M_K + M_\pi)}{M_K - 2M_\pi}\sqrt{\frac{M_K - M_\pi}{2M_K + M_\pi}}\right).\end{aligned} \tag{A19}$$

Ensemble	f_π	$K_{f_\pi}^{\mathrm{FSE}}$	$K_{M_\pi}^{\mathrm{FSE}}$	$K_{M_K}^{\mathrm{FSE}}$
A30.32	0.064 52(21)	0.9757(61)	1.0081(52)	1.002 327(1)
A40.24	0.065 77(24)	0.9406(84)	1.0206(95)	1.009 874(1)
A40.32	0.068 39(18)	0.9874(24)	1.0039(28)	1.001 299(1)
A60.24	0.072 09(20)	0.9716(37)	1.0099(49)	1.004 681(1)
A80.24	0.075 81(13)	0.9839(22)	1.0057(29)	1.002 518(1)
A100.24	0.079 36(14)	0.9900(15)	1.0037(19)	1.001 480(1)
B35.32	0.061 05(17)	0.9794(27)	1.0069(32)	1.002 466(1)
B55.32	0.065 45(11)	0.9920(10)	1.0027(14)	1.000 879(1)
B85.24	0.070 39(26)	0.9795(24)	1.0083(28)	1.003 178(1)
D30.48	0.047 35(15)	0.9938(5)	1.0021(7)	1.000 714(1)
D45.32	0.048 25(14)	0.9860(13)	1.0047(14)	1.000 000(1)

Table IX: External data used via parametric bootstrapping. The error on $K_{M_K}^{\mathrm{FSE}}$ is only estimated

Here the functions $\kappa_X^{(\prime)}$ are given by

$$\kappa_\pi = \frac{11M_K M_\pi^3 + 8M_\pi^2 M_K^2 - 5M_\pi^4}{2(M_K^2 - M_\pi^2)} \tag{A20}$$

$$\kappa_K = -\frac{67M_K^3 M_\pi - 8M_\pi^3 M_K + 23M_K^2 M_\pi^2}{9(M_K^2 - M_\pi^2)} \tag{A21}$$

$$\kappa_\eta = \frac{24M_\pi M_K^3 - 5M_K M_\pi^3 + 28M_K^2 M_\pi^2 - 9M_\pi^4}{18(M_K^2 - M_\pi^2)} \tag{A22}$$

$$\kappa_{\mathrm{tan}} = -\frac{16M_K M_\pi}{9}\frac{\sqrt{2M_K^2 + M_K M_\pi - M_\pi^2}}{M_K - M_\pi} \tag{A23}$$

$$\kappa_\pi^{'} = \frac{11M_K M_\pi^3 - 16M_K^2 M_\pi^2 + 10M_\pi^4}{2(M_K^2 - M_\pi^2)} \tag{A24}$$

$$\kappa_K^{'} = -\frac{67M_K^3 M_\pi - 8M_\pi^3 M_K - 46M_K^2 M_\pi^2}{9(M_K^2 - M_\pi^2)} \tag{A25}$$

$$\kappa_\eta^{'} = \frac{24M_\pi M_K^3 - 5M_K M_\pi^3 - 56M_K^2 M_\pi^2 + 18M_\pi^4}{18(M_K^2 - M_\pi^2)} \tag{A26}$$

$$\kappa_{\mathrm{tan}}^{'} = \frac{8M_K M_\pi}{9}\frac{\sqrt{2M_K^2 - M_K M_\pi - M_\pi^2}}{M_K + M_\pi}\,. \tag{A27}$$

Appendix B: Datatables

1. Interpolated Data

Ensemble	$a\mu_s$	aM_K	aM_π	$a\mu_{\pi K}$
	0.0185	$0.2294(3)(^{+0}_{-0})$	$0.1239(2)(^{+1}_{-0})$	$0.08046(12)(^{+0}_{-0})$
A30.32	0.0225	$0.2495(2)(^{+1}_{-0})$	$0.1239(2)(^{+1}_{-0})$	$0.08280(12)(^{+0}_{-0})$
	0.0246	$0.2597(2)(^{+1}_{-0})$	$0.1239(2)(^{+1}_{-0})$	$0.08388(12)(^{+0}_{-0})$
	0.0185	$0.2365(5)(^{+2}_{-1})$	$0.1453(5)(^{+2}_{-1})$	$0.08999(22)(^{+0}_{-0})$
A40.24	0.0225	$0.2561(4)(^{+4}_{-1})$	$0.1453(5)(^{+2}_{-1})$	$0.09269(22)(^{+0}_{-0})$
	0.0246	$0.2662(5)(^{+1}_{-2})$	$0.1453(5)(^{+2}_{-1})$	$0.09398(22)(^{+0}_{-0})$
	0.0185	$0.2343(2)(^{+0}_{-0})$	$0.1415(2)(^{+1}_{-0})$	$0.08822(10)(^{+0}_{-0})$
A40.32	0.0225	$0.2538(2)(^{+1}_{-0})$	$0.1415(2)(^{+1}_{-0})$	$0.09086(11)(^{+0}_{-0})$
	0.0246	$0.2638(2)(^{+1}_{-1})$	$0.1415(2)(^{+1}_{-0})$	$0.09210(11)(^{+0}_{-0})$
	0.0185	$0.2448(3)(^{+1}_{-0})$	$0.1729(3)(^{+4}_{-1})$	$0.10134(16)(^{+0}_{-0})$
A60.24	0.0225	$0.2637(3)(^{+1}_{-0})$	$0.1729(3)(^{+4}_{-1})$	$0.10445(16)(^{+0}_{-0})$
	0.0246	$0.2735(3)(^{+1}_{-0})$	$0.1729(3)(^{+4}_{-1})$	$0.10594(17)(^{+0}_{-0})$
	0.0185	$0.2548(2)(^{+0}_{-1})$	$0.1993(2)(^{+0}_{-1})$	$0.11184(11)(^{+0}_{-0})$
A80.24	0.0225	$0.2731(2)(^{+1}_{-1})$	$0.1993(2)(^{+0}_{-1})$	$0.11523(11)(^{+0}_{-0})$
	0.0246	$0.2824(2)(^{+2}_{-2})$	$0.1993(2)(^{+0}_{-1})$	$0.11685(11)(^{+0}_{-0})$
	0.0185	$0.2642(2)(^{+0}_{-1})$	$0.2223(2)(^{+1}_{-1})$	$0.12073(11)(^{+0}_{-0})$
A100.24	0.0225	$0.2822(2)(^{+0}_{-0})$	$0.2223(2)(^{+1}_{-1})$	$0.12436(11)(^{+0}_{-0})$
	0.0246	$0.2913(2)(^{+1}_{-1})$	$0.2223(2)(^{+1}_{-1})$	$0.12609(11)(^{+0}_{-0})$
	0.0160	$0.2053(2)(^{+1}_{-1})$	$0.1249(2)(^{+1}_{-1})$	$0.07765(11)(^{+0}_{-0})$
B35.32	0.0186	$0.2186(2)(^{+2}_{-1})$	$0.1249(2)(^{+1}_{-1})$	$0.07948(12)(^{+0}_{-0})$
	0.0210	$0.2298(2)(^{+0}_{-1})$	$0.1249(2)(^{+1}_{-1})$	$0.08091(12)(^{+0}_{-0})$
	0.0160	$0.2155(2)(^{+1}_{-2})$	$0.1554(2)(^{+0}_{-0})$	$0.09030(10)(^{+0}_{-0})$
B55.32	0.0186	$0.2282(2)(^{+1}_{-2})$	$0.1554(2)(^{+0}_{-0})$	$0.09245(10)(^{+0}_{-0})$
	0.0210	$0.2390(2)(^{+1}_{-2})$	$0.1554(2)(^{+0}_{-0})$	$0.09418(10)(^{+0}_{-0})$
	0.0160	$0.2313(3)(^{+0}_{-3})$	$0.1933(3)(^{+1}_{-0})$	$0.10530(15)(^{+0}_{-0})$
B85.24	0.0186	$0.2429(3)(^{+0}_{-0})$	$0.1933(3)(^{+1}_{-0})$	$0.10763(16)(^{+0}_{-0})$
	0.0210	$0.2535(3)(^{+2}_{-0})$	$0.1933(3)(^{+1}_{-0})$	$0.10967(15)(^{+0}_{-0})$
	0.0130	$0.1658(3)(^{+1}_{-1})$	$0.1205(4)(^{+1}_{-1})$	$0.06979(17)(^{+0}_{-0})$
D45.32	0.0150	$0.1747(4)(^{+4}_{-1})$	$0.1205(4)(^{+1}_{-1})$	$0.07132(17)(^{+0}_{-0})$
	0.0180	$0.1876(3)(^{+0}_{-1})$	$0.1205(4)(^{+1}_{-1})$	$0.07339(17)(^{+0}_{-0})$
	0.0115	$0.1503(1)(^{+0}_{-0})$	$0.0976(1)(^{+0}_{-0})$	$0.05917(6)(^{+0}_{-0})$
D30.48	0.0150	$0.1673(1)(^{+0}_{-1})$	$0.0976(1)(^{+0}_{-0})$	$0.06163(6)(^{+0}_{-0})$
	0.0180	$0.1807(1)(^{+1}_{-1})$	$0.0976(1)(^{+0}_{-0})$	$0.06336(6)(^{+0}_{-0})$

Table X: Comparison of the meson masses, M_π and M_K together with the reduced mass $\mu_{\pi K}$. The systematic uncertainties for $\mu_{\pi K}$ turn out to be negligible and thus are not shown.

Ensemble	$a\mu_s$	$aE_{\pi K}(\mathbf{E1})$	$aE_{\pi K}(\mathbf{E2})$
A30.32	0.0185	$0.3558(9)(^{+7}_{-2})$	$0.3558(7)(^{+5}_{-1})$
	0.0225	$0.3758(9)(^{+8}_{-2})$	$0.3758(7)(^{+6}_{-1})$
	0.0246	$0.3870(9)(^{+9}_{-5})$	$0.3867(6)(^{+2}_{-2})$
A40.24	0.0185	$0.3892(12)(^{+6}_{-0})$	$0.3887(11)(^{+4}_{-2})$
	0.0225	$0.4081(12)(^{+10}_{-2})$	$0.4082(11)(^{+5}_{-0})$
	0.0246	$0.4184(12)(^{+7}_{-0})$	$0.4182(11)(^{+5}_{-0})$
A40.32	0.0185	$0.3793(6)(^{+3}_{-8})$	$0.3789(5)(^{+0}_{-4})$
	0.0225	$0.3988(6)(^{+9}_{-7})$	$0.3983(5)(^{+1}_{-3})$
	0.0246	$0.4081(6)(^{+2}_{-4})$	$0.4083(5)(^{+1}_{-4})$
A60.24	0.0185	$0.4250(9)(^{+11}_{-0})$	$0.4247(7)(^{+8}_{-0})$
	0.0225	$0.4447(7)(^{+2}_{-0})$	$0.4440(6)(^{+3}_{-4})$
	0.0246	$0.4537(7)(^{+8}_{-4})$	$0.4536(6)(^{+5}_{-1})$
A80.24	0.0185	$0.4613(6)(^{+0}_{-2})$	$0.4606(5)(^{+3}_{-0})$
	0.0225	$0.4789(6)(^{+5}_{-0})$	$0.4787(5)(^{+4}_{-0})$
	0.0246	$0.4894(6)(^{+0}_{-6})$	$0.4882(5)(^{+3}_{-0})$
A100.24	0.0185	$0.4921(5)(^{+6}_{-3})$	$0.4922(4)(^{+3}_{-0})$
	0.0225	$0.5102(5)(^{+5}_{-0})$	$0.5102(4)(^{+3}_{-0})$
	0.0246	$0.5193(5)(^{+3}_{-3})$	$0.5193(4)(^{+2}_{-1})$
B35.32	0.0160	$0.3333(9)(^{+11}_{-0})$	$0.3336(6)(^{+6}_{-0})$
	0.0186	$0.3474(7)(^{+2}_{-1})$	$0.3472(6)(^{+3}_{-1})$
	0.0210	$0.3595(9)(^{+0}_{-3})$	$0.3584(7)(^{+5}_{-0})$
B55.32	0.0160	$0.3743(5)(^{+4}_{-1})$	$0.3747(4)(^{+3}_{-0})$
	0.0186	$0.3866(5)(^{+6}_{-7})$	$0.3869(4)(^{+3}_{-1})$
	0.0210	$0.3977(5)(^{+4}_{-1})$	$0.3981(4)(^{+3}_{-0})$
B85.24	0.0160	$0.4322(7)(^{+15}_{-2})$	$0.4325(6)(^{+7}_{-0})$
	0.0186	$0.4442(7)(^{+15}_{-1})$	$0.4441(6)(^{+8}_{-1})$
	0.0210	$0.4548(7)(^{+13}_{-0})$	$0.4544(6)(^{+8}_{-1})$
D45.32	0.0130	$0.2925(12)(^{+23}_{-0})$	$0.2922(9)(^{+18}_{-0})$
	0.0150	$0.3028(11)(^{+5}_{-1})$	$0.3010(9)(^{+14}_{-0})$
	0.0180	$0.3145(10)(^{+16}_{-0})$	$0.3142(8)(^{+12}_{-0})$
D30.48	0.0115	$0.2506(8)(^{+3}_{-5})$	$0.2508(5)(^{+1}_{-5})$
	0.0150	$0.2677(8)(^{+3}_{-6})$	$0.2679(6)(^{+1}_{-6})$
	0.0180	$0.2811(8)(^{+3}_{-6})$	$0.2814(6)(^{+1}_{-7})$

Table XI: Comparison of $E_{\pi K}$ for methods **E1** and **E2**

Ensemble	$a\mu_s$	$a\delta E(\mathbf{E1}) \times 10^3$	$a\delta E(\mathbf{E2}) \times 10^3$
A30.32	0.0185	$2.48(96)(^{+68}_{-20})$	$2.44(81)(^{+51}_{-8})$
	0.0225	$2.41(97)(^{+81}_{-17})$	$2.34(77)(^{+57}_{-8})$
	0.0246	$3.45(93)(^{+89}_{-49})$	$3.14(74)(^{+19}_{-22})$
A40.24	0.0185	$7.46(84)(^{+56}_{-0})$	$6.93(56)(^{+43}_{-20})$
	0.0225	$6.70(85)(^{+97}_{-19})$	$6.84(67)(^{+47}_{-1})$
	0.0246	$6.94(88)(^{+74}_{-0})$	$6.69(61)(^{+50}_{-1})$
A40.32	0.0185	$3.52(47)(^{+34}_{-83})$	$3.15(32)(^{+0}_{-38})$
	0.0225	$3.42(45)(^{+85}_{-73})$	$2.96(29)(^{+8}_{-27})$
	0.0246	$2.79(44)(^{+15}_{-42})$	$2.99(31)(^{+13}_{-39})$
A60.24	0.0185	$7.25(69)(^{+111}_{-0})$	$7.02(39)(^{+80}_{-0})$
	0.0225	$8.05(46)(^{+24}_{-3})$	$7.37(35)(^{+34}_{-36})$
	0.0246	$7.28(45)(^{+78}_{-43})$	$7.22(30)(^{+46}_{-12})$
A80.24	0.0185	$7.19(48)(^{+3}_{-22})$	$6.45(21)(^{+30}_{-0})$
	0.0225	$6.47(47)(^{+48}_{-0})$	$6.19(23)(^{+39}_{-0})$
	0.0246	$7.61(48)(^{+0}_{-57})$	$6.40(21)(^{+34}_{-0})$
A100.24	0.0185	$5.58(32)(^{+61}_{-30})$	$5.70(17)(^{+27}_{-3})$
	0.0225	$5.68(32)(^{+48}_{-0})$	$5.67(17)(^{+26}_{-0})$
	0.0246	$5.74(24)(^{+34}_{-30})$	$5.69(14)(^{+19}_{-7})$
B35.32	0.0160	$3.12(85)(^{+109}_{-0})$	$3.38(45)(^{+62}_{-0})$
	0.0186	$3.94(54)(^{+23}_{-8})$	$3.67(34)(^{+30}_{-13})$
	0.0210	$4.79(85)(^{+0}_{-33})$	$3.72(56)(^{+53}_{-0})$
B55.32	0.0160	$3.33(42)(^{+44}_{-12})$	$3.71(30)(^{+28}_{-2})$
	0.0186	$3.02(45)(^{+64}_{-74})$	$3.27(33)(^{+30}_{-8})$
	0.0210	$3.28(41)(^{+43}_{-12})$	$3.65(30)(^{+27}_{-1})$
B85.24	0.0160	$7.61(41)(^{+153}_{-16})$	$7.88(23)(^{+66}_{-0})$
	0.0186	$8.05(36)(^{+150}_{-14})$	$7.97(23)(^{+81}_{-5})$
	0.0210	$7.99(38)(^{+127}_{-3})$	$7.64(25)(^{+81}_{-9})$
D45.32	0.0130	$6.18(88)(^{+232}_{-0})$	$5.87(53)(^{+177}_{-0})$
	0.0150	$7.62(86)(^{+54}_{-12})$	$5.82(43)(^{+143}_{-0})$
	0.0180	$6.38(71)(^{+158}_{-0})$	$6.05(45)(^{+120}_{-0})$
D30.48	0.0115	$2.70(77)(^{+26}_{-53})$	$2.90(50)(^{+10}_{-53})$
	0.0150	$2.79(79)(^{+26}_{-60})$	$3.05(51)(^{+9}_{-63})$
	0.0180	$2.86(82)(^{+25}_{-65})$	$3.17(54)(^{+9}_{-69})$

Table XII: Comparison of $\delta E_{\pi K}$ for methods **E1** and **E2**

Ensemble	$a\mu_s$	$a_0/a(\mathbf{E1})$	$a_0/a(\mathbf{E2})$	$\mu_{\pi K}\, a_0^{3/2}(\mathbf{E1})$	$\mu_{\pi K}\, a_0^{3/2}(\mathbf{E2})$
A30.32	0.0185	$-0.96(34)(^{+7}_{-24})$	$-0.94(29)(^{+3}_{-18})$	$-0.077(27)(^{+6}_{-19})$	$-0.076(23)(^{+2}_{-14})$
	0.0225	$-0.95(35)(^{+6}_{-29})$	$-0.93(28)(^{+3}_{-20})$	$-0.079(29)(^{+5}_{-24})$	$-0.077(23)(^{+2}_{-17})$
	0.0246	$-1.33(32)(^{+17}_{-30})$	$-1.23(26)(^{+8}_{-7})$	$-0.112(27)(^{+14}_{-25})$	$-0.103(22)(^{+6}_{-6})$
A40.24	0.0185	$-1.27(12)(^{+0}_{-8})$	$-1.19(8)(^{+3}_{-6})$	$-0.114(11)(^{+0}_{-7})$	$-0.107(8)(^{+3}_{-6})$
	0.0225	$-1.18(13)(^{+3}_{-15})$	$-1.20(10)(^{+0}_{-7})$	$-0.110(12)(^{+3}_{-14})$	$-0.112(9)(^{+0}_{-7})$
	0.0246	$-1.23(14)(^{+0}_{-11})$	$-1.20(10)(^{+0}_{-8})$	$-0.116(13)(^{+0}_{-11})$	$-0.112(9)(^{+0}_{-7})$
A40.32	0.0185	$-1.42(17)(^{+31}_{-12})$	$-1.29(12)(^{+14}_{-0})$	$-0.126(15)(^{+27}_{-11})$	$-0.114(10)(^{+12}_{-0})$
	0.0225	$-1.42(17)(^{+27}_{-31})$	$-1.25(11)(^{+10}_{-3})$	$-0.129(15)(^{+25}_{-28})$	$-0.114(10)(^{+9}_{-3})$
	0.0246	$-1.20(17)(^{+17}_{-6})$	$-1.28(12)(^{+15}_{-5})$	$-0.111(16)(^{+15}_{-5})$	$-0.118(11)(^{+14}_{-5})$
A60.24	0.0185	$-1.37(11)(^{+0}_{-18})$	$-1.33(6)(^{+0}_{-13})$	$-0.139(11)(^{+0}_{-18})$	$-0.135(6)(^{+0}_{-13})$
	0.0225	$-1.53(7)(^{+1}_{-4})$	$-1.42(6)(^{+6}_{-6})$	$-0.160(8)(^{+1}_{-4})$	$-0.149(6)(^{+6}_{-6})$
	0.0246	$-1.43(7)(^{+7}_{-13})$	$-1.41(5)(^{+2}_{-8})$	$-0.151(8)(^{+8}_{-13})$	$-0.150(5)(^{+2}_{-8})$
A80.24	0.0185	$-1.48(8)(^{+4}_{-1})$	$-1.35(4)(^{+0}_{-5})$	$-0.165(9)(^{+4}_{-1})$	$-0.150(4)(^{+0}_{-6})$
	0.0225	$-1.39(9)(^{+0}_{-9})$	$-1.33(4)(^{+0}_{-7})$	$-0.160(10)(^{+0}_{-10})$	$-0.154(5)(^{+0}_{-8})$
	0.0246	$-1.61(8)(^{+10}_{-0})$	$-1.39(4)(^{+0}_{-6})$	$-0.188(10)(^{+12}_{-0})$	$-0.162(5)(^{+0}_{-7})$
A100.24	0.0185	$-1.27(6)(^{+6}_{-12})$	$-1.29(3)(^{+1}_{-5})$	$-0.153(8)(^{+7}_{-14})$	$-0.156(4)(^{+1}_{-6})$
	0.0225	$-1.32(6)(^{+0}_{-9})$	$-1.32(3)(^{+0}_{-5})$	$-0.165(8)(^{+0}_{-12})$	$-0.164(4)(^{+0}_{-7})$
	0.0246	$-1.35(5)(^{+6}_{-7})$	$-1.34(3)(^{+1}_{-4})$	$-0.170(6)(^{+8}_{-9})$	$-0.169(4)(^{+2}_{-5})$
B35.32	0.0160	$-1.14(28)(^{+0}_{-35})$	$-1.22(15)(^{+0}_{-20})$	$-0.088(22)(^{+0}_{-27})$	$-0.095(11)(^{+0}_{-15})$
	0.0186	$-1.43(17)(^{+3}_{-7})$	$-1.34(11)(^{+4}_{-10})$	$-0.114(14)(^{+2}_{-6})$	$-0.107(9)(^{+3}_{-8})$
	0.0210	$-1.73(26)(^{+10}_{-0})$	$-1.38(19)(^{+0}_{-17})$	$-0.140(21)(^{+8}_{-0})$	$-0.112(15)(^{+0}_{-14})$
B55.32	0.0160	$-1.38(15)(^{+4}_{-16})$	$-1.52(11)(^{+1}_{-10})$	$-0.125(14)(^{+4}_{-15})$	$-0.137(10)(^{+1}_{-9})$
	0.0186	$-1.29(17)(^{+29}_{-24})$	$-1.39(12)(^{+3}_{-11})$	$-0.120(16)(^{+27}_{-22})$	$-0.128(11)(^{+3}_{-10})$
	0.0210	$-1.42(16)(^{+5}_{-16})$	$-1.55(11)(^{+0}_{-10})$	$-0.133(15)(^{+4}_{-15})$	$-0.146(10)(^{+0}_{-9})$
B85.24	0.0160	$-1.47(7)(^{+3}_{-24})$	$-1.52(4)(^{+0}_{-11})$	$-0.155(7)(^{+3}_{-26})$	$-0.160(4)(^{+0}_{-11})$
	0.0186	$-1.57(6)(^{+2}_{-24})$	$-1.56(4)(^{+1}_{-13})$	$-0.169(6)(^{+3}_{-26})$	$-0.168(4)(^{+1}_{-14})$
	0.0210	$-1.59(6)(^{+1}_{-21})$	$-1.53(4)(^{+2}_{-13})$	$-0.174(7)(^{+1}_{-23})$	$-0.167(5)(^{+2}_{-15})$
D45.32	0.0130	$-1.89(23)(^{+0}_{-57})$	$-1.81(14)(^{+0}_{-45})$	$-0.132(16)(^{+0}_{-40})$	$-0.126(10)(^{+0}_{-31})$
	0.0150	$-2.29(21)(^{+3}_{-13})$	$-1.83(12)(^{+0}_{-37})$	$-0.163(15)(^{+2}_{-9})$	$-0.130(8)(^{+0}_{-26})$
	0.0180	$-2.02(19)(^{+0}_{-41})$	$-1.94(12)(^{+0}_{-32})$	$-0.149(14)(^{+0}_{-30})$	$-0.142(9)(^{+0}_{-23})$
D30.48	0.0115	$-2.43(60)(^{+43}_{-20})$	$-2.58(38)(^{+42}_{-8})$	$-0.144(36)(^{+25}_{-12})$	$-0.152(23)(^{+25}_{-5})$
	0.0150	$-2.59(63)(^{+49}_{-20})$	$-2.79(40)(^{+50}_{-7})$	$-0.159(39)(^{+30}_{-12})$	$-0.172(25)(^{+31}_{-4})$
	0.0180	$-2.71(66)(^{+54}_{-20})$	$-2.95(42)(^{+56}_{-7})$	$-0.171(42)(^{+34}_{-13})$	$-0.187(27)(^{+36}_{-4})$

Table XIII: Comparison of a_0 and $\mu_{\pi K}\, a_0^{3/2}$ for methods **E1** and **E2**

ChPT	$E_{\pi K}$	$\mu_{\pi K}\, a_0^{3/2} \times 10^2$	$L_{\pi K} \times 10^3$	$\mu_{\pi K}\, a_0^{1/2}$	$M_\pi a_0^{3/2} \times 10^2$	$M_\pi a_0^{1/2}$
Γ	**E1**	$-4.7(1)$	3.7(2)	0.128(2)	$-6.0(1)$	0.162(2)
	E2	$-4.59(8)$	3.8(1)	0.129(2)	$-5.8(1)$	0.164(2)
NLO	**E1**	$-4.7(1)$	3.6(2)	0.127(2)	$-6.0(1)$	0.162(2)
	E2	$-4.61(9)$	3.8(2)	0.129(2)	$-5.9(1)$	0.164(2)

Table XIV: Physical values of the scattering length and $L_{\pi K}$ after averaging over the fit ranges

Ensemble	$\mu_{\pi K}/f_\pi$	aM_K	aM_η	$\mu_{\pi K}\, a_0^{3/2}(\mathbf{E1})$	$\mu_{\pi K}\, a_0^{3/2}(\mathbf{E2})$
A40.24	1.28(2)	0.241(6)	0.317(6)	−0.12(1)	−0.106(8)
A60.24	1.37(1)	0.251(6)	0.323(6)	−0.15(1)	−0.139(9)
A80.24	1.46(1)	0.260(6)	0.327(5)	−0.16(1)	−0.153(6)
A100.24	1.52(1)	0.269(6)	0.332(4)	−0.15(1)	−0.158(6)
A30.32	1.22(1)	0.236(6)	0.314(9)	−0.08(3)	−0.08(2)
A40.32	1.28(1)	0.241(6)	0.314(9)	−0.14(2)	−0.11(1)
B85.24	1.49(1)	0.243(5)	0.296(5)	−0.17(2)	−0.178(9)
B35.32	1.27(1)	0.220(6)	0.284(8)	−0.12(2)	−0.11(1)
B55.32	1.40(1)	0.230(5)	0.283(5)	−0.12(3)	−0.14(1)
D45.32	1.45(1)	0.175(4)	0.200(4)	−0.15(2)	−0.15(2)
D30.48	1.29(1)	0.168(4)	0.196(4)	−0.15(3)	−0.15(2)

Table XV: Input Data for for the chiral analysis

CHAPTER 7

SUMMARY AND OUTLOOK

The present thesis comprises a study of elastic scattering involving pseudoscalar mesons with strangeness S up to $S = 1$ at maximal isospin. The gauge configurations employed in this study were generated using the $N_f = 2 + 1 + 1$ Wilson twisted mass formulation of lattice QCD at maximal twist. A range of pion masses from 230 to 450 MeV was used to simulate at three different values of the lattice spacing. For the valence sector we follow a mixed action approach with a light Wilson twisted mass doublet and Osterwalder-Seiler valence strange quarks at three different strange quark masses.

For the systems in question, K-K and π-K, we successfully use stochastic Laplacian-Heaviside smearing of the valence quark fields to obtain all-to-all propagators for the two and four point correlation functions. This allows us to reuse the propagators for different interpolating operators once they are generated. In both cases we have to remove thermal contributions to the two meson correlation functions, which we achieve via (weighting and) shifting of the corresponding data. To characterize the elastic interactions taking place in both cases we extract the lattice value of the s-wave scattering length a_0 from Lüscher's formula [17]. Subsequently we inter-/extrapolate our lattice data to the physical point and the continuum. For the K-K-system we are not able to use the SU(3) ChPT formula of Ref. [47] for the chiral extrapolation. The reason for that is an insufficient range of Kaon masses for a reliable fit of the ChPT formula to the data. Instead we resorted to a ChPT extrapolation in the light quark mass at leading order taking into account lattice artifacts of order $\mathcal{O}\left(a^2\right)$. Matters are different for the π-K-system. There we employ SU(3) ChPT in the chiral extrapolation. Owing to the large range of pion mass values at three distinct values of the lattice spacing the work described in this thesis adds substantially to the existing determinations of the K-K [48, 49], and π-K scattering length [45, 49–52]. Taking into account the elastic π-π scattering length [30] as well, we investigate the validity of ChPT when increasing the strangeness content of the pseudoscalar mesons participating in the interaction. As already demonstrated in the conclusion of Chapter 6, for the π-π and π-K scattering length the corrections to leading order ChPT turn out to be nearly negligible. For the K-K system the corrections still are surprisingly small. Another result of the current investigation is that lattice artifacts do not seem to play a role in chiral extrapolations at NLO as long as they are done in the following form: The dimensionless product $\mu \cdot a_0$ is extrapolated in the dimensionless variable μ / f. Here μ labels the (reduced)

mass of the system and f the corresponding decay constant. In Wilson twisted mass lattice ChPT lattice artifacts are shown to cancel through NLO for the $I = 2$ π-π-system, Ref. [53]. We confirm this behavior for the interacting π-π and π-K system but cannot make a statement about the case of K-K scattering since we did not employ full ChPT for the extrapolation to the physical point. The data we extract proves to be in good agreement within errors with other lattice determinations, cf. Refs. [45, 49–52] for π-K and Refs. [48, 49] for K-K. In the case of K-K scattering we compare two methods to fix the valence strange quark mass, both giving comparable results.

Besides all the benefits mentioned before there is still room for improvement. Our lowest pion mass corresponds to $M_\pi = 230\,\mathrm{MeV}$. This is roughly a factor of 1.6 larger than the physical pion mass. As a consequence the chiral extrapolations still could be not reliable. Furthermore there exist no experimental determination of a_0, neither for K-K, nor for π-K. Thus a determination of a_0 directly at physical pion masses would be beneficial to confirm the chiral extrapolations done in this thesis. The chiral extrapolation of the π-K scattering length involves knowledge of the LEC L_5. In order to stabilize the ChPT fits to our data we have to use this unphysical quantity as an input. Unfortunately we do not have an own determination at our disposal such that we resort to a determination done by HPQCD, cf. Ref. [46]. Albeit L_5 has been extrapolated to the continuum, it has been calculated at a different renormalization scale. To diminish the corresponding uncertainty in the chiral extrapolation a calculation of L_5 in terms of our lattice formulation would be advantageous. The miss-tuning of the sea strange quark mass, described in Chapter 6, can be improved on as well. In order to do so two approaches are possible. The first one involves a detailed knowledge of how the observables of interest, i.e. the meson masses M_π, M_K and M_η, the decay constant f_π, and the dimensionless scattering length $\mu_{\pi K}\, a_0^{3/2} = -0.0463(17)$ depend on m_s^{sea}. The observables of interest can then be corrected for the miss-tuning by using the derivative of the observables with respect to m_s^{sea}. The second approach works via taking into account the miss-tuning in setting up ChPT in the correct manner. For this one would have to re-derive the relevant chiral extrapolation formulae in a partially quenched mixed action twisted mass ChPT setup and fit the unmatched observables, stated above, in a global fit. Lattice artifacts then have to be taken into account simultaneously. As a last step of improvement a different scaling variable as the Sommer parameter r_0 could be used to interpolate our data to the physical strange quark mass. At the moment the large statistical uncertainty on r_0 contributes significantly to the interpolated values of the kaon and eta masses, entering the chiral extrapolation.

A possible extension of this work consists of investigating scattering processes of pions and kaons with a more complicated chiral structure. Of particular interest would be the resonant channel of $I = 1/2$ where the $\kappa(892)$ resonance could be characterized by its phaseshift. Complications arise in form of diagrammatically more complex correlation functions including singly disconnected diagrams, partial wave mixing which calls for a coupled channel analysis and the subduction of involved 3 momenta to the lattice octahedral group. At the moment the first and the latter issue are addressed in a study on the rho resonance such that experience of this investigation can be carried over to such a study.

To summarize, we have shown in this thesis that it is possible to extract scattering parameters for interactions involving strangeness from Wilson twisted mass lattice QCD. The reusability of

the sLapH perambulators for the correlator construction helped to save simulation time.

BIBLIOGRAPHY

[1] C. Helmes et al.,
Hadron-Hadron Interactions from $N_f = 2 + 1 + 1$ lattice QCD: Isospin-1 KK scattering length,
Phys. Rev. **D96** (2017) 034510, arXiv: 1703.04737 [hep-lat] (cit. on pp. iii, 49).

[2] C. Helmes et al.,
Hadron-Hadron interactions from $N_f = 2 + 1 + 1$ lattice QCD: $I = 3/2$ πK scattering length,
Phys. Rev. **D** ((in press)), arXiv: 1809.08886 [hep-lat] (cit. on pp. iii, 67).

[3] C. Morningstar et al., *Improved stochastic estimation of quark propagation with Laplacian Heaviside smearing in lattice QCD*, Phys.Rev. **D83** (2011) 114505,
arXiv: 1104.3870 [hep-lat] (cit. on pp. 2, 44, 46).

[4] M. E. Peskin and D. V. Schroeder, *An Introduction to quantum field theory*,
Addison-Wesley, 1995, ISBN: 9780201503975, 0201503972,
URL: http://www.slac.stanford.edu/~mpeskin/QFT.html (cit. on p. 3).

[5] J. Donoghue, E. Golowich and B. Holstein, *Dynamics of the Standard Model*,
Cambridge Monographs on Particle Physics, Nuclear Physics and Cosmology,
Cambridge University Press, 1994, ISBN: 9780521476522,
URL: https://books.google.de/books?id=aZGeknmxDjEC (cit. on p. 3).

[6] S. L. Adler, *Axial vector vertex in spinor electrodynamics*,
Phys. Rev. **177** (1969) 2426, [,241(1969)] (cit. on p. 5).

[7] J. S. Bell and R. Jackiw, *A PCAC puzzle: $\pi^0 \to \gamma\gamma$ in the σ model*,
Nuovo Cim. **A60** (1969) 47 (cit. on p. 5).

[8] C. Gattringer and C. Lang, *Quantum Chromodynamics on the Lattice*,
Lecture Notes in Physics, Springer-Verlag Berlin Heidelberg, 2010,
ISBN: 978-3-642-01849-7,
URL: https://www.springer.com/us/book/9783642018497
(cit. on pp. 6, 16, 21).

[9] C. Itzykson and J. Zuber, *Quantum Field Theory*, Dover Books on Physics,
Dover Publications, 2006, ISBN: 9780486445687,
URL: http://store.doverpublications.com/0486445682.html
(cit. on pp. 6–8).

[10] S. Scherer, *Introduction to chiral perturbation theory*,
Adv. Nucl. Phys. **27** (2003) 277, [,277(2002)], arXiv: hep-ph/0210398 [hep-ph]
(cit. on pp. 10–12).

[11] S. Weinberg, *Phenomenological Lagrangians*,
Physica A Statistical Mechanics and its Applications **96** (1979) 327 (cit. on p. 11).

[12] C. B. Lang, *The πK Scattering and Related Processes*, Fortsch. Phys. **26** (1978) 509 (cit. on p. 13).

[13] J. Gasser and H. Leutwyler, *Chiral Perturbation Theory to One Loop*,
Ann. Phys. **158** (1984) 142 (cit. on p. 13).

[14] V. Bernard, N. Kaiser and U. G. Meissner,
pi K scattering in chiral perturbation theory to one loop, Nucl. Phys. **B357** (1991) 129 (cit. on p. 14).

[15] B. Kubis and U.-G. Meissner, *Isospin violation in low-energy charged pion kaon scattering*,
Phys. Lett. **B529** (2002) 69, arXiv: hep-ph/0112154 [hep-ph] (cit. on p. 14).

[16] M. Lüscher, *Volume Dependence of the Energy Spectrum in Massive Quantum Field Theories. 1. Stable Particle States*, Commun.Math.Phys. **104** (1986) 177 (cit. on pp. 17, 18).

[17] M. Lüscher, *Volume Dependence of the Energy Spectrum in Massive Quantum Field Theories. 2. Scattering States*, Commun.Math.Phys. **105** (1986) 153 (cit. on pp. 17–20, 99).

[18] K. Rummukainen and S. A. Gottlieb,
Resonance scattering phase shifts on a nonrest frame lattice, Nucl.Phys. **B450** (1995) 397,
arXiv: hep-lat/9503028 [hep-lat] (cit. on p. 18).

[19] J. R. Taylor, *Scattering Theory: The quantum Theory on Nonrelativistic Collisions*,
Wiley, New York, 1972 (cit. on p. 18).

[20] Y. Iwasaki, *Renormalization group analysis of lattice theories and improved lattice action: two-dimensional nonlinear O(N) sigma model*, Nucl. Phys. **B258** (1985) 141 (cit. on pp. 21, 26).

[21] S. Sint, "Lattice QCD with a chiral twist",
Workshop on Perspectives in Lattice QCD Nara, Japan, October 31-November 11, 2005, 2007,
arXiv: hep-lat/0702008 [hep-lat] (cit. on pp. 22–24).

[22] A. Shindler, *Twisted mass lattice QCD*, Phys.Rept. **461** (2008) 37,
arXiv: 0707.4093 [hep-lat] (cit. on pp. 22, 24).

[23] R. Frezzotti and G. C. Rossi, *Chirally improving Wilson fermions. II: Four-quark operators*,
JHEP **10** (2004) 070, arXiv: hep-lat/0407002 (cit. on pp. 25, 26).

[24] R. Baron et al., *Computing K and D meson masses with N_f = 2+1+1 twisted mass lattice QCD*,
Comput.Phys.Commun. **182** (2011) 299, arXiv: 1005.2042 [hep-lat]
(cit. on pp. 26, 35).

[25] I. Montvay and G. Münster, *Quantum Fields on a Lattice*,
Cambridge Monographs on Mathematical Physics, 1997, ISBN: 9780521599177
(cit. on p. 27).

[26] S. Aoki et al., *Bulk first-order phase transition in three-flavor lattice QCD with O(a)-improved Wilson fermion action at zero temperature*, Phys. Rev. **D72** (2005) 054510,
arXiv: hep-lat/0409016 [hep-lat] (cit. on p. 27).

[27] F. Farchioni et al., *The Phase structure of lattice QCD with Wilson quarks and renormalization group improved gluons*, Eur. Phys. J. **C42** (2005) 73, arXiv: hep-lat/0410031 [hep-lat] (cit. on p. 27).

[28] J. J. Dudek, R. G. Edwards and C. E. Thomas, *S and D-wave phase shifts in isospin-2 pi pi scattering from lattice QCD*, Phys.Rev. **D86** (2012) 034031, arXiv: 1203.6041 [hep-ph] (cit. on pp. 32, 34, 67).

[29] X. Feng, K. Jansen and D. B. Renner, *The pi+ pi+ scattering length from maximally twisted mass lattice QCD*, Phys.Lett. **B684** (2010) 268, arXiv: 0909.3255 [hep-lat] (cit. on pp. 33, 49).

[30] C. Helmes et al., *Hadron-hadron interactions from $N_f = 2 + 1 + 1$ lattice QCD: isospin-2 $\pi\pi$ scattering length*, JHEP **09** (2015) 109, arXiv: 1506.00408 [hep-lat] (cit. on pp. 33, 49, 99).

[31] T. Chiarappa et al., *Numerical simulation of QCD with u, d, s and c quarks in the twisted-mass Wilson formulation*, Eur.Phys.J. **C50** (2007) 373, arXiv: hep-lat/0606011 [hep-lat] (cit. on p. 35).

[32] R. Baron et al., *Light hadrons from lattice QCD with light (u,d), strange and charm dynamical quarks*, JHEP **06** (2010) 111, arXiv: 1004.5284 [hep-lat] (cit. on p. 35).

[33] C. Michael, *Fitting correlated data*, Phys. Rev. **D49** (1994) 2616, arXiv: hep-lat/9310026 [hep-lat] (cit. on p. 36).

[34] U. Wolff, *Monte Carlo errors with less errors*, Comput. Phys. Commun. **156** (2004) 143, eprint: hep-lat/0306017 (cit. on pp. 36, 38).

[35] B. Efron, *Bootstrap Methods: Another Look at the Jackknife*, Ann. Statist. **7** (1979) 1, URL: https://doi.org/10.1214/aos/1176344552 (cit. on p. 39).

[36] D. N. Politis and J. P. Romano, *The Stationary Bootstrap*, Journal of the American Statistical Association **89** (1994) 1303, eprint: https://doi.org/10.1080/01621459.1994.10476870, URL: https://doi.org/10.1080/01621459.1994.10476870 (cit. on p. 40).

[37] S. Duane et al., *Hybrid Monte Carlo*, Physics Letters B **195** (1987) 216 , ISSN: 0370-2693, URL: http://www.sciencedirect.com/science/article/pii/037026938791197X (cit. on p. 41).

[38] K. Jansen and C. Urbach, *tmLQCD: A Program suite to simulate Wilson Twisted mass Lattice QCD*, Comput.Phys.Commun. **180** (2009) 2717, arXiv: 0905.3331 [hep-lat] (cit. on pp. 41–43).

[39] A. Abdel-Rehim et al., *Recent developments in the tmLQCD software suite*, (2013), arXiv: 1311.5495 [hep-lat] (cit. on p. 43).

[40] A. Hasenfratz and F. Knechtli,
Flavor symmetry and the static potential with hypercubic blocking,
Phys. Rev. **D64** (2001) 034504, arXiv: hep-lat/0103029 [hep-lat] (cit. on p. 43).

[41] M. Albanese et al., *Glueball Masses and String Tension in Lattice QCD*,
Phys. Lett. **B192** (1987) 163, URL: http://www.slac.stanford.edu/spires/find/hep/www?j=PHLTA,B192,163
(cit. on p. 43).

[42] M. Peardon et al.,
A Novel quark-field creation operator construction for hadronic physics in lattice QCD,
Phys. Rev. **D80** (2009) 054506, arXiv: 0905.2160 [hep-lat] (cit. on p. 44).

[43] S.-J. Dong and K.-F. Liu, *Stochastic estimation with Z(2) noise*, Phys. Lett. **B328** (1994) 130,
arXiv: hep-lat/9308015 [hep-lat] (cit. on p. 46).

[44] T. Umeda, *A Constant contribution in meson correlators at finite temperature*,
Phys.Rev. **D75** (2007) 094502, arXiv: hep-lat/0701005 [hep-lat] (cit. on p. 49).

[45] S. R. Beane et al., *pi K scattering in full QCD with domain-wall valence quarks*,
Phys. Rev. **D74** (2006) 114503, arXiv: hep-lat/0607036 [hep-lat]
(cit. on pp. 67, 99, 100).

[46] S. Aoki et al., *Review of lattice results concerning low-energy particle physics*, (2016),
arXiv: 1607.00299 [hep-lat] (cit. on pp. 68, 100).

[47] J.-W. Chen, D. O'Connell and A. Walker-Loud,
Two Meson Systems with Ginsparg-Wilson Valence Quarks, Phys. Rev. **D75** (2007) 054501,
arXiv: hep-lat/0611003 [hep-lat] (cit. on p. 99).

[48] S. R. Beane et al., *The K+ K+ scattering length from lattice QCD*,
Phys.Rev. **D77** (2008) 094507, arXiv: 0709.1169 [hep-lat] (cit. on pp. 99, 100).

[49] K. Sasaki et al., *Scattering lengths for two pseudoscalar meson systems*,
Phys.Rev. **D89** (2014) 054502, arXiv: 1311.7226 [hep-lat] (cit. on pp. 99, 100).

[50] Z. Fu, *Lattice study on πK scattering with moving wall source*, Phys. Rev. **D85** (2012) 074501,
arXiv: 1110.1422 [hep-lat] (cit. on pp. 99, 100).

[51] T. Janowski et al., *K-pi scattering lengths at physical kinematics*,
PoS **LATTICE2014** (2014) 080 (cit. on pp. 99, 100).

[52] C. B. Lang et al., *K pi scattering for isospin 1/2 and 3/2 in lattice QCD*,
Phys. Rev. **D86** (2012) 054508, arXiv: 1207.3204 [hep-lat] (cit. on pp. 99, 100).

[53] M. I. Buchoff, J.-W. Chen and A. Walker-Loud,
pi-pi Scattering in Twisted Mass Chiral Perturbation Theory, Phys.Rev. **D79** (2009) 074503,
arXiv: 0810.2464 [hep-lat] (cit. on p. 100).

APPENDIX A

APPENDIX

A.1 DIRAC AND PAULI MATRICES

The Dirac matrices are defined via their anti-commutator

$$\{\gamma_\mu\,,\gamma_\nu\} = 2g_{\mu\nu}\,, \tag{A.1}$$

where $g_{\mu\nu}$ is the Minkowski metric of 4-dimensional space time $g_{\mu\nu} = \mathrm{diag}(1,-1,-1,-1)$. In Dirac representation the four matrices read

$$\gamma_0 = \begin{pmatrix} 0 & \mathbb{1} \\ \mathbb{1} & 0 \end{pmatrix}\,, \qquad \gamma_k = \begin{pmatrix} 0 & -i\tau_k \\ i\tau_k & 0 \end{pmatrix}\,, \tag{A.2}$$

with $\tau_k\,, k \in \{\,1,2,3\,\}$ the Pauli matrices

$$\tau_1 = \begin{pmatrix} 0 & 1 \\ 1 & 0 \end{pmatrix}\,,\ \tau_2 = \begin{pmatrix} 0 & -i \\ i & 0 \end{pmatrix}\,,\ \tau_3 = \begin{pmatrix} 1 & 0 \\ 0 & -1 \end{pmatrix}\,. \tag{A.3}$$

In addition one defines

$$\gamma_5 = \gamma_0\gamma_1\gamma_2\gamma_3\,, \quad \gamma_5^2 = \mathbb{1}\,. \tag{A.4}$$

In Euclidean space time the anti-commutation relation Equation (A.1) changes to accommodate the euclidean metric:

$$\{\gamma_\mu^{(E)}\,,\gamma_\nu^{(E)}\} = 2\delta_{\mu\nu}\mathbb{1}\,. \tag{A.5}$$

The Dirac matrices in Euclidean space (E) are obtained from their Minkowski space (M) counterparts by

$$\gamma_{1,2,3}^{(E)} = -i\gamma_{1,2,3}^{(M)} \tag{A.6}$$

$$\gamma_4^(E) = \gamma_0^(M)\,. \tag{A.7}$$

LIST OF FIGURES

List of Tables